LUT UNIVERSITY
LUT School of Energy Systems
LUT Mechanical Engineering

*Mukesh Kumar Gupta*

# SIMULATION OF VERTICAL PEOPLE TRANSPORTATION SYSTEMS

Examiner(s): Professor Aki Mikkola
D. Sc. (Tech.) Kimmo Kerkkänen

## ABSTRACT

LUT University
LUT School of Energy Systems
LUT Mechanical Engineering

Mukesh Kumar Gupta

**Simulation of vertical people transportation systems**

Master's thesis

2021

89 pages, 53 figures, 5 table

Examiners: Professor Aki Mikkola

D. Sc. (Tech.) Kimmo Kerkkänen

Supervisors: D. Sc. (Tech.) Gabriela Roivainen and M.Sc. (Tech.) Tarvo Viita-aho

Keywords: Multibody dynamics subsystem, Elevator system simulation, Vibration analysis, synthetic data

This thesis was focused on generating synthetic data of several parameter configurations from elevator system simulations model that could be utilized in prescriptive maintenance policies. An existing simulation model of the elevator system was used as a foundation for the elevator system model. To represent the characteristics of the studied elevator and to make the model more parametric, new elements were included and multiple modifications were made to the based model. For system simulation of the elevator system, SimulationX software was used.

The simulation model was validated using the measurement data from the real elevator. The maximum peak to peak value at the nominal speed of lateral and vertical vibrations were the main criteria for the model validation. In the validation comparisons, there was a good correlation between measurement data and simulation data. A brief investigation of model behavior was made while replacing one of the components with another component for same functionality in the model.

All together 72 combinations of nominal run parameter configuration were simulated by four different elevator specifications. Sensitive analysis showed that in the majority of cases, the simulation model exhibited its sensitivity and robustness in projecting the dynamic behavior of elevator systems. However, in few cases the deviation of the results from expectation. The fundamental causes for this deviation were investigated and corrective action was suggested to avoid this deviation. Finally, three load case scenarios were modeled and evaluated to showcase the capabilities for other malfunction modeling and more effectively creating synthetic data using dynamic simulation.

**ACKNOWLEDGEMENTS**

One of the most challenging yet enlightening periods of my life has come to end. I would like to use this chance to appreciate everyone who assisted me during this project. I am grateful for their excellent supervision, invaluable constructive criticisms, and friendly suggestions. I am grateful to them for giving their honest and enlightening perspectives on a variety of project-related difficulties.

I would like to express my deepest gratitude to my supervisor D. Sc. (Tech.) Gabriela Roivainen and M.Sc. (Tech.) Tarvo Viita-aho from KONE Corporation, for believing in me and getting me on board in this project, and for their invaluable assistance, research direction, and support during the research process, without that my thesis would not have been possible. I would also like to thank Olli Peura from Elomatic Oy for teaching and helping me out not only about software but also about elevator system.

I would also want to show my thankfulness to Professor Aki Mikkola and D. Sc. (Tech.) Kimmo Kerkkänen from LUT university for providing me with invaluable advice and, constructive feedback, suggestions during my thesis.

Last but not least I would like to thank my friends and my family for their direct or indirect support on this time.

Mukesh Kumar Gupta
Vantaa 03.09.2021

**TABLE OF CONTENTS**

## LIST OF SYMBOL AND ABBREVIATIONS

| | |
|---|---|
| $d_p$ | Distance between points |
| *dq0* | Direct quadrature zero |
| $f$ | Lower limit frequency for the eigenfrequency |
| $\mathbf{F}_n$ | Normal contact force |
| $H$ | Hermite polynomial |
| $I_a$ | Armature circuit |
| $i_d$ | Current in axes d |
| $i_q$ | Current in axes q |
| $J_{eq}$ | Equivalent inertia of the motor, load and pulley |
| $J_{F,panel}$ | Inertia for one floor panel |
| $J_{R,panel}$ | Inertia for one roof panel |
| $K$ | Motor constant |
| $K_e$ | Back electromotive force coefficient |
| $k_{iI}$ | Integral gain for current |
| $K_{i\Omega}$ | Integral gain constant for speed |
| $k_{pI}$ | Proportional gain for current |
| $k_{PWM}$ | Quadrant Pulse-Width-Modulation converter |
| $K_{p\Theta}$ | Proportional gain constant for position |
| $K_{p\Omega}$ | Proportional gain constant for speed |
| $kr_z$ | Rotational stiffness in z-axis |
| $kt_x$ | Translational stiffness x-direction |
| $kt_y$ | Translational stiffness y-direction |
| $L_d$ | Inductance axes d |
| $L_{dq}$ | Inductance at axes d and q |
| $L_q$ | Inductance axes q |
| $m$ | Constraint equations |
| $m_{floor}$ | Mass of the floor panel |
| $m_{roof}$ | **M**ass of the roof panel |
| $m_{Total}$ | Total mass of the car |
| $n$ | Generalized coordinates |
| **n** | Normal vector |

| | |
|---|---|
| $p$ | Motor pole pairs |
| $R$ | Winding resistance |
| $R_a$ | Armature resistance |
| $T_{em}$ | Motor torque |
| $t_{sat}$ | Saturation time |
| $u_d$ | Voltage in axes d |
| $u_q$ | Voltage in axes q |
| $V_a$ | Armature voltage |
| $V_c(s)$ | Control voltage |
| $v_n$ | Relative normal velocity |
| $\xi$ | Scalable variable |
| $\Theta_m$ | Position at time |
| $\mu$ | Scaling factor |
| $\omega$ | Angular velocity |

| | |
|---|---|
| AABB | Axis-Aligned Bounding Box |
| AAT | Automatic Adjustment Tool |
| ANCF | Absolute Nodal Coordinate Formulation |
| ANN | Artificial Neural Network |
| BB | Internal width of the car |
| BTF | Back to Front |
| BV | Bounding Volume |
| CAD | Computer-Aided Design |
| DBG | Distance Between Guiderail |
| DOF | Degrees of Freedom |
| DOP | Discrete-Orientation Polytope |
| DT | Decision Tree |
| FD | Fault Diagnosis |
| FEM | Finite Element Method |
| FFT | Fast Fourier transform |
| FMI | Functional Mock-up Interface |
| FMU | Functional Mock-up Unit |
| FP | Fault Prediction |

| | |
|---|---|
| IoT | Internet of Things |
| LR | Logistic Regression |
| MBS | Multibody System |
| MSO | Maintenance Strategy Optimization |
| OBB | Oriented Bounding Box |
| OSG | Over Speed Governors |
| PI | Proportional-Integral |
| PMSM | Permanent Magnet Synchronous Machine |
| RAMS | Reliability, Availability, Maintainability and Safety |
| RF | Random Forest |
| RUL | Remain Useful Life |
| SVM | Support Vector Machine |

# 1 INTRODUCTION

Different types of analysis are carried out in different scenarios when a new machine is designed or developed for better performance. These include analysis of vibration, failure mode, and impact, repair, improvement of the control system, and parameter optimization. These analyses in today's world are made virtually with the help of different computer simulation software. Computer simulation is a very useful technique in product design, product development as well as in product maintenance. The computer simulation provides greater improvements in system performance predictions comparison with earlier techniques that were mainly built on analytical solutions or empirical testing. The main benefit of computer simulations of equipment is that it allows the effects of design variables on dynamic behavior to be studied quickly and effectively. Using simulation decreases the requirement to construct actual prototypes, thereby speeding up the cycle of product development. Computer simulation is thus an important part of a wide variety of industrial design and development processes.

In the simplest form, a process for building a system simulation model and validating it with a real system is shown in Figure 1. In a simulation, an actual system or component of a system is investigated. The model is therefore a formulated based on an ideal description of the system. This phase is often difficult and challenging since the modeler must select the essential elements of the system because leaving out any essential elements leads to an invalid model and adding redundant elements complicates the model. After modeling, an appropriate simulation tool can be selected depending on the system requirements and level of accuracy needed and simulation can be run to produce the simulation results. The model validation is performed in the next step where the simulation result is compared with the experimental data and theoretical prediction of the same system. The model validation focuses on the detection and reduction of simulation model defects by comparing simulation results from the model to the experimental results. The simulation model undergoes continuous improvement until the model validation is successful and a clear conclusion is drawn. This validated model now can be used in various ways to predict the system operation by introducing changes in the inputs of the system. (Yin & Mckay 2018, p. 2-4.)

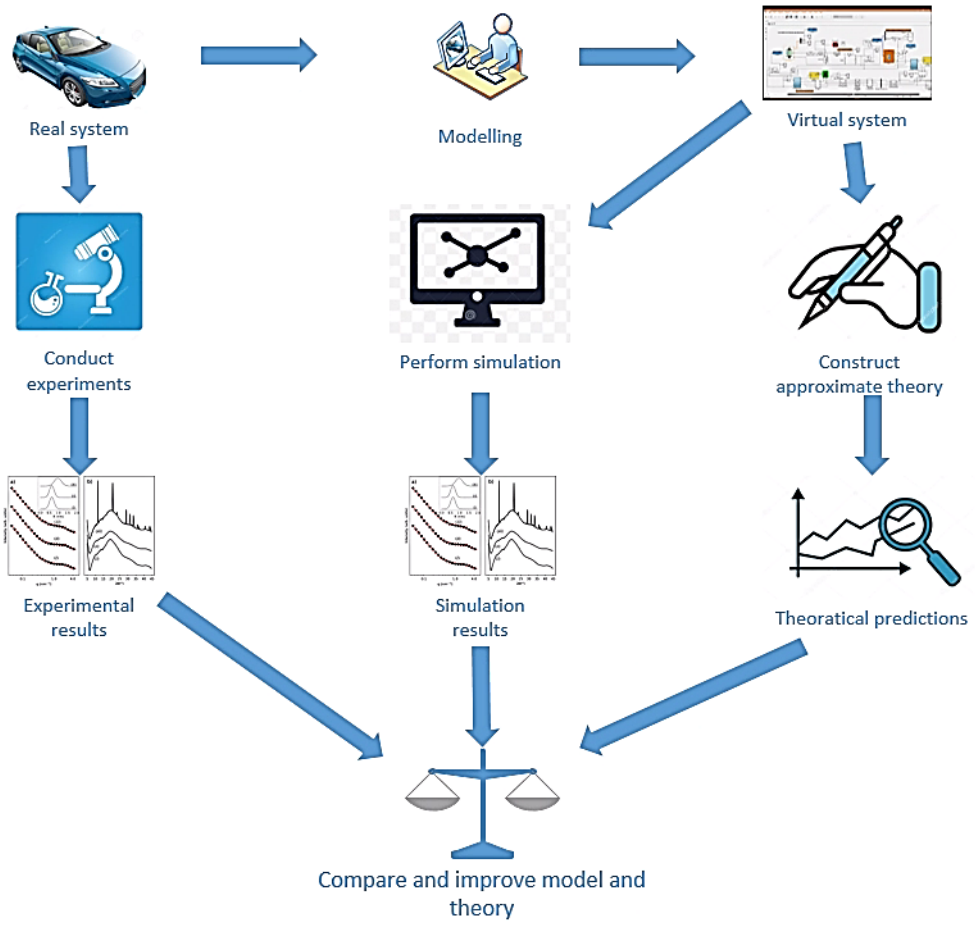


**Figure 1.** System simulation, validation, and analysis process.

Many enterprises have usually viewed maintenance departments as expense sources that do not contribute to the growth of a company. This perspective has changed significantly in recent decades. Managers also recognized the cost savings are possible from successful maintenance processes. Maintenance is now seen as an important part of the product lifecycle, which leads to product quality, plant productivity, and the capacity to reach delivery deadlines. There are various types of maintenance policy for example corrective maintenance, preventive maintenance, predictive maintenance, and prescriptive maintenance available as per the industry's needs and requirements. The primary inputs for these maintenance policies for instant are the failure data, which are collected from sensor data, Reliability, Availability, Maintainability, and Safety (RAMS) data, or generated synthetic data. Simulation plays a vital role in producing synthesis data which further can be used for various purposes and in this case as data for prescriptive maintenance purposes. (Kelvin 2007, p. 2.)

## 1.1 Motivation

KONE Corporation is one of the leading industries in the elevator and escalator business in the world. The elevator and escalator by KONE Corporation can be seen in Figure 2. The demand for the elevator is increasing with the increase in the number of buildings, malls, and skyscrapers and so is the competition between competitors. Therefore, for improving performance, lifetime and ride experience in the elevator, KONE corporation has started to build a virtual system-level model of an elevator. This virtual elevator model will provide an excellent opportunity to understand deeply the dynamics of the elevator and the behavior of the critical component during the operation, which can be utilized in the development and maintenance phase. The final goal of the project is to connect it with the digital twin concept, which has an enormous number of ways to help and develop the ride experience, and quality of the elevators in the future. Digital twin technology also provides an opportunity to monitor the product's health throughout its lifetime and provide prescriptive maintenance (Parrott & Warshaw 2017, p. 2-5).

**Figure 2.** KONE'S elevator and escalator (KONE 2013).

## 1.2 Research problem

In Predictive maintenance policy, to prevent unexpected failure of system or component, history-based data is used through machine learning and artificial intelligence to estimate the maintenance requirements. Physics-based simulation of a real system provide opportunities to produce system behavior data for all kind of parameter configurations, along with the faulty component. The synthetic data obtained from the physics-based virtual model

can be used in machine learning and artificial intelligence to find the signature pattern for the simulated case. Prescriptive maintenance is the combination of predictive maintenance policy and physics-based simulation policy along with machine learning and artificial intelligence to not only search for failure signature pattern but also gives information to avoid or delay equipment failure. In order to implement prescriptive maintenance, greater engineering effort is required as shown in Figure 3. (Aspentech 2021.)

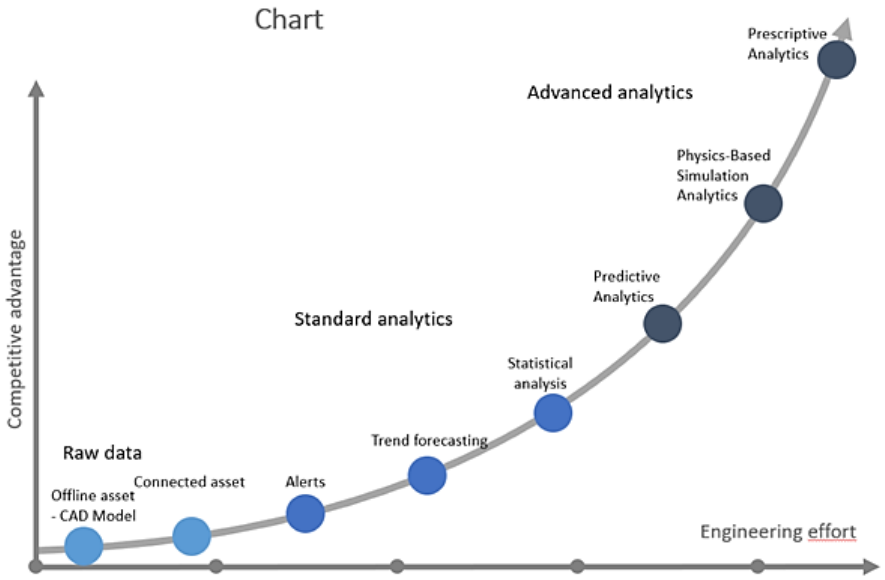


**Figure 3.** Digital twin value chat (Edrmedeso 2020).

In principle, creating synthetic data from a physics-based virtual system appears to be a straightforward approach, but in practice, it is not. Some of the greatest challenges in the process are creating a sensitive and robust virtual model of the system, modeling of the malfunction condition or component in the system and identification of the malfunction's signature pattern and many more.

### 1.3 Objectives and research questions

During the analysis of the model, the accuracy of the model behavior increases as the level of detail increases but at some point, increasing the detail in the model has no longer an effect on the results. Therefore, knowing the optimal number of the detail of the system is required to build a generic model. Once the generic model is built, by changing important parameters in this case travel distance, different masses, different stiffnesses, different damper, etc. the entire family of the elevator can be analyzed.

The main objective of this project is to validate the computed results such as car position, velocity, vibration, etc. obtained from the system-level model of the elevator with the data collected from the measurements. The fulfillment of the requirement for this goal is obtained by comparing the calculated and measured signals at the peak to peak value vibration and should be when the load, speed, travel is maximum or minimum. The results should be in the same range and the differences explicable. To gain further reliability of the model, sensitivity analysis of different nominal run cases will be performed. Physics-based simulations are becoming increasingly relevant as computer power increases. Simulations are a viable alternative for getting synthetic data for product platform parameters configurable scenarios. A preexisting physic-based simulation model of a KONE elevator system from different platforms constructed prior to the thesis will be utilized as a reference model for modeling the elevator system in the thesis. The second objective of this thesis is to model the top three different load cases that occur in the elevator system which are listed below.

1. Sag and bounce: - when the passenger getting in and out of the elevator car
2. Buffer run: - when the car does not stop at the lowest level and hits the buffers.
3. Counterweight run: -when the car does not stop at the top floor and the counterweight hits the buffer.

The main research questions of the thesis are listed below.

- How detailed a system-level model of an elevator is required to obtain the result closed to the physical product?
- Why the selected parameters are the most important ones while changing from one elevator family to another without losing accuracy in the results?
- How most common load cases in the elevator system can be modeled in the virtual environment?
- How synthetic data obtained from simulation can be used for prescriptive maintenance?

# 2 METHODS AND METHODOLOGY

In this chapter, the importance of simulation in the implementation of prescriptive maintenance is discussed. The methods which can be used for modeling and analysis of the different elevator components are mentioned.

## 2.1 Maintenance policies and their primary requirements

Maintenance requires all steps possible to maintain or restore the correct operation of equipment or machines. The aim is to eliminate the possibility of failures that can lead to machine breakdown or unscheduled downtimes, or that could escalate to safety problems. For example, wear, progressive damage, or material deformation due to force that develops in several mechanical parts, for example, roller bearings, O-rings, or gears, is the common cause of failure. Systematic maintenance processes improve machine availability, minimize costs and encourage appropriate maintenance plans to be scheduled. Traditional, preventive maintenance requires the routine monitoring of devices according to a set timeline or fixed target based on the simplistic presumption that faults occur most of the time. However, this strategy does not work most of the time for the reason being failure takes place before planned maintenance or maintenance is performed even though it was not required. (Centomo et al. 2020, p. 1782.)

### 2.1.1 Predictive maintenance

Predictive maintenance aims at solving the strategy of the fixed schedule by implementing a procedure to predict specific possible failures. The purpose is to have maintenance unless is really required, i.e., not too soon, or too late. Predictive maintenance has the benefit of substantially reducing maintenance costs by allowing better use of capacities and preventing operation downtimes. (Centomo et al. 2020, p. 1782.)

Predictive maintenance is focused on the prediction of faults based on the data collected by different sensors, for examples vibration, temperature, humidity, or acoustic sensors. Thus, it is important to preset data that describe the different states of the machine for example location sensors or switches as well as the actuator status. Based on preset data and collected data from the decision for maintenance are called out. Due to a large number of data

collection, manual tracking, and decision-making are impossible. That is why machine learning and particularly deep learning are the best fit for data processing. They are often used for predictive maintenance tasks like Remain Useful Life (RUL), Root Cause Analysis also referred to as Fault Diagnosis (FD), Fault Prediction (FP), and Maintenance Strategy Optimization (MSO). But before the use of the Machine Learning (ML) algorithm, all sets of data labeled with the respective fault and patterns or shape of signals have to be discovered. This data is then used as a source of information for predicting when which failure has taken place. Figure 4 illustrates the predictive maintenance working processes and various technologies use to accomplish an effective process. (Çınar et al. 2020, p. 8211; Klein & Bergmann 2018, p. 3.)

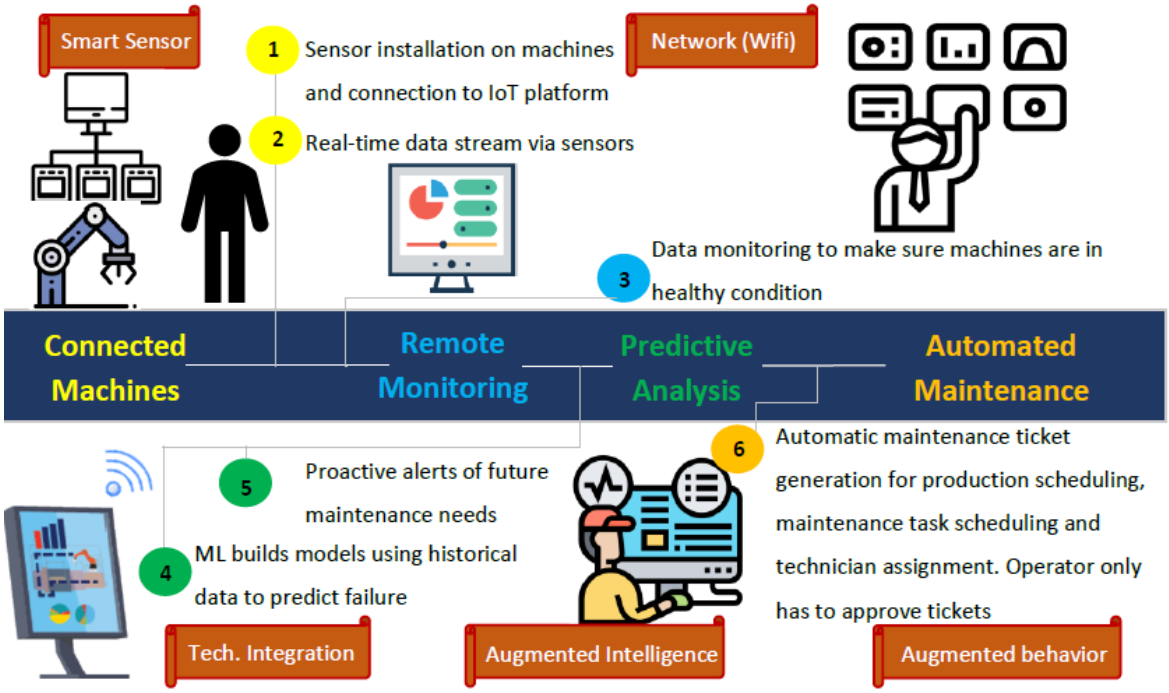


**Figure 4.** Predictive maintenance working principle and used technologies (Çınar et al. 2020, p. 8211).

The collection of data and creating algorithms from machine learning in predictive maintenance are the most challenging phase in the process. There are two approaches for data collection described in detail in the next sub chapters, and many methods for application of ML algorithm in predictive maintenance such as Artificial Neural Network (ANN), Support Vector Machine (SVM), Decision Tree (DT), Random Forest (RF), Logistic

Regression (LR), Extreme Gradient Boosted Trees (XGBoost), Gradient Boosting Machines (GBM), Linear Regression, Symbolic Regression (SR) (Çınar et al. 2020, p. 8211).

### 2.1.2 Prescriptive maintenance

Prescriptive maintenance works in cooperation with preventive maintenance and physics-based simulation to indicate not only what and when a breakdown will occur, but also why it will occur when the behavior of equipment had changed. Prescriptive maintenance will take the study a step further by determining alternative choices and their potential effects in order to reduce any harm to the system. The data and analysis will continue in the period prior to the maintenance activity, with the potential consequences and suggestions being continually adjusted and changed, increasing the credibility of the results. The analytical engine will keep monitoring the machine after the maintenance activity is done to see if the maintenance was effective. (Kovacevic 2017.)

A machine learning model that is developed on sensor and service data is required for prescriptive maintenance to be successful. The artificial intelligence model would be increasingly accurate when more high-quality data becomes available, recognizing more indicators of maintenance requirements and failure signatures while providing fewer false positives. During training a prescriptive maintenance algorithm, higher-level information about an industry may be supplied to the machine learning algorithm. This allows the program to consider important factors for example maintenance costs and product downtime. The machine learning model is trained using specialized hardware, which might be local, or cloud based. The model is code that may be installed on-premises or in the cloud, therefore a means to reach and operate it is necessary. This can be readily connected with various asset management software packages, easing the process of implementing the prescriptive maintenance model's suggestions. At last, prescriptive maintenance needs a company's willingness and ability to put into practice the machine learning suggestions. Hypothetical outcomes created by a prescriptive maintenance program give options that were previously either left by chance or tried and tested. (Aspentech 2021.)

In many sectors and industries, predictive maintenance has been proven to be accurate. A company or organization's physical operations can benefit from the power of machine

learning by implementing prescriptive maintenance suggestions. The difference between prescriptive maintenance and predictive maintenance is that prescriptive maintenance gives a range of alternatives and outcomes from which to choose. In many cases, prescriptive maintenance can also detect capital expenditure needs months before they could even appear to human operators giving time to the company for economy purchases. (Aspentech 2021.)

### 2.1.3 Methods of data collection

The primary method for determining the health condition of machines is by observing the machine which can be successfully achieved by the implementation of a sensor. The IoT sensor such as accelerometers, gyroscopes, pressure sensors, etc. is normally used for this process. The data coming from the sensor then can be utilized for the ML algorithms for predictive maintenance. However, the implementation of these sensors is not straightforward and vary many cases not appropriate especially for already existing machines and equipment. The failure data of machines are generally collected by a method called run-to-failure. This method can be very time-consuming and costly for larger sets of data. Once data has been collected, there come difficulties for data handing and drawing conclusions that can be used in predictive maintenance. (Centomo et al. 2020, p. 1786.)

Although there is not enough or sufficient data available for analysis from the actual system, it is possible to generate them. There are four ways to generate the sensor data: fully synthetical, synthetical based on previous data, synthetical based on a virtual simulation model, and finally based on a simplified physical model (Klein & Bergmann 2018, p. 4).

For the generation of fully synthetic data, sensor data is produced using a parameter-based algorithm. This method may slightly drift from its concept because its results are based on the statical model. (Klein & Bergmann 2018, p. 5.) The procedure made by Hahsler et al. can be used for generating and analyzing fully synthetic data (Hahsler et al. 2017, p. 1-45).

Generation synthetic data based on previous data can be archived by generating new data based on fundamental properties of existing data distribution. This could be achieved by preparing a generative and discriminative neural model by either directly learning the distribution parameters or indirectly using a generative adversarial time-series network. (Klein & Bergmann 2018, p. 5.)

Synthetical data generation based on a virtual simulation model uses a computer simulation platform for creating a model with the property of the actual model which can be used for data generation. An engineer can model faulty components or a variety of failure scenarios by adjusting temperatures, flow rates, or vibrations or adding a sudden fault in the system. These faults containing model can be simulation and results containing failure data can be labeled and stored processed for further analysis. Many industries have used this approach for creating virtual factory, machine health testing applications. (Klein & Bergmann 2018, p. 5.)

Synthetical data generation based on a simplified physical model uses a similar approach but instead of using a virtual model, it uses a simplified physical-based model. The models can be replicated in two different ways. One using actual components which are used in real machines and the other using not real components. The benefit of the second method is the remarkably low cost of constructing such a model. Lego Mindstorms and Fischertechnik (FT) provides such construction of the model at a low cost. (Klein & Bergmann 2018, p. 6.)

## 2.2 SimulationX - a system simulation software

SimulationX is a Multiphysics software tool based on Modelica (Modelica is a non-proprietary, objects-oriented, multi-domain equations-based programming language that may be used to simulate complicated physical systems) modeling language for modeling and simulating of mechanical system, hydraulic, pneumatic, electro-material, control system, along with thermal and magnetic systems. This provides great opportunities for simulating and multi aspects of the model without unitizing co-simulation as shown in Figure 7. It can be used to model, analyze, and optimize sophisticated, nonlinear, dynamic systems. The graphic user interface of SimulationX software is shown in Figure 5. A user interface is used to describe simulation models interactively. Domain-specific libraries contain ready-to-use model components. SimulationX employs well-known symbols and input values. The user-defined component can be constructed by assembling already available elements with TypeDesigner. A model of component or system can be made through diagram view or 3D view or text view. It also provides the opportunity to calculate the natural frequencies of the model. It has a real physics element; thus, it can run in real-time. The great majority of SimulationX applications are focused on drive systems, hybrid powertrains, mechatronics,

and vehicle dynamics. Furthermore, constructing the hoisting model (virtual prototype of an elevator) and network modeling in SimulationX not only offers the user a realistic and current engineering solution, but it also saves time and has a long lifetime. This technology is also compatible with software like as Microsoft Word, Excel, and COMSOL. (SimulationX 2016.)

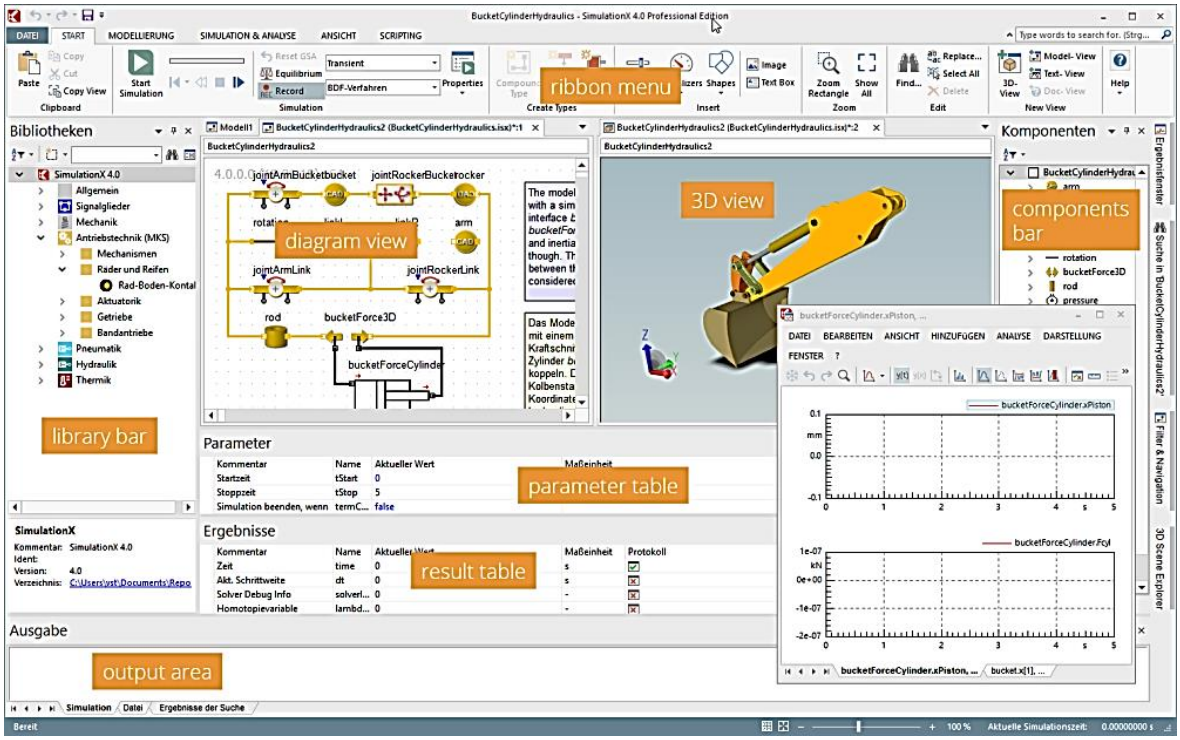


**Figure 5.** Graphic user interface of SimulationX software (SimulationX 2016).

## 2.3 Method of modeling of electronics and control

In his chapter, the electrical motor modeling method and the controller modeling method for actuating and controlling the elevator system are presented.

### 2.3.1 Electrical motor modeling

The dynamic modeling of the motor as a mathematical model based on voltage equation. For instant, the voltage equations from motor modeling are listed below, which are based on Liu, et al. work (Liu et al. 2015, p. 1121).

$$u_d = ri_d + L_d \frac{di_d}{dt} - p\omega L_q i_q \quad (1)$$

$$u_q = ri_d + L_d \frac{di_d}{dt} - p\omega(L_q i_q + K_e) \quad (2)$$

Where $u_d$ and $u_q$ are voltage in axes $d$ and $q$ , $r$ represents winding resistance in every phase, $L_d$ and $L_q$ represents inductance axes $d$ and $q$, $\omega$ angular velocity of the mechanical part, $K_e$ is back electromotive force coefficient, $p$ is motor pole pairs and $i_d$ and $i_q$ is current in axes $d$ and $q$ (Liu et al. 2015, p. 1121).

The generation of the equation contains various assumptions and neglection such as the model is linear regardless of the eddy current and hysteresis loss, neglecting the impact of cogging and armature reaction, the winding is completely symmetrical in three phases (Liu et al. 2015, p. 1121). An inverter can also be modeled to convert DC power to AC power and desired sinusoidal or trapezoid signals can be produced as per request for permanent magnet synchronous machine (PMSM). To connect the one-dimensional electrical parts with the MBS part, the interface elements can be used.

### 2.3.2 Controller modeling

Controllers are made up of software and hardware that are designed to run algorithms rapidly and efficiently. Such algorithms aim to increase the speed of complex transactions involving mathematical and logical equations. This algorithm may either be hardwired into the controller's structure or run as customized code on a microprocessor. Each digital control system is optimized for the system it operates in order to maximize performance and achieve the fastest response time possible. The control system is used to impose the position, speed, and current of electric power on the elevator that enhances the precise and accurate response of the elevator to position requirements. (Ford et al. 2016, p. 309.)

Figure 6 (a) shows the working principle of Cascaded control system. The position controller is shown in figure 6 (d) where $\Theta_m$ is position and $K_{p\Theta}$ proportional gain constant. The speed controller is shown in figure 6 (c) where $\omega_m$ is speed, $K_{i\Omega}$ integral gain constant, $K_{p\Omega}$ is proportional gain constant, $I_a$ is armature circuit, $K$ is motor constant, $T_{em}$ is motor torque, $J_{eq}$ is equivalent inertia of the motor, load and pulley and current controller is shown in figure 6 (b) where $R_a$ is armature resistance, $k_{pI}$ is the proportional gain, $k_{iI}$ is integral gain, $V_c(s)$ is control voltage, $k_{PWM}$ is 4-quadrant Pulse-Width-Modulation converter, $V_a(s)$ is voltage *Te*

torque. These controllers are working together with three cascaded loops by utilizing the motor position sensor and current output. Feedback controllers are designed to regulate a system accurately and rapidly based on real-time feedback received from the system themselves, with no need for external adjustment. A correctly built control scheme can reduce a process's steady-state error to zero in a short period with little oscillations and minimal overshoot. Proportional-Integral (PI) controller corrects gap between desired and measured speed or current with respect to the given proportional and integral values and Proportional (P) controller that will properly adjust errors in the location of the drive. (Ford et al. 2016, p. 310.)

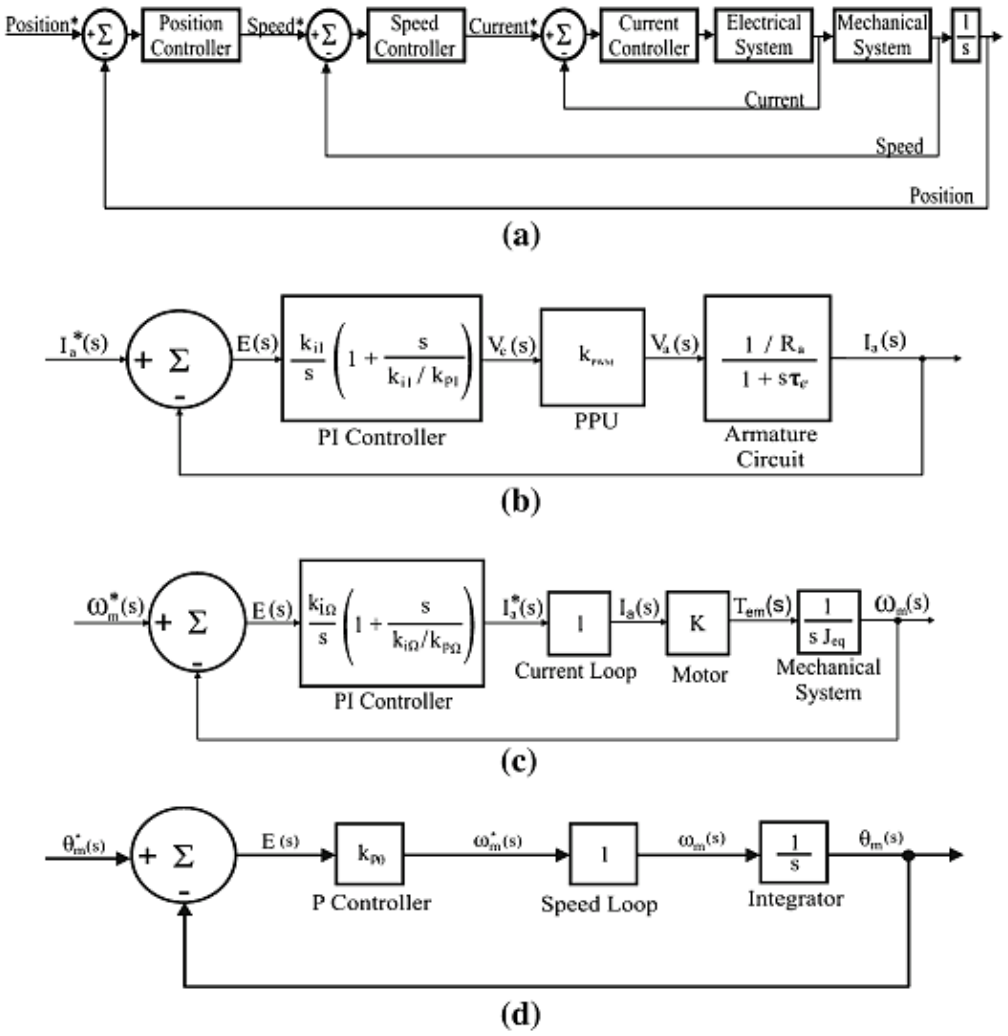


**Figure 6.** Cascaded control system (a), controlled loops for current (b), speed (c) and position (d) (Ford et al. 2016, p. 311).

The elevator controlled are consists of motion controller, PI controller and controlled inverter. The motion controller determines the required velocity for the PI controller depending on the current position, velocity, and desired floor. The PI controller will determine how much torque is needed depending on the difference between the intended elevator velocity (from motion controller) and the present elevator velocity. The inverter controls the machine's electric phases by establishing an initial set of currents. A coordinate transformation of the machine into a direct quadrature zero (*dq0*) representation is used for this control. The control then comprises many components, including a PI controller for the currents *d* and *q* with the specified gain calculated by the inductance $L_{dq}$ and specified in the parameter.

## 2.4 Functional mock-up interface and co-simulation

Functional Mock-up Interface (FMI) is an autonomous platform for the sharing of models and simulation of complex models using a mix of XML files and compiled C-code. FMI contains a series of basic functions for exchanging data and synchronizing sub-systems in interaction stages. These sub-systems are referred to as FMI slaves, while the co-simulation supervisor is referred to as FMI master. This provides an opportunity to have the same model simulation in different platforms for different analyses and therefore investment in a model portfolio significantly increases. (Modelon 2020.)

Functional Mock-up Unit (FMU) is a file that includes a model of simulation complying with the FMI specification (with the extension.FMU). FMUs are divided into two categories by the FMI standard: model exchange FMUs use differential equations to describe dynamical processes. The FMU must be connected to a numerical solver in order for the model to be simulated. The solver decides the phase size and how to calculate the state at the next time step after setting the FMU internal state and asking for the state derivatives. The other FMI standard is co-simulation where FMUs have their built-in numerical solver. The import tool selects the inputs for FMU, orders the FMU to go further to the given time, and reads the results for FMU after that point. (Modelon 2020.)

Co-simulation is a technique where one aspect of the model for example physical model is combined with another aspect for example mathematical model to perform a simulation giving a deep level understanding of an entire system as shown in Figure 7. This technique

also can be used for studying multi-physical models where for example rigid bodies are modeled on one platform and flexible bodies or acoustics or CFD or structural are modeled on other and are coupled together to capture the system behavior in detail. This approach is suited for the test of mechanical design, device specifications, system compatibility analysis, and control system testing. (Baobing & Baras 2013, p. 71; Brezina et al. 2011, p. 59.)

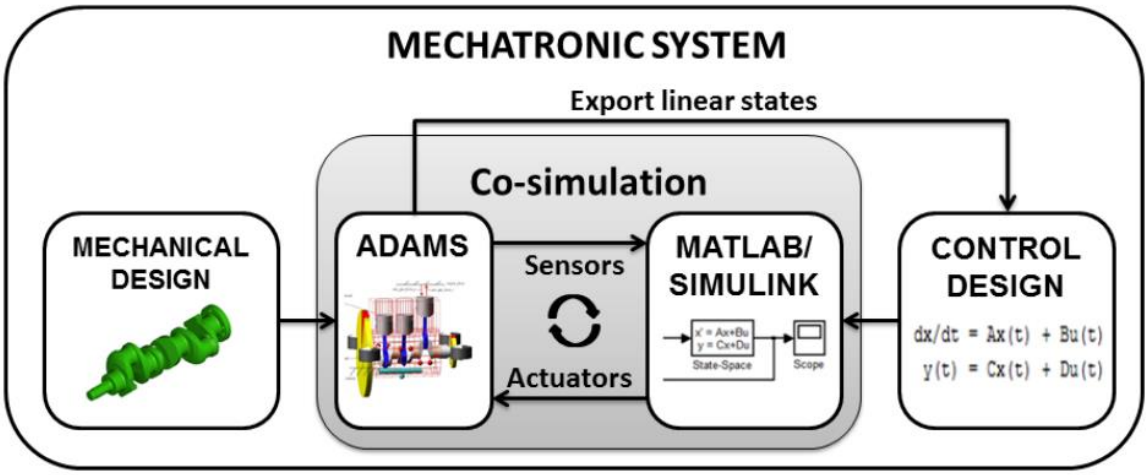


**Figure 7.** Co-simulation of entire system (Brezina et al. 2011, p. 59).

SimulationX software is used for simulation of electrical, mechanical and controller all in the same platform explained in detail in section 2.2. This platform also provides a facility for co-simulation with another aspect if required. FMU technique has been utilized to import a real motion control algorithm for the elevator. The Initial motion control algorithm is in MATLAB Simulink Which is exported using FMI Co-Simulation Target for Simulink®CoderTM. It allows to export MATLAB Simulink functions as FMUs and reimport them into SimulationX. Especially for the FMU import behavior, some parameters can be edited on the pages “FMI Settings” and “Master Algorithm” in SimulationX.

## 2.5 Principles of a multibody system

According to Flores ( 2015, p. 1). “a multibody system encompasses a collection of rigid and/or flexible bodies interconnected by kinematic joints and possibly some force elements.” The method of multibody system dynamics can be described as an efficient way of studying such mechanical systems. This method is extremely successful for mechanical systems which contain several bodies interconnected with mechanical joints as shown in Figure 8. Examples of the use of multibody structures, including automotive vehicles, mechanisms,

robots, and biomechanical systems. Recently, there has been a significant rise in the application of this multibody system dynamics approach to analyze the mechanical structure. (Flores 2015, p. 1-2.)

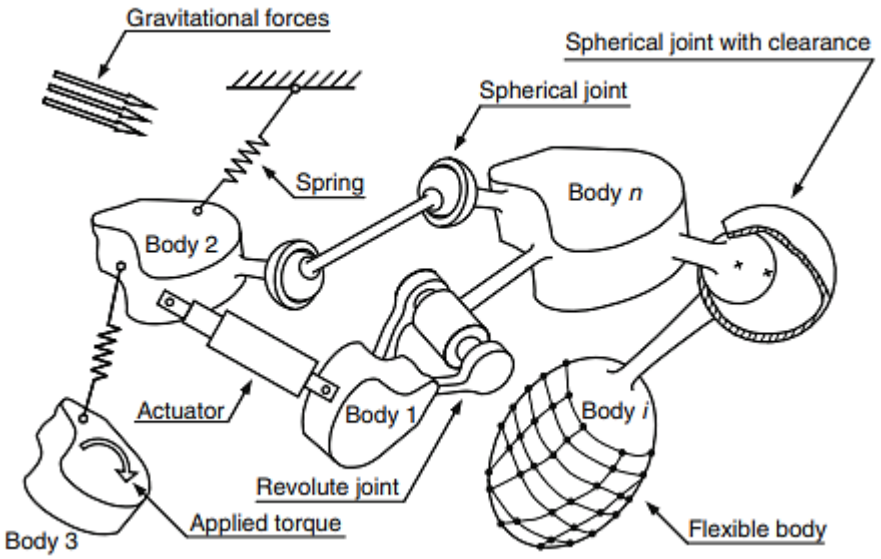


**Figure 8.** Multibody system representation (Flores 2015, p. 2).

There are several techniques to formulate equation of motions for computational multibody dynamics. Some techniques allow producing motion equations in a differential-algebraic equations whereas some in a minimum group of basic differential equations and a number other intermediate approaches offer different alternatives as shown in Figure 9. Depending on application and priorities, each formula has its own benefits and restrictions. (Flores 2015, p. 3.)

The most basic method of generating equations of motion is with a large set of differential-algebraic equations. A group of translation and rotational coordinates defines the structure of a rigid body. To describe kinematic joints between bodies, algebraic constraints are implemented, and then the Lagrange multiplier technique is used to define joint reaction forces. This formulation is called body-coordinate formulation. Body coordinate formulation is also called as the absolute coordinate formulation or Cartesian coordinate formulation. While these formulations are simple to build, one of the key disadvantages is their computational inefficiency. These types of formulations are adopted in many commercial multibody simulation software such as ADAMS and DADS. This formulation method is

employed to the generation of dynamic analysis of the multibody system in this thesis. (Nikravesh 2004, p. 83.)

The other formulations of equations of motion are point-coordinate (or natural coordinates) formulation and joint-coordinate formulation. The point coordinates formulation method is based on the constrained Newton equations therefore the rotational coordinates are excluded. In joint coordinates formulation, relative coordinates and velocities are used and it results in much fewer sets of equations. Through a systematic method, these equations are obtained by translating the body-coordinate formulation to the joint space. (Flores 2015, p. 7.)

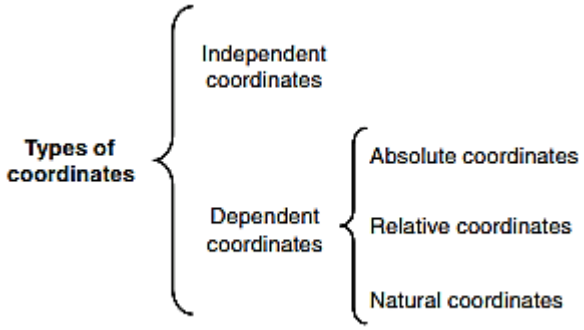


**Figure 9.** Most commonly used coordinate types in Multibody system (Flores 2015, p. 7).

### 2.5.1 Coordinates system

Global and local coordinate system is used in the formulation of multibody spatial system. The global coordinate system is to define the frame of inertia and the local coordinates system is to define the local properties of points belonging to a particular body. The local coordinates systems translate and rotate with the motion of the body and, therefore, its position and rotations differ with time. The method of translating local coordinate into global coordinate is defined by a transformation matrix. (Flores 2015, p. 11-12.) The description of the position vector and local coordinates can be seen in Figure 10.

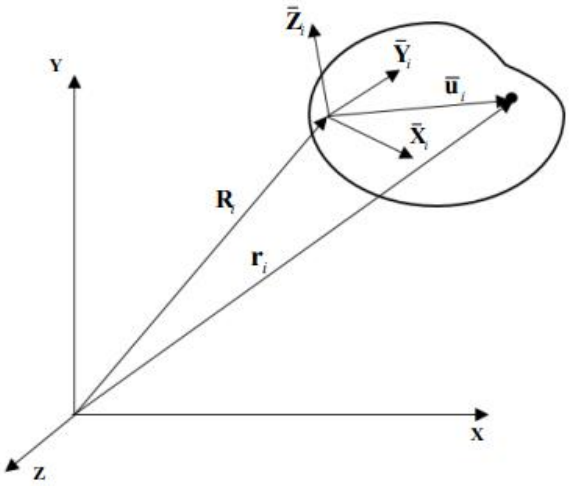


**Figure 10.** Description of the position of a point in the spatial body (Flores 2015, p. 12).

There are numerous methods in spatial multibody systems for defining the rotational coordinates such as Euler angles, Bryant angles, Rodrigues equation, and Euler parameters. Each method has its own advantages and disadvantages. Sometimes a combination of two separate rotation representation processes could be used to get the best output. Details information can be found in (Flores 2015, p. 11-12).

### 2.5.2 Generalized coordinates

Generalized coordinates are classified as a collection of convenient and typically independent coordinates for the purpose of explaining the configuration of a specific system. The quantities of independent generalized coordinates determine the number of degrees of freedom of the system if external constraints are applied to the system then that results in some dependence among the generalized coordinates. For example, if a specific configuration is represented by *n* generalized coordinates and m constraint equations (m<n), the difference *n-m* is equal to the system's total degrees of freedom (DOF). Various terms for velocity, acceleration, and equation of motion are required to be produced for the study of multibody dynamics. The number and type of generalized coordination rely on the selection of the kinematic description of the system. Therefore, to achieve a simple expression for the velocity, acceleration, and motion equation, it is necessary to choose the appropriate generalized coordinates. (Amirouche 2006, p. 46.)

### 2.5.3 Constraint equation

In multibody system modeling, the constraints indicate a restriction on one or more bodies' kinematic degrees of freedom. In other words, mechanical joints are expressed through constraints equations and are linked to generalized coordinates. Therefore, the constraint equations impose the dependency in generalized coordinates. The constraint equations are functions of the generalized coordinates and, in some cases, time. In general, the number of generalized coordinates is higher than the number of constraints equations. (Amirouche 2006, p. 45-48.)

The kinematics constraints are classified into two categories namely holonomic and nonholonomic. If the constraints depend on generalized coordinates and possibly on time then it is called holonomic, otherwise, it is nonholonomic. The holonomic constraints in the multibody system are further divided into two categories that are, scleronomic and rheonomic. If constraints do not include time as an explicit variable, they are called scleronomic and if constraints are a function of time, they are called rheonomic. The detailed kinematic equation formulation based on the vector of body coordinates can be shown in (Flores 2015, p. 31-35).

Modeling of the joints is an essential step during the study of multibody dynamics. In a multibody system, multiple bodies are linked with joints. Joints also provided restrictions to the relative motion of the bodies. There are various types of joints in mechanical systems. The various joints type minimizes the number of DOF in the system. Revolute joints, translational joints, spherical joints, cylindrical joints, screw joints, and planar joints are commonly used joints during the modeling of the multibody system. These basic joints are being used to establish joints with different mechanisms. (Flores 2015, p. 7.) Complicated joints can be constructed utilizing a combination of several types of simple joints. The formulation of the kinematic joint constraints for the spherical joint, revolute joint and the spherical-spherical joint is shown in (Flores 2015, p. 43-48). Different properties of different types of joints can be seen in Table 1.

*Table 1: Joint types and total DOF (Mathworks 2021).*

| Joint Type | Total DOF | Restriction of Translational DOF | Restriction of Rotational DOF |
|---|---|---|---|
| Revolute | 1 | 3 | 2 |
| Spherical | 3 | 3 | 0 |
| Translational | 1 | 2 | 3 |
| Universal | 2 | 3 | 1 |
| Fixed | 0 | 3 | 3 |
| Cylindrical | 2 | 2 | 2 |
| Prismatic joint | 1 | 2 | 3 |
| Bearing joint | 4 | 2 | 0 |

### 2.5.4 Dynamic analysis of multibody system

The dynamic equation of motion can be derived from different techniques. The dynamic analysis of the system includes determining dynamic equilibrium and dynamic equilibrium can be represented by second-order differential equations. If the system is unconstrained, the equation of motion could be formed with Newton-Euler equations. If the system is constrained, there are several other processes to solve the equation of motion of spatial multibody systems namely Lagrange multiplier method, the Embedding technique, the Baumgarte method, the penalty method, and the augmented Lagrangian formulation. (Flores 2015, p. 61.)

In the augmented formulation, the dynamic equations appear with constraint forces and are represented as redundant coordinate. For unknown accelerations and constraint forces, the constraint relationship is used with the differential equation of motion. In this process, a sparse matrix structures are formed. The augmented formulation, however, has the downside of rising the dimensionality of the problem and, needs father advanced numerical algorithms to calculate the resulting systems of differential and algebraic equations. (Flores 2015, p. 61.)

The Lagrangian dynamics are based on a higher systematic and universal method for designing the augmented equation of motion. The Lagrange multiplier technique is utilized in the Lagrangian method to describe generalized constraint forces and to generate an

augmented formulation where the coefficient matrix is symmetric. In the formulation of the augmented equation of motion, Lagrange multipliers are mostly used. There are equal number Langrage multipliers and constraints equations in the system. This equation has constraints in terms of acceleration and the constant equation vanishes after differentiating the constraint equations two times with respect to time. Therefore, to overcomes this downside, a constraint stabilization method for example Baumgarte stabilization method, a penalty formulation or an augmented Lagrangian method can be introduced. Figure 11 shows the algorithm for dynamic analysis of multibody systems on the basis of the standard Lagrange multipliers method. (Flores 2015, p. 60-68.)

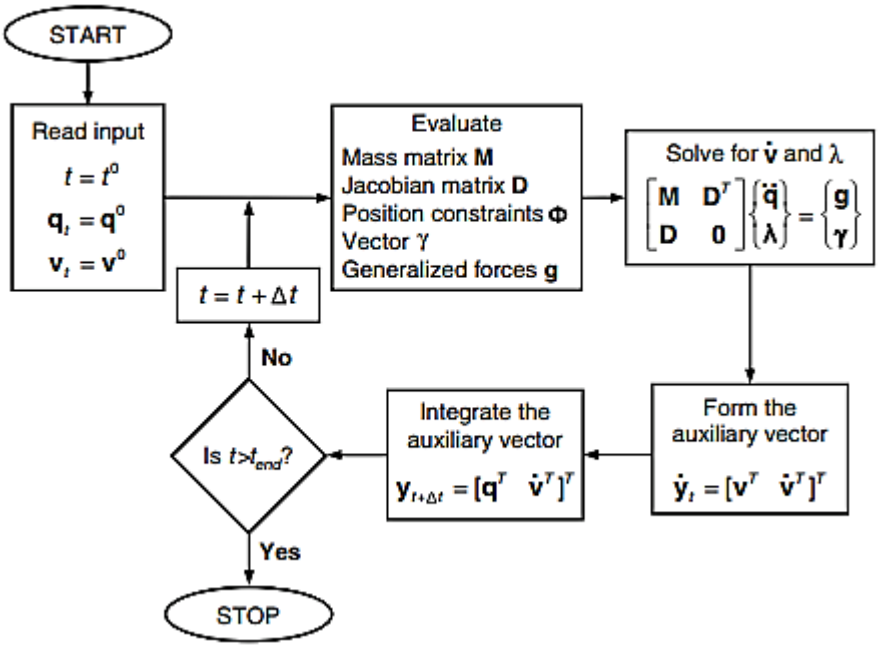


**Figure 11.** Flowchart based on the standard Lagrange multipliers method for dynamic analysis of multibody systems (Flores 2015, p. 63).

### 2.5.5 Collision and contact modeling methods

When studying a real multibody system, contact modeling is an important modeling aspect. Contact modeling's main feature is to detect the collision point and give the reactions of the collision. It is also used to evaluate the contact forces between two bodies. Two computational methods, named finite element analysis (FEM) and multibody system (MBS) can be used to perform contact analysis. FEM is the most effective content analysis tool and compared to MBS, the results are very accurate, but takes longer processing time. In this

project, the collision and contact modeling will provide the results of the buffer crash of the elevator car and counterweight. (Baharudin 2016, p. 41.)

There are two key stages in contact modeling i.e., collision detection and collision response. The detection of collision's time and the location is accounted in the collision detection model whereas, the contact force between the two bodies is accounted in the collision reaction model. Since the protocol must be carried out in real-time, a correct contact algorithm must be used to decide the time and location contact takes place and computes the contact response. (Baharudin 2016, p. 42.) One can see in Figure 12 below, the general algorithm for contact detection and content response models.

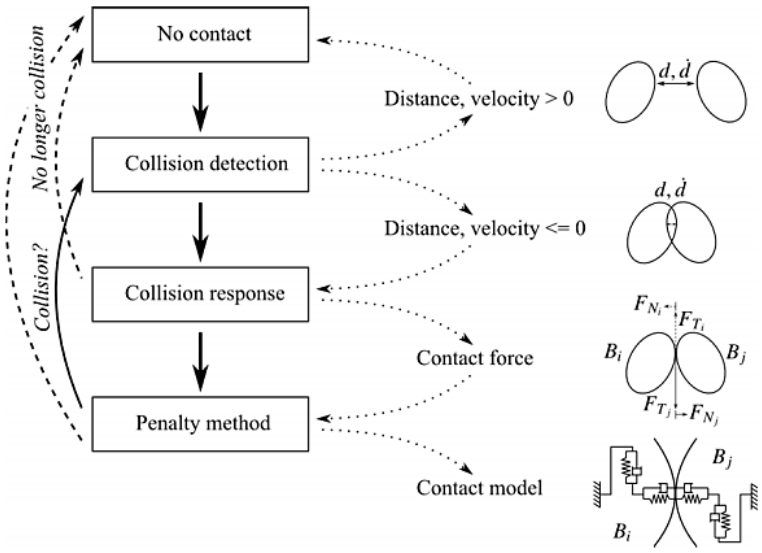


**Figure 12.** Contact detection and content response modeling algorithm (Baharudin 2016, p. 42).

For the collision detection between two geometrically different bodies, bounding volume (BV) techniques can be used. This approach functions to estimate when bodies intersect and utilize spheres or boxes that summarize the complicated geometrical entity into a simple form as shown in Figure 13. The collision detection mechanism can be greatly enhanced using these simple forms. For collision detection, a variety of bounding techniques may be utilized, like Axis-Aligned Bounding Box (AABB), Discrete-Orientation Polytope (k-DOP), and Oriented Bounding Box (OBB) (Baharudin 2016, p. 41).

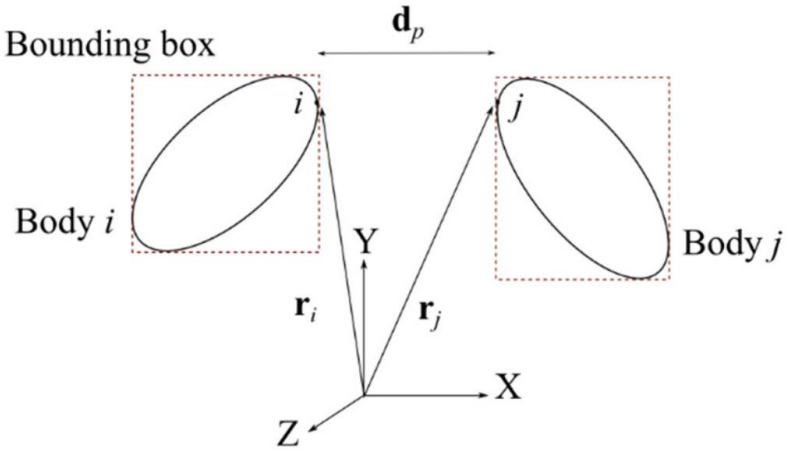


**Figure 13.** Bounding box approach for contact modeling (Baharudin 2016, p. 42).

For collision response, many techniques, for example, penalty methods, analytical methods, and impulse methods, can be used. Penalty methods are the technique in contact modeling that enables minor penetrations among bodies at the contact point and these are considered as soft contact. With the spring-damper components, the penetration interval is integrated. The contact force is measured and introduced in the equation of motion as an external force. In the analytical methods, the contacts are solved with the constraints which lead to the addition of an extra dimension to the equation of motion and contribute to the computational expense. In the impulse methods, the contact forces of colliding bodies are not computed, and instead, the velocities at the contact point are computed and introduced directly to the bodies. (Baharudin 2016, p. 42.)

The kinematic of the contact point can be represented with the help of Figure 13. Multibody formulations can be used to determine the position of the two points. The two-point are *i* and *j*, the distance between them is $\mathbf{d}_p$, is expressed below (Baharudin 2016, p. 43).

$$\mathbf{d}_p = \mathbf{r}_j - \mathbf{r}_i \tag{3}$$

The **n** normal vector of the contact is expressed below (Baharudin 2016, p. 43).

$$\mathbf{n} = \frac{\mathbf{d}_p}{\|\mathbf{d}_p\|} \tag{4}$$

The normal magnitude between two points $d_p$ is determined below (Baharudin 2016, p. 43).

$$d_p = \mathbf{n}^{\mathrm{T}}\mathbf{d}_p \tag{5}$$

By differentiating equation (5) with respect to time, the relative normal velocity $v_n$ between two points can be determined below (Baharudin 2016, p. 43).

$$v_n = \mathbf{n}^{\mathrm{T}}(\dot{\boldsymbol{r}}_j + \dot{\boldsymbol{r}}_i) \tag{6}$$

When a collision takes place, a spring-damper is applied at the contact point to identify forces of contact and $d_p$ becomes as penetration distance at the contact point. The normal contact force, $\mathbf{F}_n$ at the contact point is expressed below (Baharudin 2016, p. 43).

$$\mathbf{F}_n = -\left(Kd_p + Cv_n\right)\mathbf{n} \tag{7}$$

Where *K* is the coefficient of the stiffness and *C* is the damping factor (Baharudin 2016, p. 43).

### 2.5.6 Rope modeling methods

Wire ropes are commonly used in various engineering areas because of their excellent mechanical characteristics and comprehensive applicability. Wire rope is used extensively in the hoisting industry; thus, it is necessary to anticipate the consequences of using wire rope. Generally, wire rope experiences the combined force conditions of tension, bending, contact, friction, impaction, and vibration. It is difficult to explain the stress progression and deformation of the cabling at the operating phase because of the dynamic loading state. Thus, many researches had been conducted by constructing a mechanical model of wire for understanding stress analysis, failure mechanism, mechanical properties, and lifetime predictions. (Huang et al. 2018, p. 37.)

The principle of wire rope with respect to the behavior of deformation and strength under different loading conditions has been discussed in detail. Multiple contributions are made for non-linear static and dynamic finite element and multi-body simulations of spatially

discrete cable models. The most common approach for modeling wire rope is as a series of elastic links, connected by spherical joint (Spiegelhauer & Schlecht 2020, p. 68). Figure 14 shows the modeling method of cables. Linear finite element models use straight elastic elements to link individual particles or lumped masses and finite segment models consist of rigid elements joined by spherical joints. These models usually ignore the bending stiffness of the wire, excluding finite segment, model torsional spring at the joints. For modeling cable-pulley structures, nonlinear finite element models are common. The continuous existence of the formulations of curved elements is beneficial since the contact forces could be described as continuous functions of the cable position and velocity. It has been possible to simulate the cables without pre-tensions or under compressions with high order non-linear finite elements. In the multibody simulation, if the wire rope is experiencing large deformations, then the non-linear dynamic behavior can be studied by the absolute nodal coordinate formulation (ANCF) method. (Westin 2018, p. 3.)

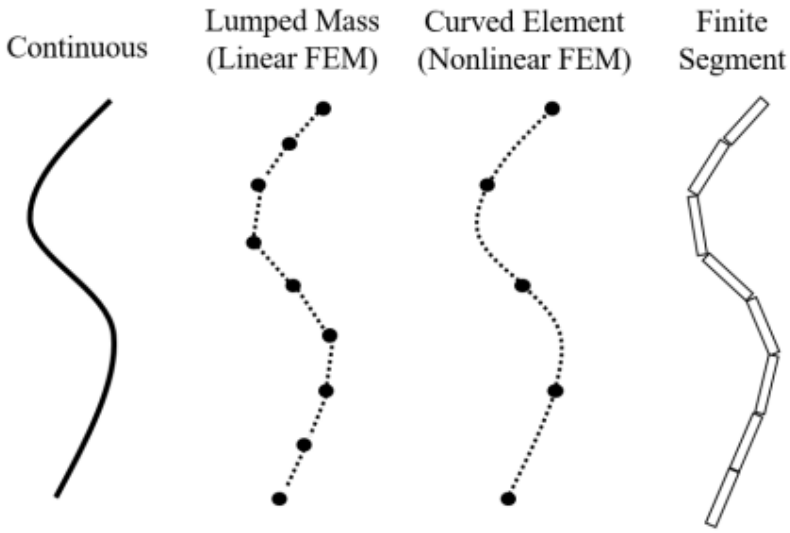


**Figure 14.** Modeling methods of cable (Westin 2018, p. 3).

The rope and pulley available in SimulationX software are based on the mechanics MBS domain. The rope is models as a rope spring which symbolizes a free rope section or strand for the analysis of longitudinal rope oscillations. Internally, it is discretized into masses and spring-damper and this element evaluates stiffness and damper forces between the connection points. The rope, pulley and drum models are grouped in to ready to use pulley and drum.

# 3 ELEVATOR ARCHITECTURE

The components of real elevator systems are introduced first, followed by virtual modeling of each elevator system component in SimulationX software. At last, the modeling of three load case situations of the elevator system is present.

## 3.1 Real elevator system

An elevator is a machine to transfer people and objects vertically, in other words, called as "vertical people's transportation system". The use of elevators is not limited to high-rise structures but also applies to low-rise structures. From manual hoisted elevators to traction sheave elevators, they have evolved with time. Elevator cars are suspended from one end of the rope and counterweights are attached to the other end of the rope. All elevators use traction-based hoisting mechanisms. They help to balance both the cars and their riders, as well as providing enough traction to prevent ropes from slipping off of their loop. Figure 15 represents the elevator and its basic components.

The Elevator motor (E-machine) is the power source in the elevator system. KONE uses motor named EcoDisc© which is a gearless permanent magnet synchronous machine developed by KONE corporation back in 1996. This is the first room-less (MRL) elevator drive built to position the motor in the guide shaft. This motor offers several advantages, including improved material and energy economy, the absence of oil, frequency control, and low friction gearless design, all of which contribute to consume just half the power needed by equivalent traditional systems. Steel rope travels through the drive pulley and the wire tension is given by the weight of the hanging car and counterweight. Suspension ropes convert the work done by the machinery into the movement of the car. When these ropes travel over the traction sheave, they are moved by friction between the ropes and sheaves. (Ford et al. 2016, p. 308.)

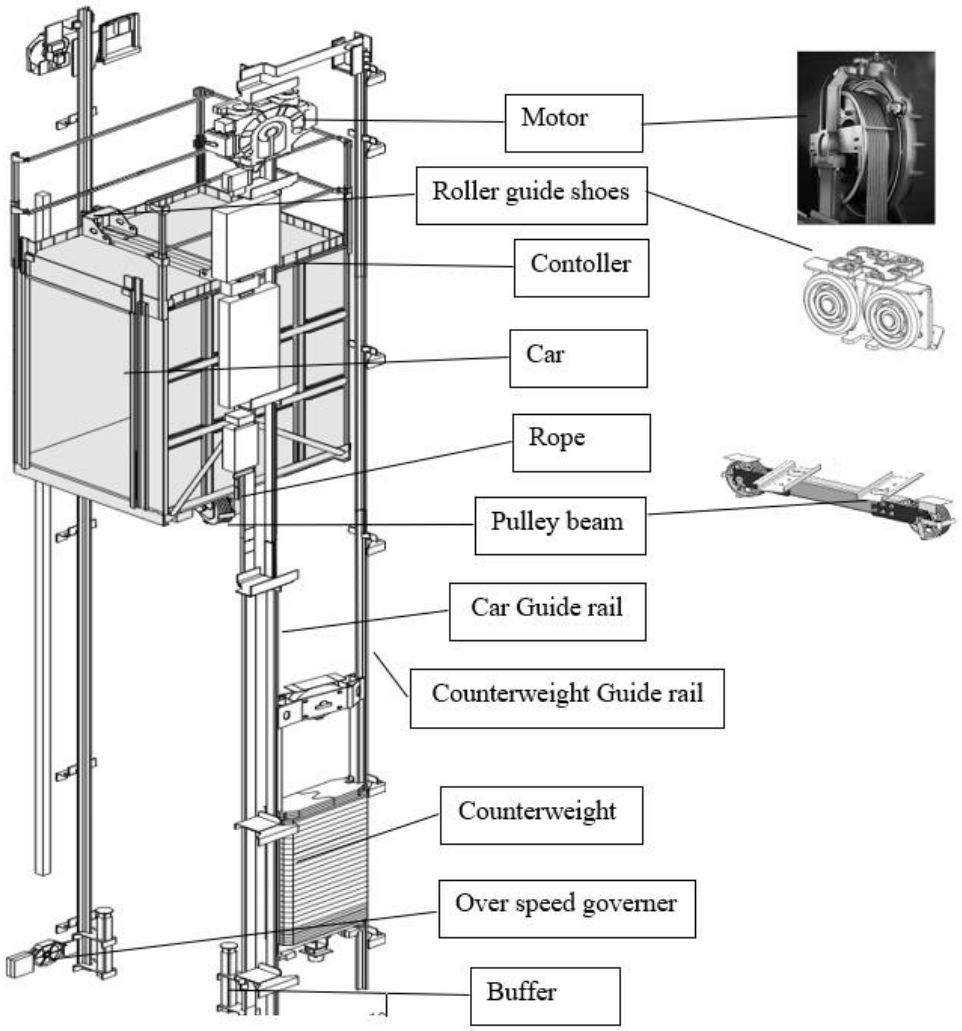


**Figure 15.** Elevator and its components.

E-machine is controlled by electric drives called a controller. Depending on the input current and voltage, the control system operates the E-machine at varying torque and speed levels. Electricity and communication between passengers such as selection of floor are supplied to and from the elevator car employing traveling cable to the controller. The controller is located at top of the shaft and the traveling cable is connected to the car's bottom while enabling unrestricted car movement.

The elevator car is that which travels vertically to transport passengers from one floor to the other. Elevator cars are either firmly connected to a sling or utilizing springs and dampers. The sling is a frame assembly that wraps around the elevator car and is supported by suspension ropes and guide rails. It serves as the car's main support framework. The Pulley

beam is part of the sling allocated at the bottom of the car, where spring or dampers are used to minimize vibrations coming from suspension ropes.

Guide shoes are used to ensure the contact of the car to the guide rail throughout the travel. There are four guide shoes, two on each side of the car. There are two types of guide shoes i.e. roller and sliding guide shoes. The use of roller or sliding guide shoes is dependent on the quality of ride requirement or speed for that elevator. Roller guide shoes have lower friction for rolling contact over sliding contact. Sliding guide shoes uses oil as a lubrication agent to lower the friction. Typical roller guides employ damping material or springs to absorb the vibration, but due to higher comfort standards, active and passive dampening mechanism are now used to decrease lateral elevator vibrations, particularly in high-rise buildings. (Kheir 2015, p. 1085.)

Car guide rails and counterweight guide rails are used to ensure a car and counterweight traveling in a straight line. They are firmly attached to the shaft walls with brackets and to each other with fishplates. To provide a smooth and comfortable ride, guide rails should always be installed accurately. (Ishii 1994, p. 44.)

The elevator system consists of two types of doors. Car doors that are attached to the elevator car and move with it. Every landing floor has a landing door. When the elevator is traveling, both doors are shut to protect people from dropping down. Passengers can securely enter and exit the elevator when it reaches the landing floor.

Overspeed governors (OSG) are speed monitors that check elevator speed and, if it exceeds the allowed limit due to anomalous acceleration, activate safety mechanisms and put the elevator to a safe stop. If the electrical Overspeed governor fails to stop the car, a mechanical safety device kicks in and is activated by clutching the guide rails tightly and bring the car to a stop.

Elevator systems also consist of buffer at the bottom of the pit under the car and under the counterweight. It provides added safety to the passenger in case the car won’t stop at the landing floor and run the pit. At buffer impact, buffer absorb and disperse the kinetic energy of the falling elevator and lessen the falling impact´s force.

3.2 Modeling of an elevator system

The modeling of the elevator at the system level has been done in SimulationX software. The development in the model of the elevator has been carried out in sense to capture position, velocity, vibration, motor torque, guide shoes forces, along with many other phenomena of different components in the spatial direction. The most significant components contributing to the dynamic and electric behavior of the elevator are modeled separately as components. These elevator components models are already available in KONE's library. A simplified representation elevator system and modeled components are shown in Figure 16. The SimulationX model for the elevator system is presented in Figure 17.

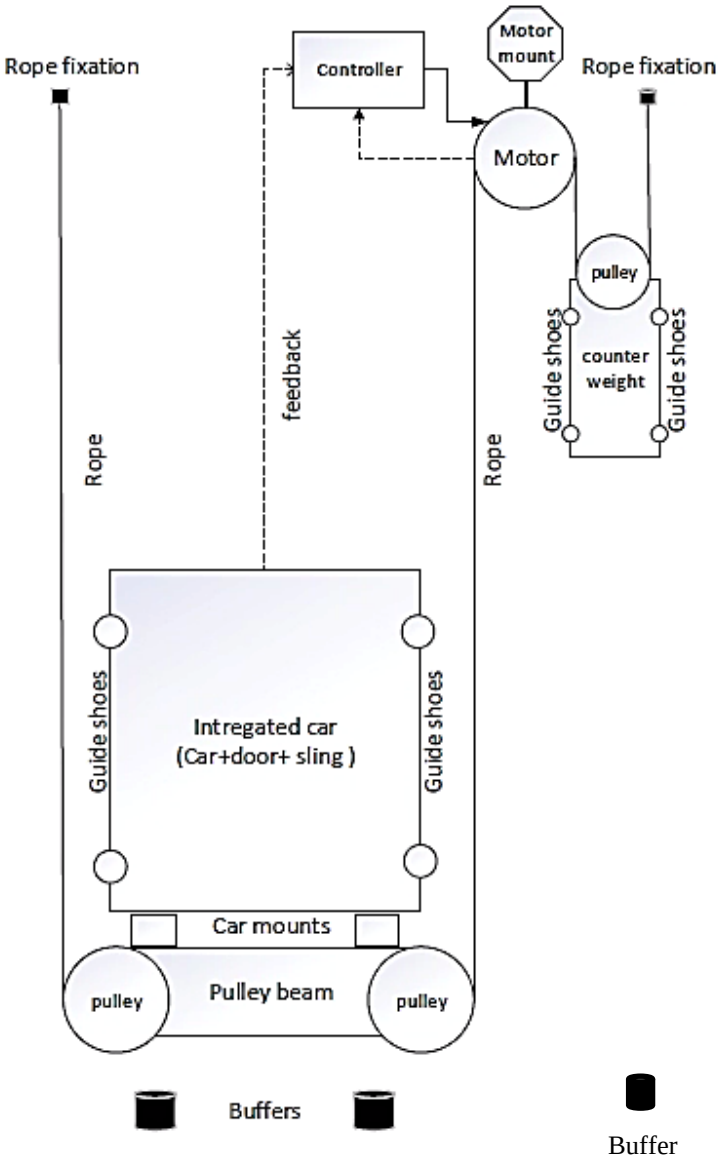


**Figure 16.** Simplified elevator system.

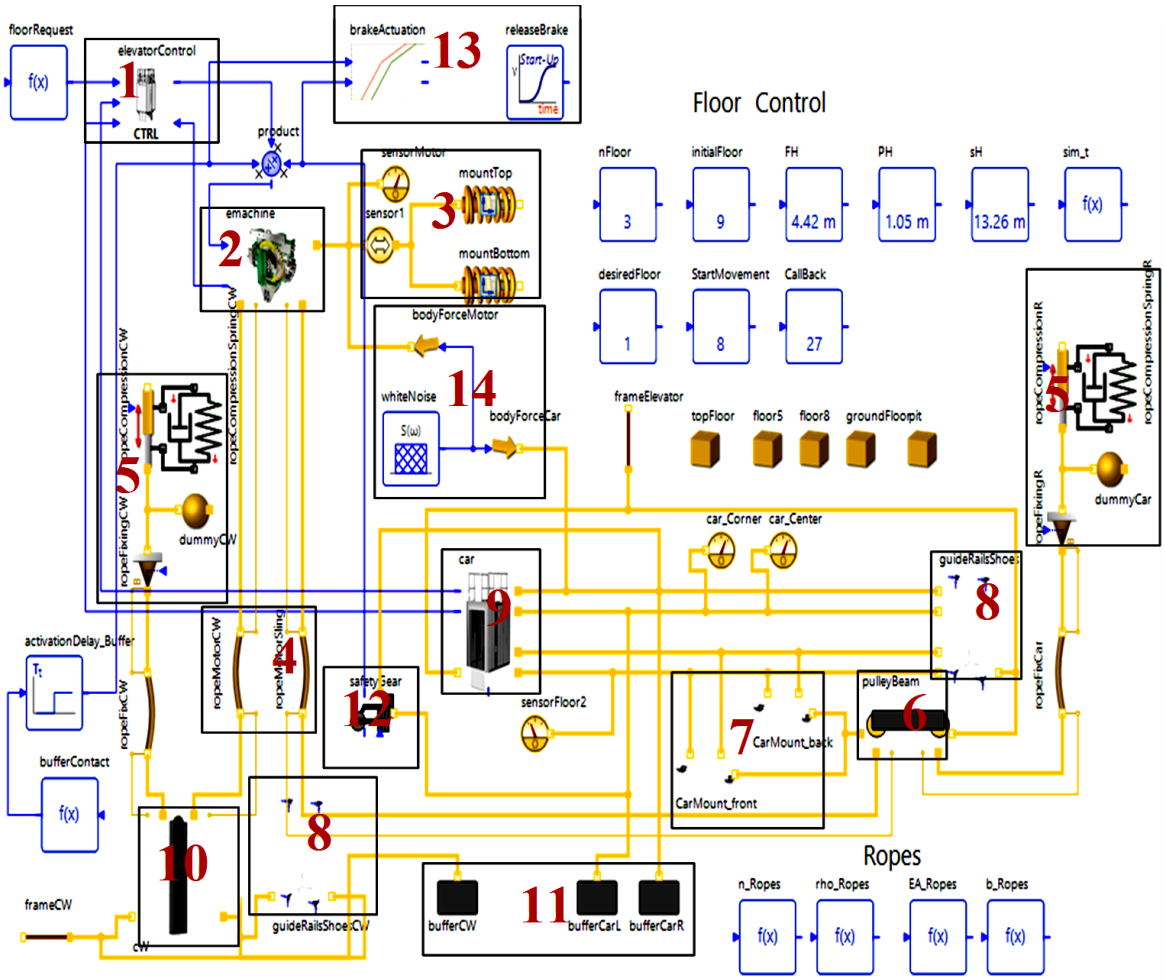


**Figure 17.** Elevator system model in SimulationX (1) controller, (2) motor, (3) motor mount, (4) rope, (5) rope fixation, (6) pulley beam, (7) car mount (damper pad), (8) guide shoes, (9) car, (10) counter weight, (11) buffer, (12) overspeed governor, (13) brake actuation, (14) white noise.

Controller (1, Figure 17) modeled includes motion controller, PI feedback, feedforward, and normalization based on method discussed in section 2.3.2. Motion controller has been imported in the mode with FMU as discussed in section 2.4. The motion controller's main inputs are floor request, car vertical position, and velocity of the car. Based on these inputs, the motion controller calculates the desired car velocity trajectory. The desired velocity trajectory is fed into the PI controllers where it continuously calculates the difference between required vertical velocity set by the motion controller and measured vertical velocity which comes from the measured rotational speed of the electric motor. PI corrects this difference with respect to the proportional and integral values provided. This corrected

required vertical velocity is added with the feedforward controller where it calculates the static load based on mass different results and the dynamic load based on the system mass results to give static torque and dynamic torque. In the normalization part, the scale output of the required torque is calculated.

The motor (2, Figure 17) contains electrical as well as mechanical components as discussed in section 2.3.1. The mechanical component such as traction sheave, the mass of the motor, degree of freedom limitation was modeled with the MBS methodology and the electrical part's contains axial flow synchronous machine, and modeling is done with the mathematical formula for the voltage equations of PMSM. Motor mount (3, Figure 17) is modeled as the 3-dimensional (3D) spring with stiffness and damper properties. The stiffnesses used for motor mount are calculated from the Finite elements method (FEM) analysis with 12 kN load on the shaft. Translational and rotational stiffnesses are used to mount the motor at top and bottom positions. The bottom mount represents the motor bed plate where the motor is assembled with a damper pad. The bed plate is vibrating with eigenfrequencies of 17,9 Hz, 20,25 Hz, 24,63 Hz 26,31 Hz, 28,71 Hz and 53,21 Hz. The damping value has been obtained from a similar component.

The ropes (4, Figure 17) in the system are modeled as rope elements as mentioned in section 2.5.6, and their primary inputs as linear density, axial stiffness and damper, and number to ropes. The length of the rope on either side of the car and counterweight are model as the position of the car and counterweight depended. Rope fixation (5, Figure 17) is modeled with a prismatic joint allowing a vertical degree of freedom and stiffness and damping value to represent the connecting point. The stiffnesses used in rope fixation are calculated from the Finite elements method (FEM) analysis and the damping value has been obtained from a similar component.

The pulley beam (6, Figure 17) is modeled with MBS-bodies and pullies with pulley element with its point masses, the center of gravities and inertia of tensors, and positioned to represent the skewed pully beam. The car mount (7, Figure 17) is modeled as a linear 3D spring to represent elastic behavior and positioned under the car and pulley beam. With the correct stiffness and damping ratio of these springs, a true damper can be represented in the model.

The stiffnesses utilized for car count are computed using the FEM, and the damping value is acquired from a similar component.

Guide shoes (8, Figure 17) are modeled with a 1-dimensional spring and damper to represent the contact point of guide shoes and guide rials in x-axis and y-axis. The same model of guide shoes is used to represent roller and sliding guide shoes. The stiffness used for roller guide shoes is obtained from the force-displacement curves of FE analysis for 1 mm displacement to the compression force. For roller guide shoes, the stiffness value is the same in both x-axis and y-axis direction however for the sliding guide shoe, the stiffness value is different in both x-axis and y-axis direction and has a higher friction coefficient value. The stiffnesses used for sliding guide shoes are as the measure in the lab for the load-deflection test, and the result is found to be nonlinear. The current modeling structure in SimulationX supports only linear spring constants, and thus a linear estimate is given for x-axis and y-axis stiffness values. The damping value is acquired from a comparable component.

Guide rails are modeled as a function of the guide rails misalignments in form of curves through with the excitation for the guide rail shoes are provided. The measurement of the guide rail misalignment is a complicated procedure due to the compact arrangement of the elevator system. Therefore, the modeling strategy is to scale the values of measured misalignments, so they cover the entire available database of measured guide rails misalignments with automatic adjustment tool (AAT).

Initially, the elevator car (9, Figure 17) has been modeled as a rigid body with MBS-bodies which included car door and sling, with point masses, centers of gravity, and inertia of tensors with respect to their position. The door and car were rigidly connected and at the end, the entire car component could have 6 degrees of freedom. With this car model, the vertical vibration accuracy was compromised and was not accurate enough for capturing the local modes of the car. Therefore, a flexible car was introduced and discussed in the next subsection. Counterweight (10, Figure 17) is modeled similarly to a rigid car and with a pulley element.

Buffer (11, Figure 17) is modeled by simplifying the real components. The modeling is based on a polynomial buffer force description where the seven degrees of the polynomial is used.

Visualization of the buffer is a rubber pad. Position of buffer contact and buffer characteristic has been applied as per specification and as output, deflection, combine buffer force, spring force, and damping force can be plotted. Over speed governor (12, Figure 17) is modeled based on detecting car speed and provide elevator safety brakes when the speed of the car is over the limit. Brake actuation (13, Figure 17) is a model based on safety gear signal. Delays and brake force characteristics are taken into account. If safety gear is activated or if the buffer gets in contact with the car, time count and time-dependent brake behavior is activated. Time can be set for the break to be released and the elevator motion to begin in the break release element.

The motor is modeled as an ideal motor as mentioned in section 2.3.1, which means that not all the excitations from torque ripples, bearings, manufacturing tolerances are represented. To overcome this simplification, white noise (14, Figure 17) is used as an initial excitation of the motor. This will provide initial excitation to the motor. Idealities in modeling car, hoisting components (guide rails, ropes, guide shoes), air pressure in the shaft, etc. reduce scientifically the excitations transmitted to the car component. For this reason, the car is excited with white noise, in order to see if during the ride any resonance may be built on. The white noise signal is applied as a body force element to the motor mass and car mass in 3 spatial directions.

The geometrical information of the entire elevator has been collected from the Computer-Aided Design (CAD) files and elevator installation layout. The masses, center of gravity and inertia tensors are taken from Creo model of respective components.

### 3.2.1 Flexible car modeling

In flexible car modeling, the car's roof and floor are modeled separately, and the entire car including the sling door and in-car load is divided into two components as shown in Figure 18. The car is then joined via joints and springs providing flexibility to the car. The springs connecting the components can be tuned to the FE computed eigenfrequencies of the roof and floor. In this way, the local mode of the car can be implemented in the model.

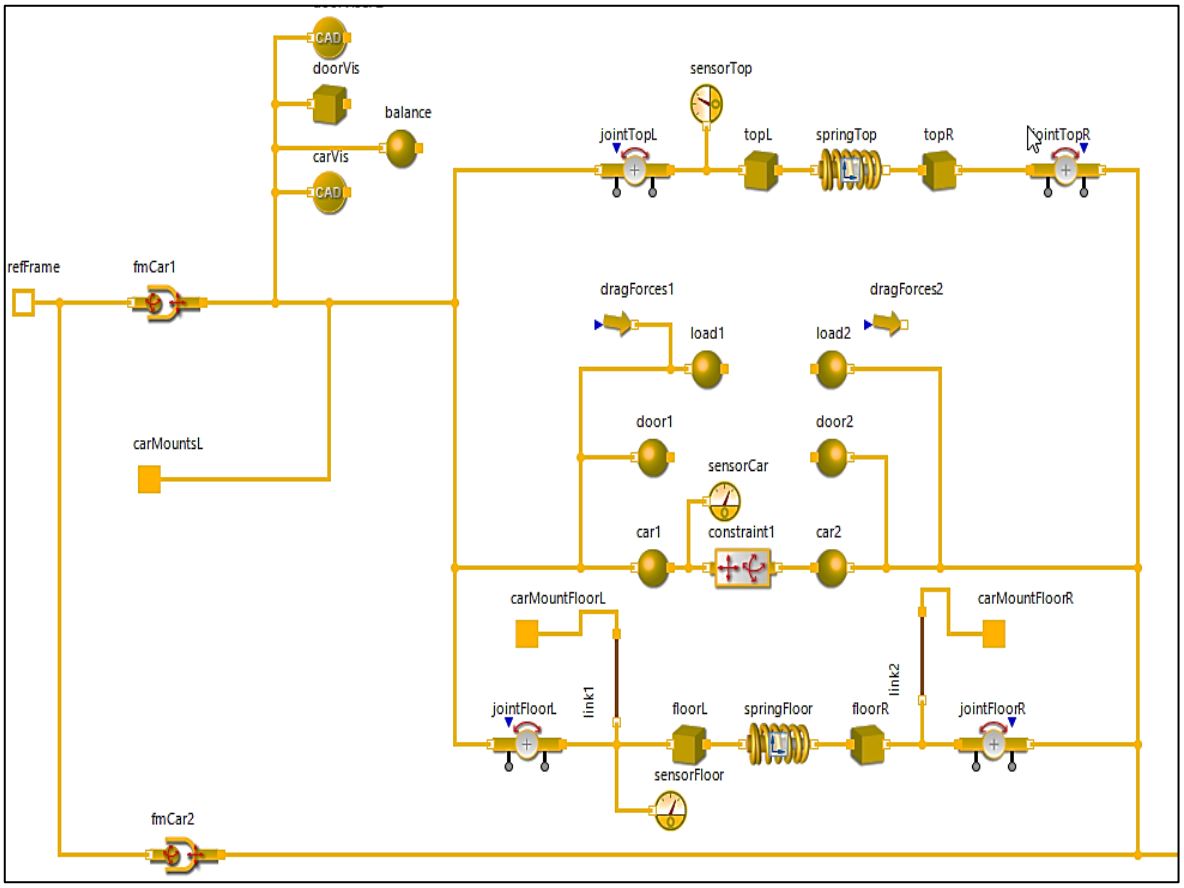


**Figure 18.** Flexible car model.

A separate study for frequency response analysis was done to compute in-car eigenfrequencies excited during car movements and induce in-car vibrations. FE method has been used for this study utilizing Abaqus software. Eigenfrequency extraction with Lanczos solver for frequency range 0,3 – 150 Hz has been used. The geometrical specification, material data and connection between subsystem is made as per elevator car. During that frequency analysis, the elevator car was attached to the ground through the guide shoes and pulley beam mounting stiffness and analysis was done in static condition. The loading force of 10 N has been applied in the vertical direction, on the bottom of the sling. Significant vertical response of the car floor and roof for vertical excitation with 10 N has been expected as a result. No damping was used during the analysis.

In the simulation model, frequency obtained from frequency response analysis is given to the floor and roof of the car to capture local modes and potential resonances, through fine-tuning the stiffness value of spring joining two parts of the floor and roof of the flexible car.

The correct stiffness value of spring could be obtained by multiple iterations of the stiffness value of spring joining two parts of the floor in the SimulationX software. Figure 19 depicts the influencing stiffness values for eigenfrequency tuning. The translational and rotational stiffness is necessary to be estimated.

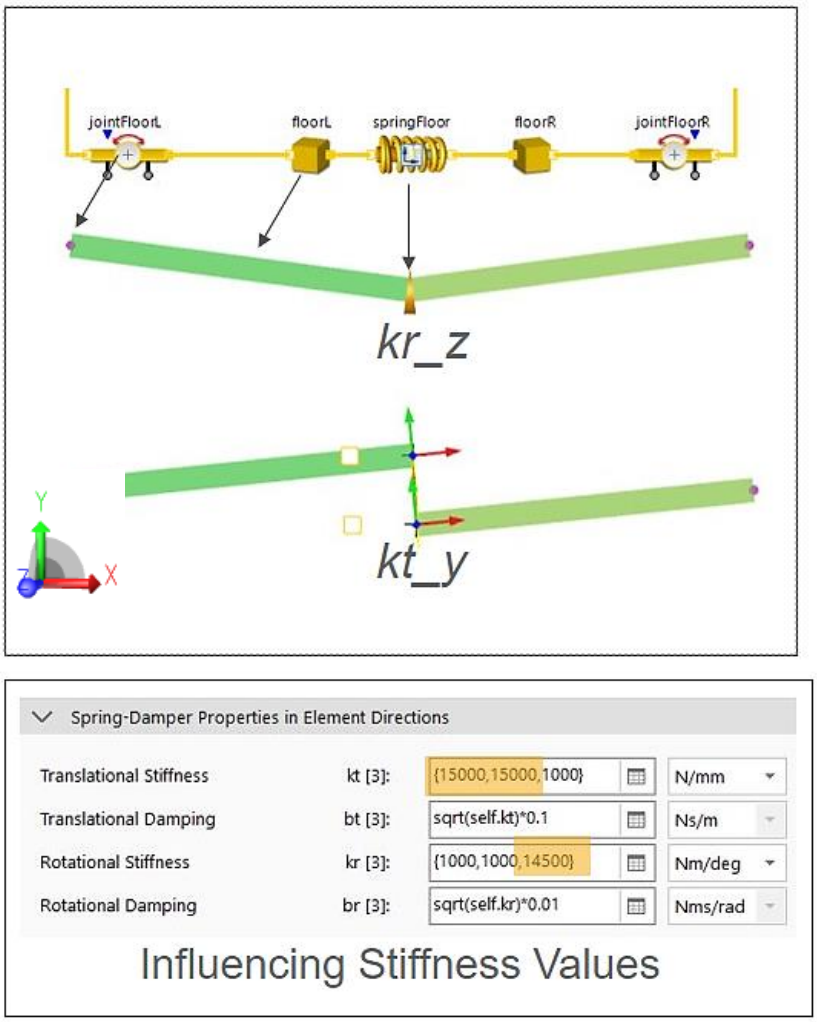


**Figure 19.** Influencing stiffness values

Bending mode comes mainly from rotational stiffness around the z-axis (*kr_z*). Due to the kinematic assembly of two rotational joints, floorL and floorR can move independently in translational y-direction shown in Figure 19. Movement is dependent on *kt_y* (Translational y-direction) and leads to outer phase mode (no bending mode). The frequency of this must be shifted outside the interesting frequency range (<150 Hz). Translational x-direction (*kt_x*) is not constrained during flexible car model as it is necessary for squeezing effect of car, thus must be restricted by *kt_x* and must be set appropriately.

*kt_x* can have too high an influence on lateral vibrations which is not wanted. If rigid behaviour is wanted, one could set value infinite high which leads to extremely high eigenfrequency and however, that leads to decrease of performance (simulation time) therefore appropriate value *kt_x is* necessary which should shift eigenfrequency (longitudinal vibration mode) outside interesting frequency range and can be calculated by formula mentioned below.

$$kt_x \geq \frac{m_{Total}\pi^2 f^2}{2} \tag{8}$$

Where $m_{Total}$ is the total mass of the car and $f$ is the lower limit for the eigenfrequency e.g. $f$ = 200 Hz.

This calculated value should be input in the simulation model for floor and roof and its influences much be checked and if eigenfrequency is too low then the stiffness must be adjusted.

The bending mode of the roof can be obtained analytically for estimation *kr_z* (rotational stiffness around z-axis) however for floor stiffness simplified model of car damper pad and pull beam should be used. This is because, in this platform models, damper pads have an influence on floor bending mode. The roof and floor estimation formula are mentioned below.

- Estimation roof stiffness

$$kr_z = 2\pi^2 \cdot f^2 \cdot J^* \tag{9}$$

- estimation floor stiffness

$$kr_z \leq 2\pi^2 \cdot f^2 \cdot J^* \tag{10}$$

Where $J^* = J_{F,panel} + \frac{\mathrm{m_{Floor}}}{32} \cdot BB^2$ or $J^* = J_{R,panel} + \frac{\mathrm{m_{Roof}}}{32} \cdot BB^2$

Where $k_{rz}$ is rotational stiffness around z-axis, $J_{F,panel}$ and $J_{R,panel}$ is inertia for one panel floor and roof, the value taken from SimulationX (in Centre of mass), $\mathrm{m_{Floor}}$ is mass value for the entire floor, BB is Internal width of the car

From this approach, the upper limit will be obtained therefore choose a lower value for cars and iterate to matching eigenfrequency via eigenfrequency Analysis in SimulationX.

The same value obtained for the *Kt_x* can place here but this led to too high stiffness and may lead to performance issues. Therefore, its own value should be determined as mentioned below.

$$k_y \geq \frac{4}{BB^2} \cdot (2\pi^2 f^2 \cdot J^* - k_{rz}) \tag{11}$$

$$\text{Where } J^* = \frac{J_{F,panel}}{2} + \frac{\mathrm{m_{Floor}}}{32} \cdot BB^2 \text{ or } J^* = \frac{J_{R,panel}}{2} + \frac{\mathrm{m_{Roof}}}{32} \cdot BB^2$$

By following the above-mentioned procedure, the stiffness value can be calculated and tuned to any wanted eigenfrequency of the floor. However, during the tuning of the eigenfrequency of the floor at 81 Hz, its rotational stiffness value around x-direction $\mathrm{kr_z}$ is calculated to be 100 Nm/deg at the frequency of 83,9 Hz. This value for rotational stiffness value is significantly small and this also limits the tuning of floor eigenfrequency lower than 84 Hz. While looking at the potential energy distribution at this frequency, it is found that the damper pads have a high influence and store higher potential energy as shown in Figure 20. In reality, the damper pads have an influence on floor eigenfrequency but should not limit the eigenfrequency, therefore this issue must be overcome.

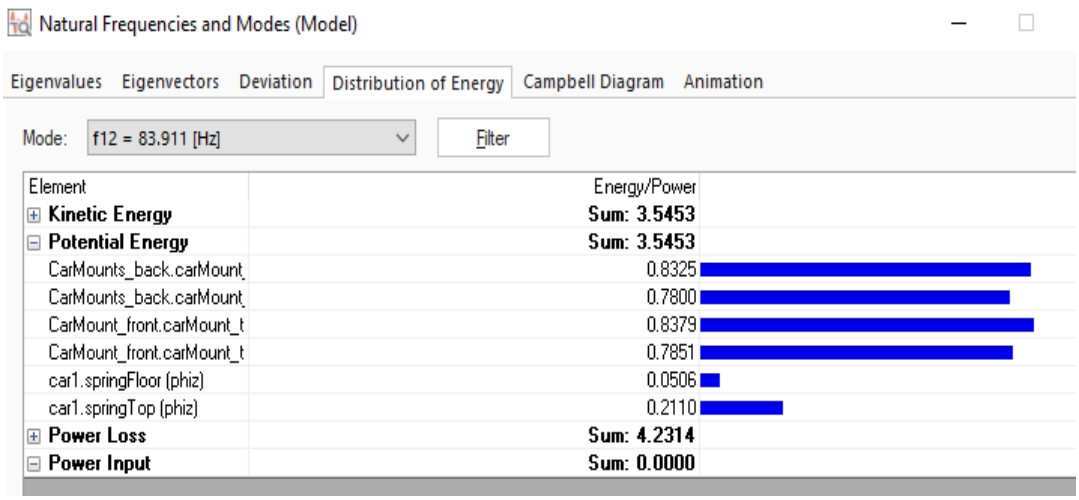


**Figure 20.** Potential energy distribution at 84 Hz floor frequency.

There are two ways to achieve the higher rotation stiffness value and be able to tune even lower frequency than 81 Hz of the floor. By increasing the mass of the floor. This means including the overall structure of the floor (i.e. floor and sling beam) till now only floor masses are used. However, this is a case-specific solution and will be applied for this thesis work to get going. The rotational stiffness value, in this case, is 1300 Nm/deg which still is the small value and the involvement of damper pads are still high. The other option is by changing the connection of damper pad from the floor of the car to the rigid frame of the car. This involves a big model change hence further investigation is required to see its effect on the other components and their results. For this reason, this option is not used during this thesis work. The elevator components along with inputs are needed for the SimulationX elevator model as presented in Table 2.

*Table 2: Elevator components and their inputs required for modeling in SimulationX*

| **COMPONENTS** | **INPUTS** |
|---|---|
| Car | Dimensions, load, mass, center of gravity, the inertia of tensor, type of car isolations and positions, eigenfrequency of floor and roof, etc. |
| Sling | Mass, the center of gravity, inertia of tensor, positions of pulley beam, guide shoes, buffer counterpart, traveling cable, compensation chain, interface car-sling (stiffness and damper), etc. |
| Door | Mass, type, the position of the center of mass in relation to the car |
| Guide shoes | Type, stiffness, damper, end stops clearance, friction |
| Counterweight | Type, mass, the center of gravity, inertia of tensor, pulley's position, mass, inertia |
| Ropes | linear mass, numbers of ropes, stiffness, damper, fixation spring |
| Over-speed governor | Motor shut down speed, activated speed, delays from detection to actuation |
| Buffers | Type, stiffness, damper, non-linearity fitting polynomials |
| Guide rails | Misalignments for car, scaled misalignments for simulating different installation accuracy |

*Table 2 continues: Elevator components and their inputs required for modeling in SimulationX*

| **COMPONENTS** | **INPUTS** |
|---|---|
| Machinery | Electrical:- Nominal motor torque, number of pole pairs, number of slots, stator resistance, synchronous inductance, etc.<br>Mechanical:- the mass of stationary parts and rotating parts, rotor inertia, rotor diameter, mounting position, stiffness and damper, etc.<br>Brakes:- Brake torques value, actuator delay brake 1, Actuator delay brake 2 |
| Controller | Type, car position Controller FMU |
| Layout | Positions of machinery, head room, pit, counterweight, guide rails, buffers, etc. |

## 3.3 Load case modeling

The procedure for modeling sag and bounce, car buffer crash and counterweight buffer crash situation in SimulationX software is discussed in this chapter.

### 3.3.1 Sag and bounce

When an elevator is loaded, it tends to slide down from its starting position, and when it is unloaded, it returns to its initial position, which is known as sag, and bouncing occurs when the car returns to its initial position as shown in Figure 21. The sag and bouncing have a negative impact on the ride comfort of an elevator and most customer complaints relate to the bouncing of the car. Car bounce amplifies especially during the unloading of many passengers at the same time. Some of the most important parameters contributing to these phenomena are rope properties (number or rope, length of rope, elasticity of rope, damper of rope), amount of load, excitation time i.e. loading time and loading off time.

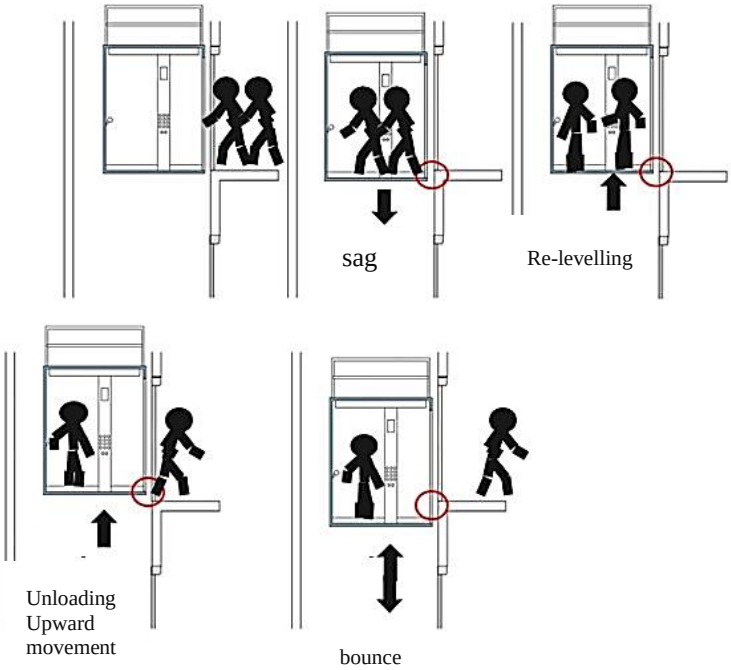


**Figure 21.** Sag and bouncing of the elevator.

The modeling of this real-life load case can be achieved with the SimulationX model of the elevator. This is a static case situation; therefore, the car of the elevator is set to stay at the requested floor throughout the simulation period and load (passenger) specification is only varying. The loading) and unloading of the car can be model from the formulation listed below, as an extra element and its result can be placed as load in the car.

$$m(\mu) = \begin{cases} \dfrac{1}{2} & (3\mu - \mu^3, \mu \leq 1 \\ m_c, otherwise \end{cases} \tag{12}$$

Where $\mu$ is scaling with force is calculated by $\mu = t/t_{sat}$ where $t_{sat}$ is saturation time and $m_c$ mass of passenger loading.

Hermite interpolation can be used for simulating the loading off of passengers from the car is mentioned below.

$$F(\xi) = H_1(\xi)m_1 + H_2(\xi)m_2 \tag{13}$$

Where $m_1$ is mass at time instances at $t_1$, $m_2$ mass at time instances at $t_2$, $\xi$ is scalable variable calculated from $t \in [t1\ t2\ ]$ and $H_1$, $H_2$ Hermite polynomials.

$$H_1(\xi) = \frac{1}{4}(2 - 3\xi + \xi^3) \tag{14}$$

$$H_1(\xi) = \frac{1}{4}(2 + 3\xi - \xi^3) \tag{15}$$

### 3.3.2 Car buffer run

The concept of buffer run is coming for the real-life situation when the elevator car cannot find the ground floor and collide with the buffer instead which is located in the pit. This collision can happen with any speed in between the given minimum to maximum allowed speed of that elevator model. To represent this real-life situation in the SimulationX model, the position of the first floor or any other floor requested floor needs to be positioned well below the buffer location. This means that the requested floor could be at -5m. If the requested floor is set to zero, the car will crash with the buffer, but at a slower speed than the permitted speed. This is because the car will be already in retardation when it approaches to ground.

### 3.3.3 Counterweight buffer run

Counterweight buffers (attached to counterweight bottoms) crash to the ground when the elevator car is unable to locate the top floor, resulting in a buffer run. The model strategy for counterweight buffer is like the car buffer run modeling where the elevator is requested to go above the top floor.

# 4 RESULTS AND RESULTS ANALYSES

In this chapter, the virtual elevator system model is validated and analyzed. Sensitivity analysis of several configurations has been made and the result and analysis of three load cases have been discussed.

## 4.1 Models validation and comparison

In this chapter, two elevator models from the same platform but with different specifications are modeled and simulated, and these elevators are with maximum load capacity of 480 kg and 630 kg. Both elevator models are simulated with roller guide shoes and sliding guide shoes. Short representations of these elevators with their type of guide shoes are listed in Table 3. The calculation type is transient, and the simulation run control parameter is shown in Figure 22 below.

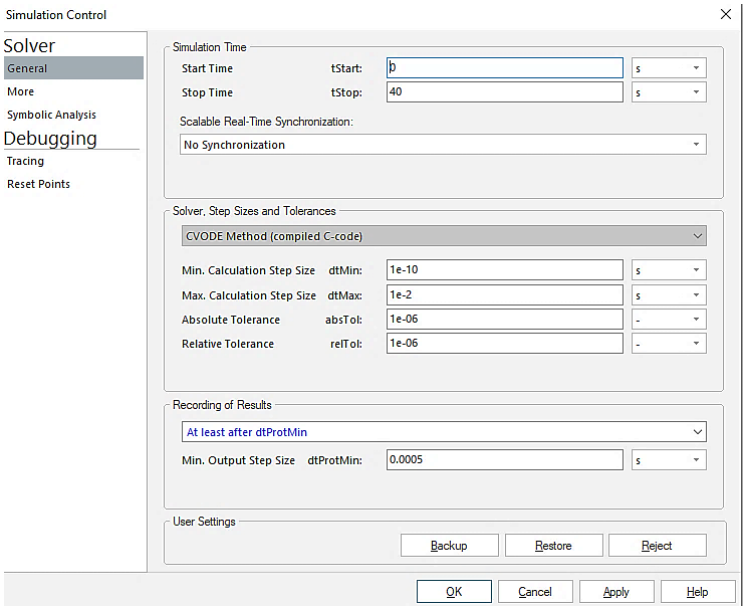


**Figure 22.** Simulation type and simulation control parameter.

*Table 3: Elevators specification*

| Elevator Name | Elevator and type of guide shoes |
|---|---|
| Elevator 1 | rated load 630 kg with roller guide shoes |
| Elevator 2 | rated load 630 kg with sliding guide shoes |
| Elevator 3 | rated load 480 kg with roller guide shoes |
| Elevator 4 | rated load 480 kg with sliding guide shoes |

The measured data is obtained laboratory. The measurement was taken from Elevator 1 and Elevator 2 for the position, velocity and vibration in all 3 directions. During the measurement, 3-dimensional direct current (DC) accelerometer was used. The placement of the sensor was in the center of the floor therefore, the validation data of the simulation model is also taken from the center of the floor. The measured and simulated data are filtered with a lowpass filter of 12 Hz in the lateral direction and 80 Hz in the vertical direction as any vibration higher than these frequencies will not be felt by humans. The simulated model has adopted initial position, velocity, acceleration, maximum jerk, final jerk distance as per the measurement data. Elevator 1 and Elevator 2 are validated with respective measured data.

The Galileo (gal) unit is used to describe the amplitude of the vibrations in this project where 1 gal is 9.8 mm/s$^2$. Vibration amplitude has been used to describe vibration intensity. Vibration is quantified using the peak-to-peak value since the maximum excursion point is essential for ride comfort. A single zero-crossing separates two peaks with opposite sign magnitudes is described as peak to peak value shown in Figure 23.

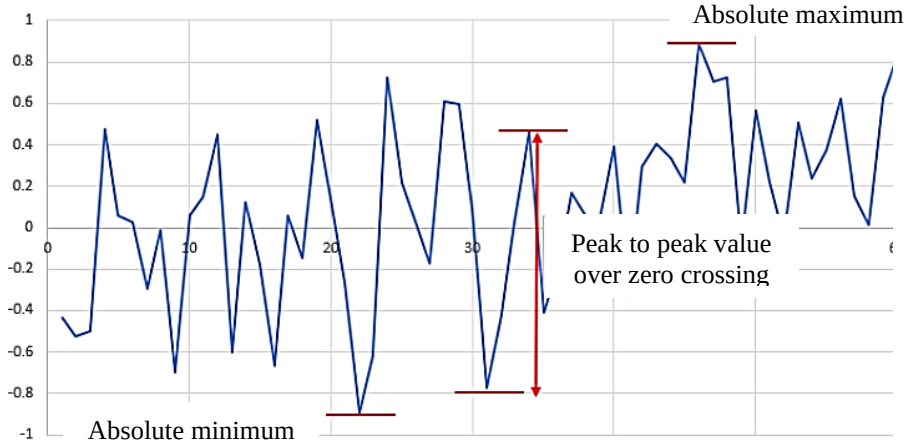


**Figure 23.** Characteristics of peak to peak value.

For the vibration validation, only the information of data at the nominal speed is taken into account. The target is to identify the component's contribution to in-car vibration. For this reason, a constant frequency of excitation is needed, which can be obtained only when the speed is constant. The analysis would be more complicated if acceleration and deceleration are included, although but they are equally important. The nominal speed is achieved in between 12 to 25 seconds of run time. The X-axis is in back to front direction of the elevator car. The Y-axis is in distance between guide direction of the elevator. The Z-axis is the vertical axis of the elevator as can be seen in Figure 24.

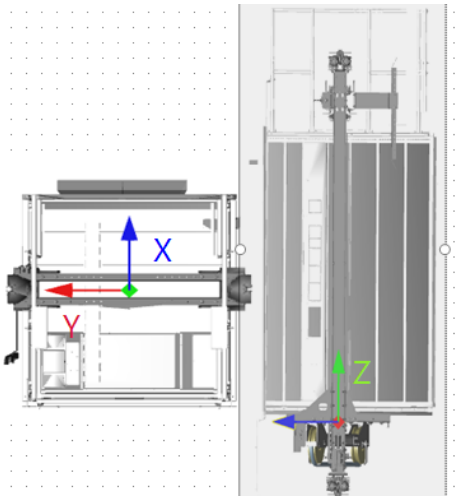


**Figure 24**. Measurement coordinate system.

### 4.1.1 Time domain validation

The position and velocity profile of Elevator 1 and Elevator 2 with sliding guide shoes are simulated and compared with the measured results. The graph of simulated and measured data fits well for both models as shown in Figure 25. The simulation is down run from the top floor to the ground floor at nominal setting and in-car load 80 kg, representing one person's weight.

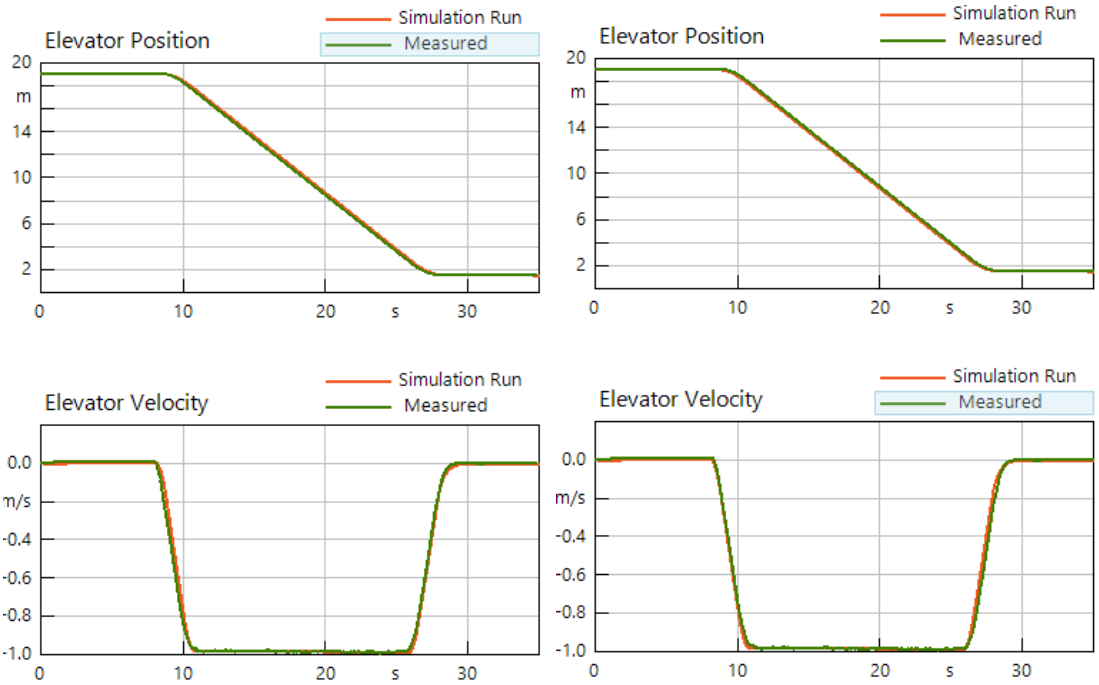


**Figure 25.** Position and velocity curve simulation vs measured for Elevator 1 (left) and Elevator 2 (right).

Graph of simulated results compared with the measured result of Elevator 1 is shown in Figure 26. The vibration value of the graph has not been shown in this thesis work because of confidential reasons. In-car vibration of this elevator has shown that X-axis simulated graph's peak to peak value to be 2 times higher than the measured value. This large deviation is caused because of the guide rail misalignments data used in the simulation which is for the different elevator. The misalignment of this elevator is not available. The Y-axis peak-peak value of simulated data is 1,8 times higher than the measured data. In Z-axis, simulated peak to peak values is in good correlation in peak to peak value of the measured data.

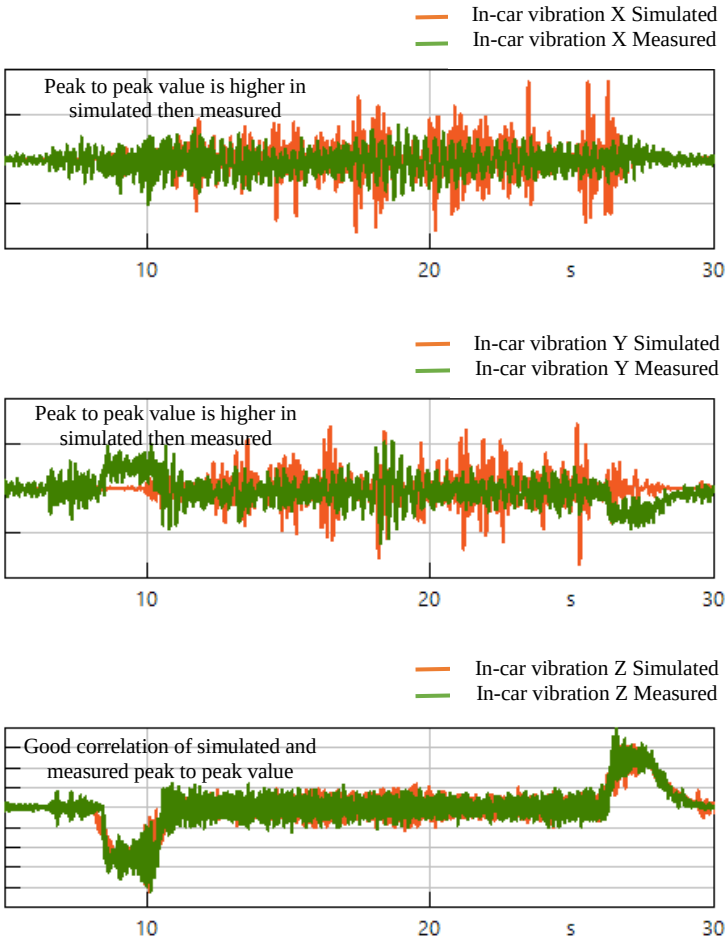


**Figure 26.** In-car vibration curve simulation compared to measure data of Elevator 1.

To make the correct representation of guide rail misalignment, the scaling factor can be used as discussed in section 3.2 of this thesis. Guiderail misalignment has been measured only for the different laboratory elevator then modeled. Guide rail misalignment of this elevator has peak to peak maximum value of 1,97 mm in y-axis which is close to 2 mm and falls under very poor category based on internal requirement. Similarly, in x-axis direction guide rail

misalignment has peak to peak maximum value of 1.46 mm which is close to 1.5 mm and falls under the poor category based on the internal requirement. The assumption is, that modeled elevator has more accurately installed guide rails. Therefore, to represent more accurate installed guide rails, an average of right and left guide rail misalignments were considered and scaled down with a factor of 0.4 (in average right and left guide rail) which resulted in peak to peak value of 0.7 mm in y-axis direction and x-axis direction, the reducing factor used was 0.7 (in average for right and left guide rail) which resulted in peak to peak value of 0.75mm. After scaling down of misalignments the elevator model has shown a good graph fit with the measured graph as can be seen in Figure 27.

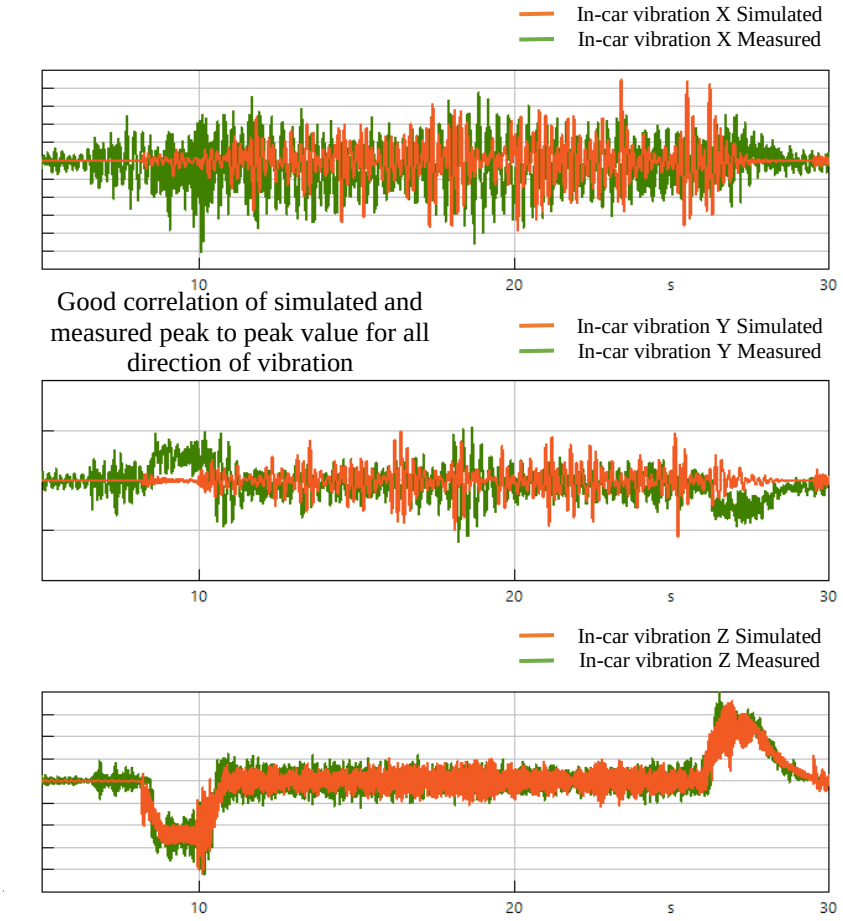


**Figure 27.** In-car vibration curve simulation compared to measure data of Elevator 1 after correct representation of guide rial misalignment.

Elevator 2 is validated with measured data as seen in Figure 28. The data measured is for the elevator with sliding shoes but with a different experimental motor than the one used in the simulation model. Here also guide rail misalignment scale factor of 0.4 in y-axis direction and 0.7 BFT direction of measure elevator has been used. The sliding guide shoes is modeled

by changing stiffness in y-axis and x-axis direction and friction coefficient of 0.2 as discussed in section 3.2.1. High correlation in all three directions vibration can be seen.

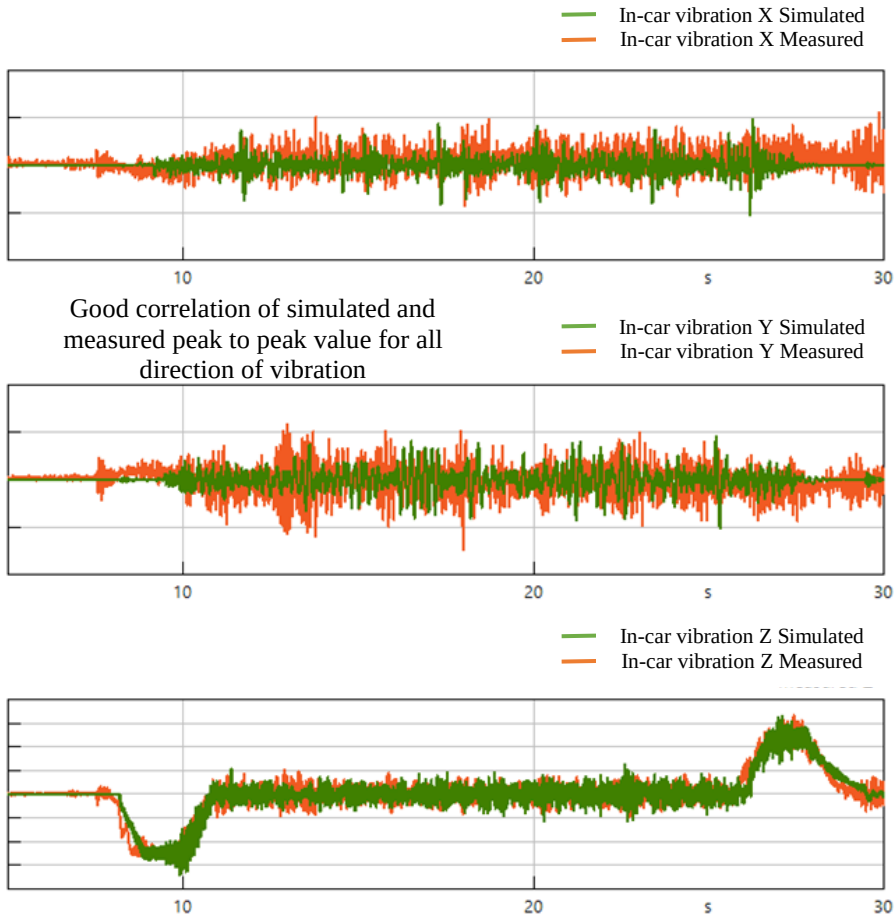


**Figure 28.** Elevator 2 simulated vibration vs measured vibration.

The modeling of the elevator rated load 480 Kg model has been done with its specifications. The guide rail misalignment has been used same as of model elevator rated load 630 Kg. Due to the unavailability of the measured data for this elevator, validation was not possible. However, this model was assumed to be model accurately as elevator rated load 630 Kg and elevator rated load 480 Kg comes from the same elevator platform and has only differences in the geometrical, mass and inertia specification. The elevator rated load 630 Kg and elevator rated load 480 Kg were both modeled using the same technique with the same stiffness and damper for the majority of the components.

### 4.1.2 Frequency domain validation

The peak to peak validation has shown good results in the last chapter, however, it is important to validate the model on the frequency domain. The frequency domain validation will provide the model to gain more reliability. From frequency domain validation, it is possible to find out at what frequencies the system is vibrating and help to find what is the root cause of these frequencies. The Frequency domain validation of Elevator 1 and Elevator 2 has been done. Figure 29 shows the Fast Fourier transform (FFT) graphs of the measured and simulated signal where the roller guide shoes have been used. The vertical vibration of the elevator is only discussed in the frequency domain as vertical vibrations provide information on the status of several components, such as guide shoe wear, incorrect motor bedplate design, and improper guide rails installation, and so on along with the opportunity to develop ride comfort.

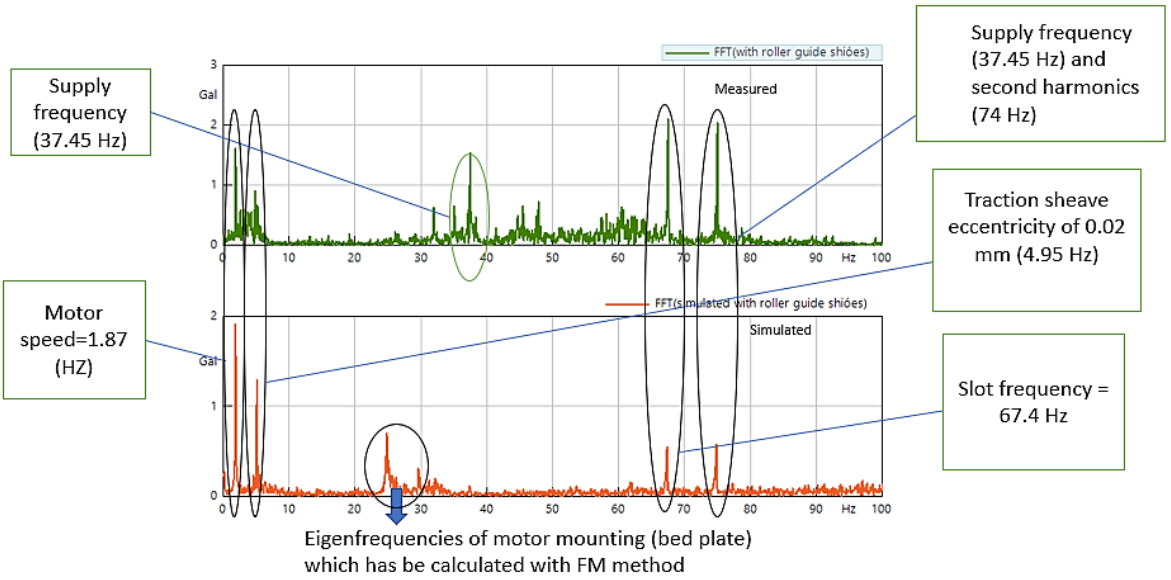


**Figure 29.** FFT of Elevator 1 of measured and simulated data.

In the above figure, the FFT graphs have shown similar resonances taking place at similar frequencies on both measures and simulated signals. The supply frequencies at 37.45 Hz and its second harmonics at 74 Hz, the motor speed at 1.87 Hz, traction sheave eccentricity at 4.45 Hz, slot frequency at 67.4 Hz are seen in both measured signal and simulated signals. These are fundamental frequencies of motor which are traveling from motor via rope to pulley beam to car. In the simulated signal the supply frequency is not seen, however, the eigenfrequency of the motor mounting has been seen at 24 Hz. This motor mounting eigenfrequencies had been also seen in the FEM calculation eigenfrequencies for modes for

the same motor as discussed in section 3.2. During the frequency response analysis (see section 3.2.2), the floor mode at 107 Hz is found for this elevator which has been tuned in the model. However, this floor mode is not visible in the FFT since the graph plotting is only fitted to 100 Hz because the measurement data is only credible up to that frequency.

The FFT graph for the measured and simulated signal of Elevator 2 is present in Figure 30. The fundamental motor frequencies are clearly seen in both the graphs; however, the measured signal has also shown excitation at the frequency 94 Hz can be seen in a blue square box in Figure 30, which is not motor excitation. As discussed in section 3.2.2, the frequency response analysis of the elevator with sliding guide shoes shows the floor mode at 92 Hz for this elevator therefore, it is concluded that this frequency could be coming from the floor resonance. In the result, the floor eigenfrequency is seen in the simulated signal in a similar frequency range to the measured signal.

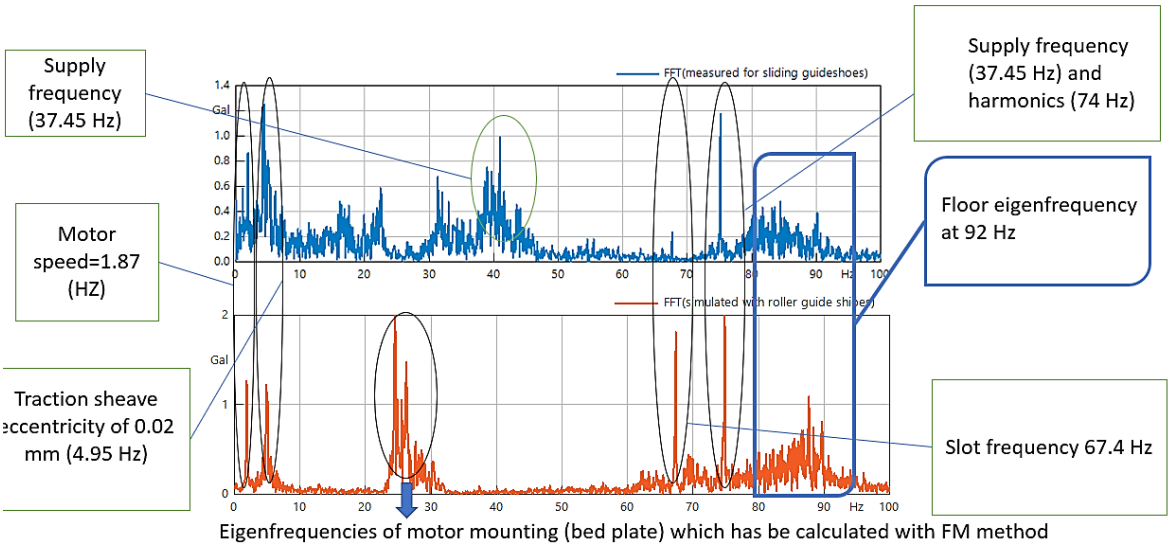


**Figure 30.** FFT of Elevator 2 of measured and simulated data.

### 4.1.3 Comparison of roller and sliding guide shoes

The difference between roller guide shoe and sliding guide shoes modeling is the stiffness value, friction coefficient value and floor eigenfrequencies as shown in Table 4. The elevator car floor eigenfrequency is dependent on the stiffness value of guide shoes therefore difference in stiffness value of roller and sliding guide has led to the difference in the floor eigenfrequencies. The roller guide has roller assembly consists of three separate identical rollers. Each of the rollers is fixed to the guide roller frame with damper isolation pads. The

all rollers in the roller guide have an initial compression of 1 mm against the guide rail in reality which is not used in the SimulationX model. The sliding guide shoe consists of a u-shaped plastic sliding insert, 2-part sheet metal frame and a rubber isolator and has a clearance of x-axis direction of 1mm which again is not used in the SimulationX model.

*Table 4: Different between roller and sliding guide shoes model*

| Roller guide shoes | Sliding guide shoes |
|---|---|
| 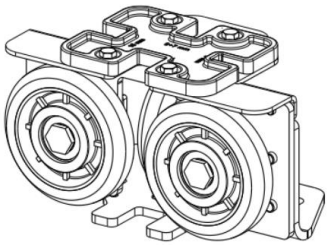 | 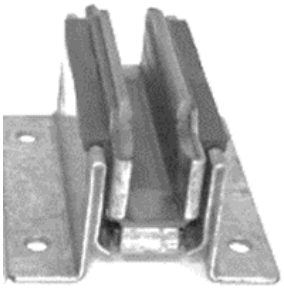 |
| • Stiffness of 250 N/mm in both y-axis and x-axis direction<br>• The friction coefficient of roller assembly is 0.05<br>• Floor eigenfrequency for Elevator 1 is 87 Hz and in Elevator 3 is 94 Hz | • Stiffness of 175 N/mm in y-axis and 325N/mm x-axis direction<br>• The friction coefficient of sliding assembly is 0.2<br>• Floor eigenfrequency for Elevator 2 is 96 Hz and in Elevator 4 is 81 Hz |

Comparison Elevator 1 and Elevator 2 has been carried out to understand its impact in the lateral and vertical vibration and as well all in frequency domain seen in Figure 31. In X-direction, the higher stiffness value of sliding guide shoes (325 N/mm in x-axis), has higher vibration amplitude in time domain result and in frequency domain result, slight shift toward higher frequency can be seen in the FFT graph. Similarly, in Y-direction, lower stiffness value of sliding guide shoes (175 N/mm in y-axis), lower vibration amplitude and slight shift toward lower frequency can be seen in FFT. In Z-direction, less vibration can be seen in sliding guide shoes as the floor eigenfrequency is tuned to be 94 Hz, which requires higher rotational stiffness than of 87 Hz (roller guide shoes). A higher stiffness value has lower vibration. The effect of the difference of guide shoes stiffness value can be also seen in the forces of guide shoes.

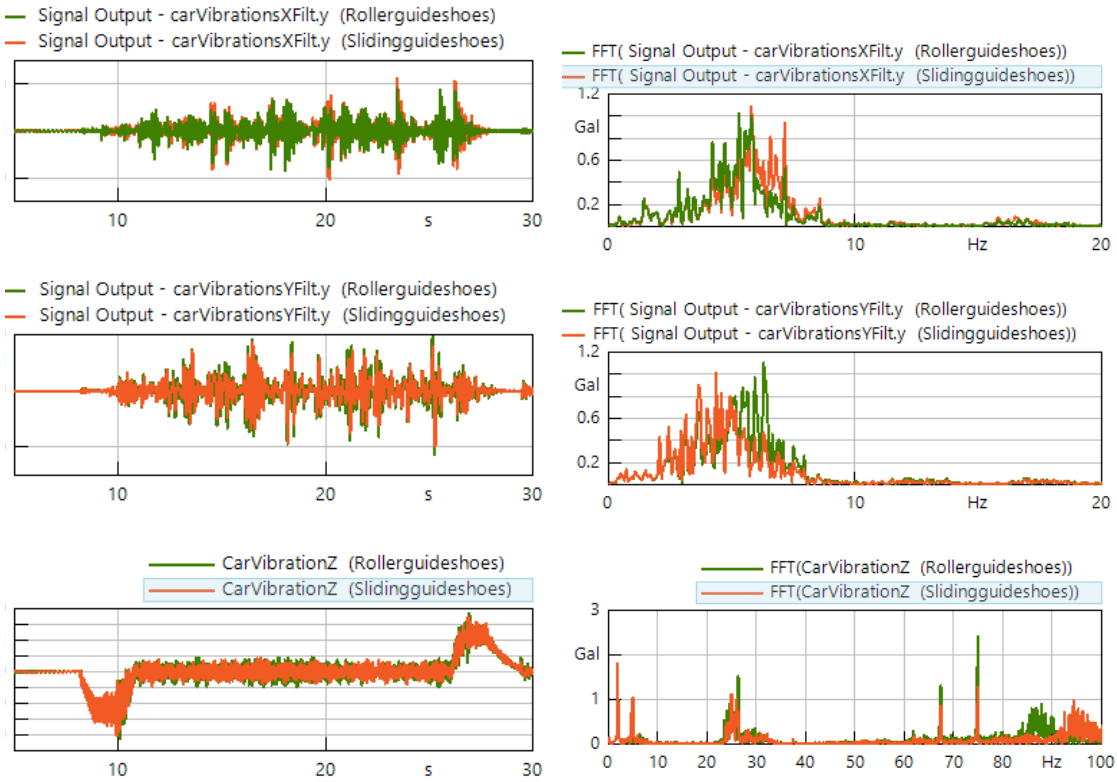


**Figure 31.** Time and frequency domain vibrations of roller guide shoe and sliding guide shoes.

The torque produced by the motor changes as the friction coefficient increases from 0.05 to 0.2 When the power loss caused by friction in the guide shoes is greater, the needed motor torque is increased to keep the elevator cars moving smoothly. This creates a fluctuation in motor torque generation as can be seen in sliding guide shoes in Figure 32. This finding can be used to diagnose a lubrication deficiency that generated a high friction coefficient between the guide rail and guide shoes.

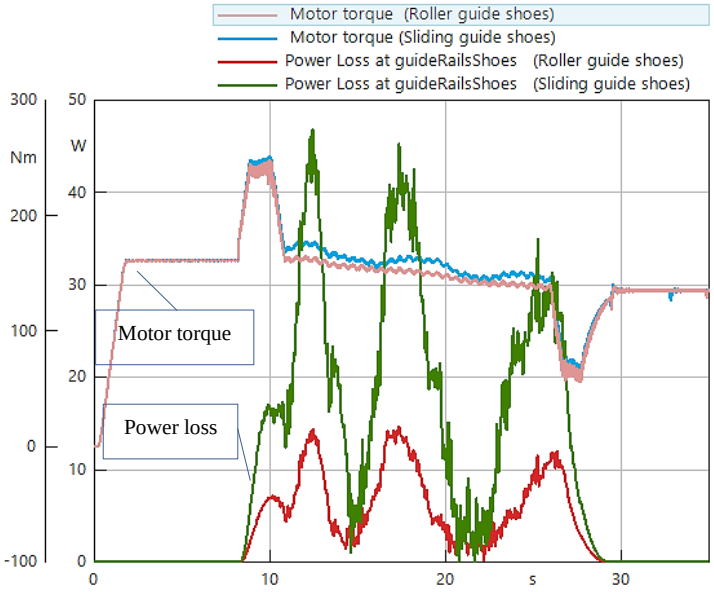


**Figure 32.** Motor toque and power loss of roller guide shoe and sliding guide shoes.

### 4.1.4 Validation analysis

The time and frequency domain validation comparison with two different elevators was successful as the simulated results correlated well with the laboratory measured quantities of elevators. In time domain vibration validation, maximum peak to peak values at nominal speed were the main criteria for the validation. The time domain validation demonstrates not only a correlation in the peak to peak value at the nominal run but also a well-fitted vertical vibration at the time of acceleration and deceleration period. However, there were some minor deviations between the simulation and measured data of the position and velocity of the car at acceleration and deceleration mainly caused by the difference in car movement time, jerk value and inertia between simulated and measured data. The shift in the vibration phase is observed in measured data during acceleration and deceleration in the y-axis vibration, which is produced by measurement error and is not seen in simulated results. Validation comparisons also reveal many differences in the shape and amplitude of measured data and simulation data curves. Factors contributing to these discrepancies include characteristics differences between actual elevators and their simulated counterparts, such as stiffness and damper coefficient of different components, and guide rails misalignment. These differences might also explain why some excitation frequencies are not visible in the simulated FFT when compared to the observed FFT.

## 4.2 Sensitivity analysis

To verify and get reliable the model, a sensitivity analysis is performed by altering several parameters. Elevator 1, Elevator 2, Elevator 3, and Elevator 4 are used for sensitivity analysis. The parameters chosen for these analyses are nominal run parameters such as load, no. of rope, traveling cable linear density, compensation chain linter density, travel height, speed, acceleration, and balancing ratio of counterweight. During each simulation run, only one parameter is changed, and the rest are kept with the default parameter. The purposes of this study are to observe model sensitivity and as well as to generate synthetic data for malfunction identification.

The default parameter of the simulation run all model

- Run type: - Down run from (top to 1st floor)
- Travel height 18 m (+1.1 m pit) from Elevator 1
- Travel height 13.26 m (+1.05 m pit) from Elevator 3
- In-car load 80 Kg
- Acceleration 0.5 m/s^2
- Rope number – 4
- Speed 1 m/s
- Nominal Jerk: 0.64 $m/s^3$
- Traveling cable liner density 0.435 Kg/m
- No compensation chains
- Motor

A total of 72 variants run are simulated and peak to peak value of lateral and vertical vibration for up run and down run. The combination of variants is presented in Table 5. As a result of the sensitivity study, it was discovered that white noise causes random deviations discussed in section 4.5, and hence white noise was not set as constant during sensitivity analysis. The lateral vibration and vertical vibration for all the simulation runs are analyses for the down run only. For a better comparison of the four model's peak to peak value of vibration, the bar chart is used.

To find maximum the peak to peak value from the vibrations result in the time domain is a time-consuming process and most like to make a mistake. The python script was developed

to circumvent these issues. The simulation data was entered into Python, and the script determined the highest peak to peak value as well as the precise time when the peak to peak occurred.

*Table 5: Variants combination*

| Case | Description / Variants | Model | Model | Model | Model |
|---|---|---|---|---|---|
| 1 | Incar load 80 kg | Elevator 1 | Elevator 2 | Elevator 3 | Elevator 4 |
| 2 | Incar load 315 kg | Elevator 1 | Elevator 2 | Elevator 3 | Elevator 4 |
| 3 | Incar load 630 kg | Elevator 1 | Elevator 2 | Elevator 3 | Elevator 4 |
| 4 | Rope 5 | Elevator 1 | Elevator 2 | Elevator 3 | Elevator 4 |
| 5 | Rope 6 | Elevator 1 | Elevator 2 | Elevator 3 | Elevator 4 |
| 6 | Travelling cable linear density 0,809 kg/m | Elevator 1 | Elevator 2 | Elevator 3 | Elevator 4 |
| 7 | Travelling cable linear density 1,842 kg/m | Elevator 1 | Elevator 2 | Elevator 3 | Elevator 4 |
| 8 | Compensation chain 1,5 kg/m | Elevator 1 | Elevator 2 | Elevator 3 | Elevator 4 |
| 9 | Compensation chain 3 kg/m | Elevator 1 | Elevator 2 | Elevator 3 | Elevator 4 |
| 10 | Travel 35 m | Elevator 1 | Elevator 2 | Elevator 3 | Elevator 4 |
| 11 | Travel 55 m | Elevator 1 | Elevator 2 | Elevator 3 | Elevator 4 |
| 12 | Travel 75 m | Elevator 1 | Elevator 2 | Elevator 3 | Elevator 4 |
| 13 | Balancing 40% | Elevator 1 | Elevator 2 | Elevator 3 | Elevator 4 |
| 14 | Balancing 50% | Elevator 1 | Elevator 2 | Elevator 3 | Elevator 4 |
| 15 | Acceleration 0,3m/s^2 | Elevator 1 | Elevator 2 | Elevator 3 | Elevator 4 |
| 16 | Speed 0,63 m/s | Elevator 1 | Elevator 2 | Elevator 3 | Elevator 4 |
| 17 | Speed 1,6 m/s | Elevator 1 | Elevator 2 | Elevator 3 | Elevator 4 |
| 18 | Speed 1,75 m/s | Elevator 1 | Elevator 2 | Elevator 3 | Elevator 4 |

### 4.2.1 Load case

During elevator system operation, the in-car load i.e. the number of passengers often fluctuates. Because of the variable elevator load, the vibration behavior is predicted to change. The changes in eigenfrequency and decrease in car oscillation amplitude are expected when increasing the load in the all elevator model. The peak to peak value for all four models is presented in Figure 33. (Herrera et al. 2014, p. 125.)

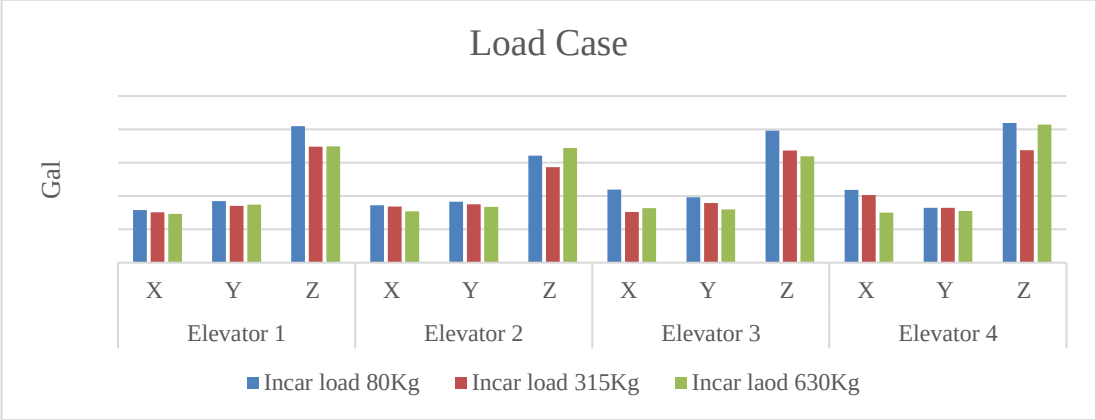


**Figure 33.** Load impact in peak to peak value of in-car vibration.

The Elevator 1 and 3 models has responded as predicted, with a drop in the peak to peak value in all three directions of vibration as shown in Figure 33. Similar lateral vibration responses can be found for both models with sliding guide shoes, however, the vertical vibration amplitude is the smallest when the load is 315 kg. When the load in the car is half of the rated load, the elevator car to counterweight balancing ratio is approximately 50%, and the motor torque necessary to carry out the operation is at its lowest. Less motor torque is generated, which results in less vibration being produced and transferred to the vehicle via the suspension rope. Vibration reduction can be seen in Figure 34 of Elevator 2.

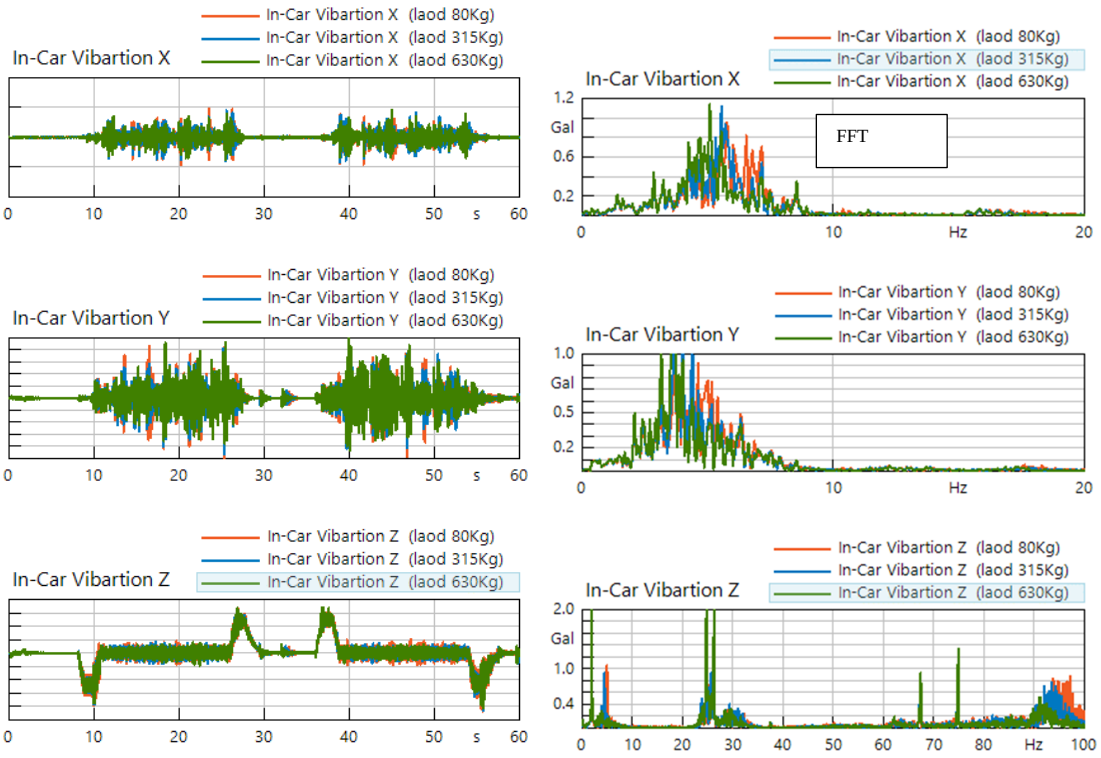


**Figure 34.** Vibration and frequency domain at different load cases.

### 4.2.2 Rope case

When the number of suspension ropes increases, the tension on each rope is decreased making the system more flexible. Due to the flexible hoisting system, rope oscillation is decreased, and less vibration is transmitted to the car, causing less vibration in-car. Figure 35 depicts the effect of changing the number of ropes on car vibration. The number of ropes is varying from 4, 5 and 6 for all four-elevator models. The peak to peak values are fluctuating and no clear trend can be seen, however lateral and vertical vibration peak to peak values are close to each other. It could be explained as the model has randomness shown in subsection 4.2.9 therefore it is challenging to draw a clear conclusion from this study. Overall, less vibration can be seen while increasing the rope number from 4 to 6. However, no significant change in the peak-to-peak value.

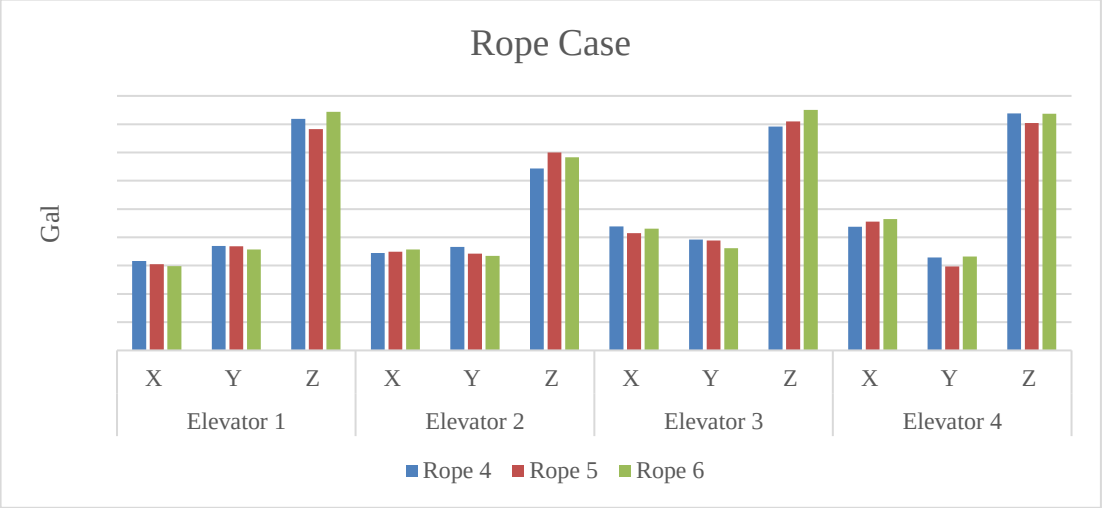


**Figure 35.** Number of rope impact in peak to peak value of in-car vibration.

The number of suspension rope impacts are investigated without any randomness in the model, by using the same white noise for all simulation runs. For this investigation, Elevator 3 was employed, and all three rope variations (4,5,6) were used. When the number of ropes is increased, the peak to peak value of both lateral and vertical vibration is found to decrease. However, this shift in the peak to peak value of lateral vibration occurs within 1 gal of vibration, but vertical vibration has a vibration drop of almost 10 gals. The model has responded as expected when the randomness was eliminated.

### 4.2.3 Speed case

For speed variations between 0.63 m/s to 1.75 m/s, the same motor but of different versions are used. For speed 0.63m/s and 1m/s motor_V1 has been used and for speed 1.6 m/s and 1.75 m/s motor_V2 has been used for the simulation. The masses and inertia of tensor of rotation component and mounting translation and rotational stiffness were kept constant for both motor versions.

The speed of an elevator has a significant influence on the quality of the ride i.e. vibration. The effect of guide shoes and misalignment of the guide rails is amplified as travel speed increases (Lemiao et al. 2020, p. 6). As a result, at lower speeds, the vibration amplitude should be smaller, while at higher speeds, it should be larger. When the speed is reduced from 1m/s to 0.63 m/s, the lateral vibration is reduced by more than 50 %, as shown in Figure 36. When the speed is raised from 1 m/s to 1.75 m/s, the lateral vibration has risen by about 250%. When it comes to lateral vibration, all four models behave well. Figure 36 illustrate that the vertical vibrations for all model are changing from each other. The vertical vibration Peak to peak value has no clear trend and it is challenging to conclude it. This could also be because of randomness present in the model.

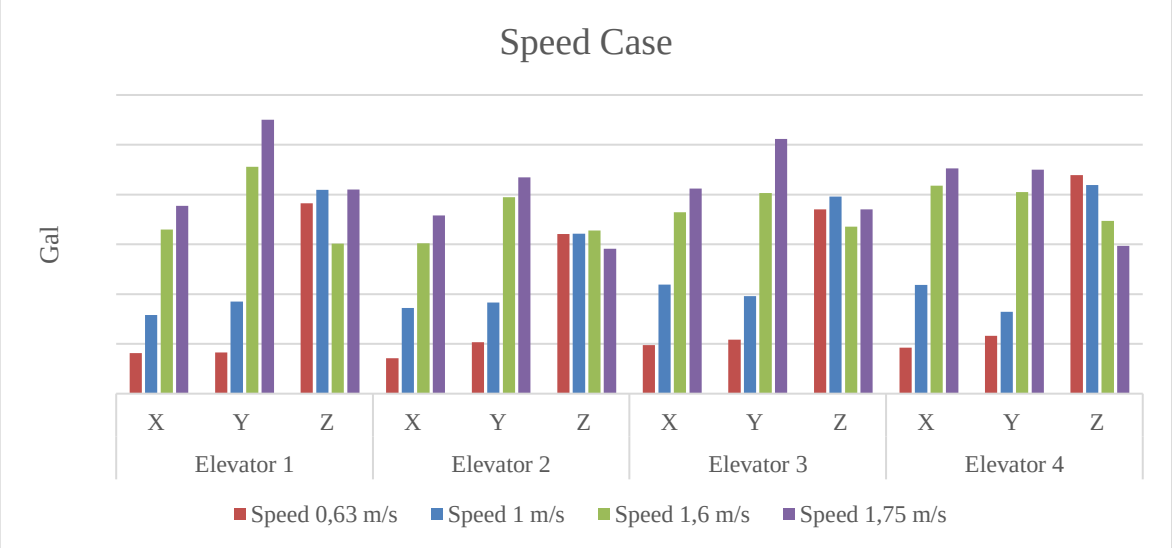


**Figure 36. S**peed impact in peak to peak value of in-car vibration.

To examine the influence of speed changes in the lateral direction in full depth, the Elevator 3 model has been used. This study discusses how the guide rail's misalignment impact is

exacerbated when speed increases from 1m/s to 1,75 m/s, as well as its reaction to vibration. Figure 37 depicts a right rail misalignment (right up), with higher two peaks at 3,1 m and 10,19 m height which is contributing to the highest vibration in the Y direction for both speed profiles. Higher speed causes a greater shift in the displacement and forces on the guide shoes, resulting in increased vibration throughout the car. The Peak to peak value at speed 1,75 m/s is 2.5 times higher than of at speed 1 m/s. Figure 37 at the right bottom shows this effect in guide shoes.

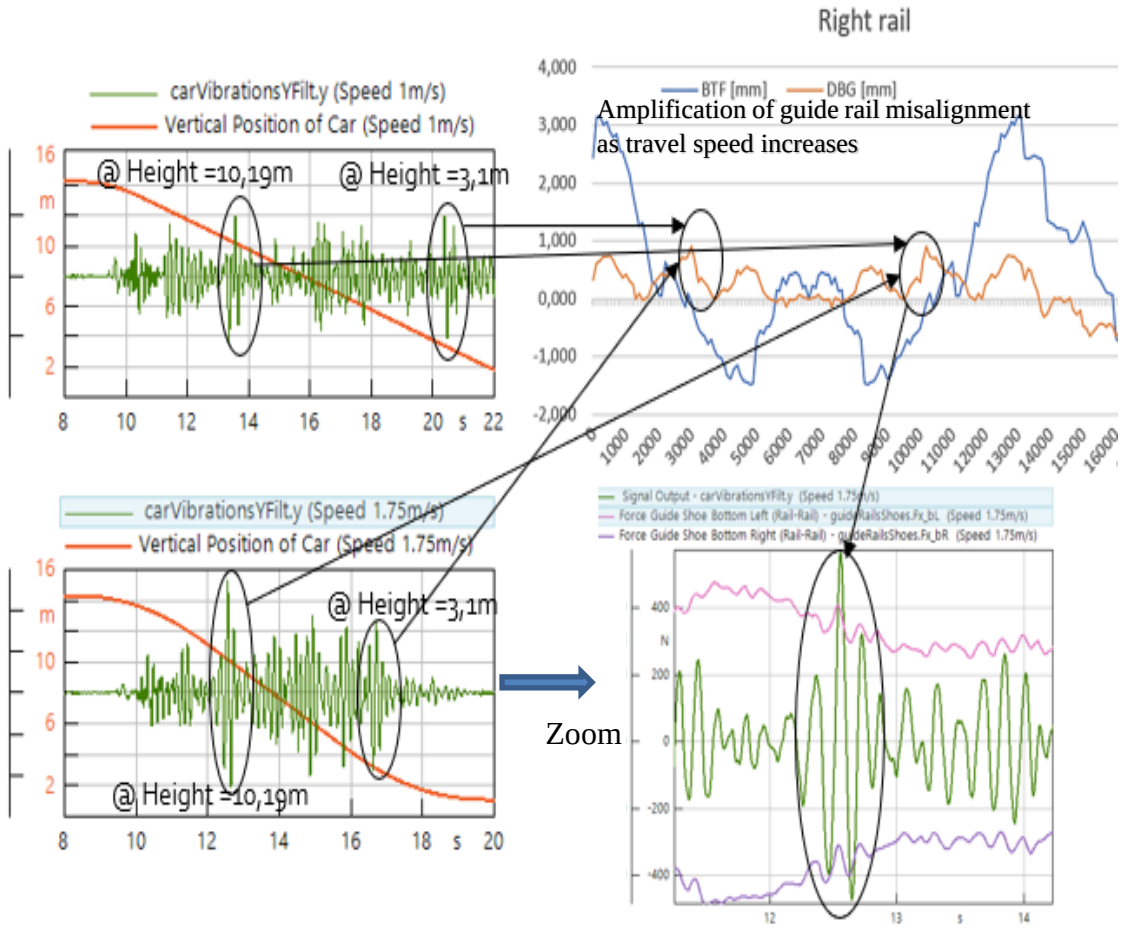


**Figure 37.** Speed impact to guide shoes forces and to the lateral vibration.

In the model, the supply frequency and slot frequency are proportional to the speed to make the model parametric. Reducing the speed lowers the supply frequency and slot frequency, and vice versa. The FFT graph of car vertical vibration Figure 38 clearly shows these variations in slot and supply frequency. In the lateral direction, one can observe that the lower speed has a smaller frequency amplitude than the higher speed in the FFT.

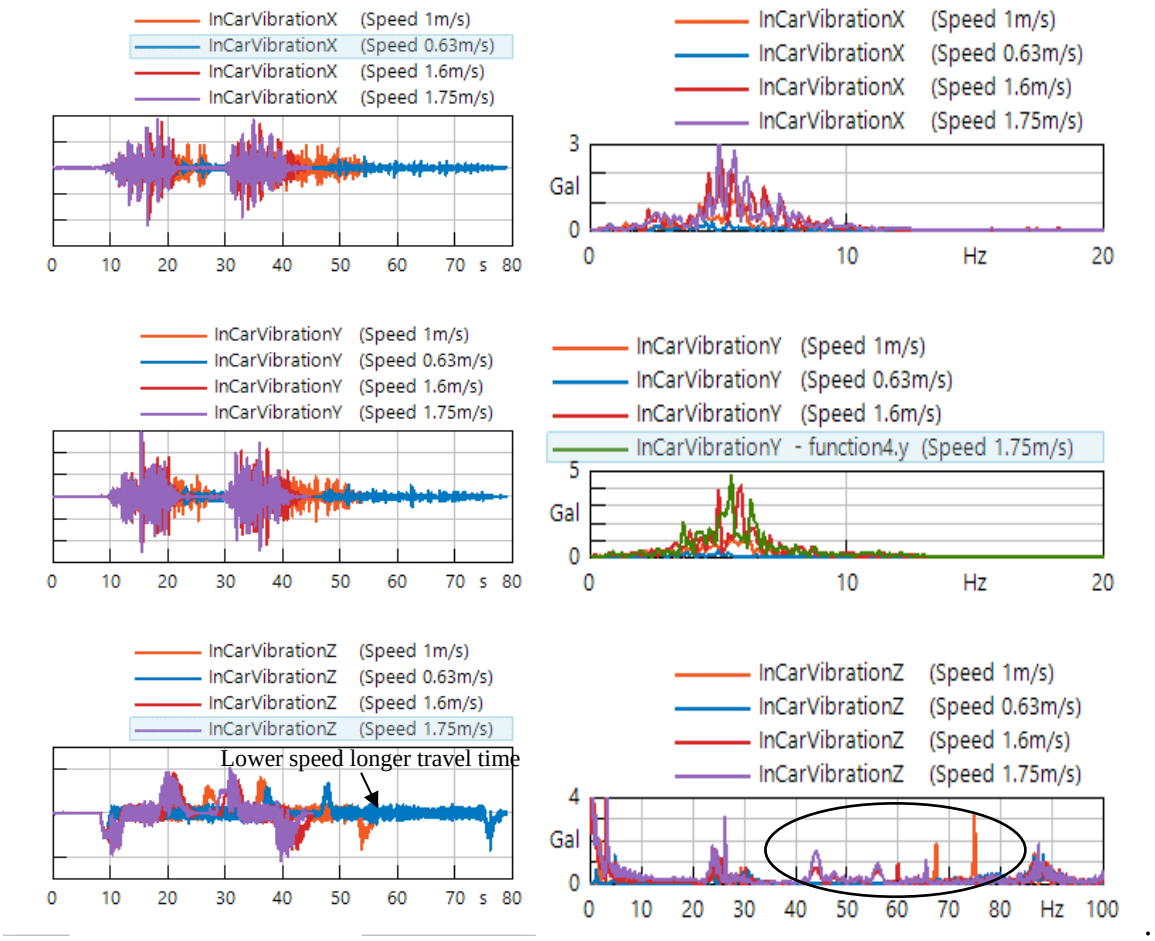


**Figure 38.** Vibration and frequency domain at different speed cases.

### 4.2.4 Travel height case

For the travel height variation, four different shaft heights of 18 m, 35 m, 55 m, and 75 m are used. This travel height variation is made in the SimulationX model by changing the location of the motor's vertical position. The suspension rope connecting the motor to the car and counterweight is changed automatically in the model while shaft height is changed. Measured data for guide rail misalignment is available only up to 32 m, therefore, to implement guide rail misalignment up to 75 m, the measured data is mirrored and repeated. Figure 39 illustrates higher vibration in both lateral and vertical direction when the travel height is increased from 18 m height therefore detailed investigation for lateral and vertical vibration is required.

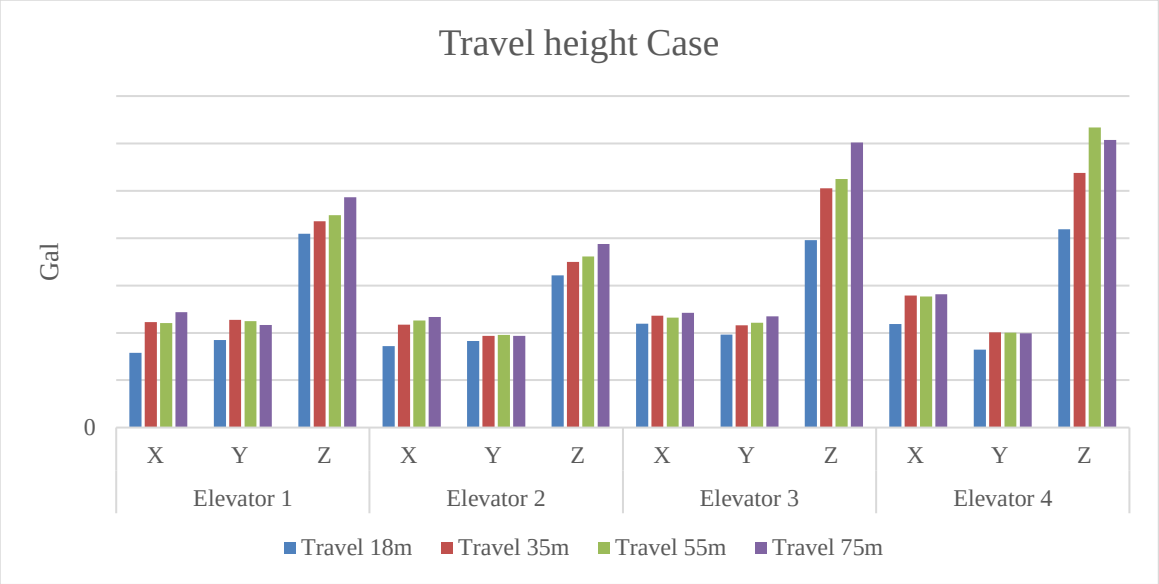


**Figure 39.** Travel height impact in peak to peak value of in-car vibration.

The Elevator 1 was used to investigate the impact of changes in travel height in the lateral and vertical directions in detail. This model's travel height is set at 55 m. When investigating the guide rail misalignment further, it is discovered that there are peaks with greater amplitude beyond 20 m. This is explained by the fact that as the height of the guide rial shaft increases, so does the number of guide rail segment slices, resulting in a greater misalignment in the structure. Manufacturing error (if the guide rails are not manufactured straight) and assembly error also known as human error (brackets are used to rigidly fix guide rail to the building walls and fishplate are used to guide rials to each other) are the most common causes of guide rail misalignment. As a result, larger guide rail misalignments can occur after the 18 m height, contributing to a higher peak-to-peak value on the lateral vibration. This is visible in all models with a travel height greater than 18 m. The highest peak to peak value in the X-direction is at time 41,8 m, and a bigger misalignment in the right rail can be observed at time 44,3 m, which demonstrates that when top guide shoes (vertical distance between guide shoes 2,5 m from top to bottom guide shoes) pass over this misalignment, a peak is created, as shown in Figure 40. There is also regular excitation after every 2.5 m of travel after 20 m of shaft height. This is excitation caused by misalignment at guide rail slices. The length of one guide rail segment is 5 m, and the distance between guide shoes is about 2.5 m, resulting in contact of a guide shoe to a guide rail edge every 2.5 m, lead to greater vibrations every 2.5 m. Similarly, the larger the misalignment in the Y-direction, the higher the vibration.

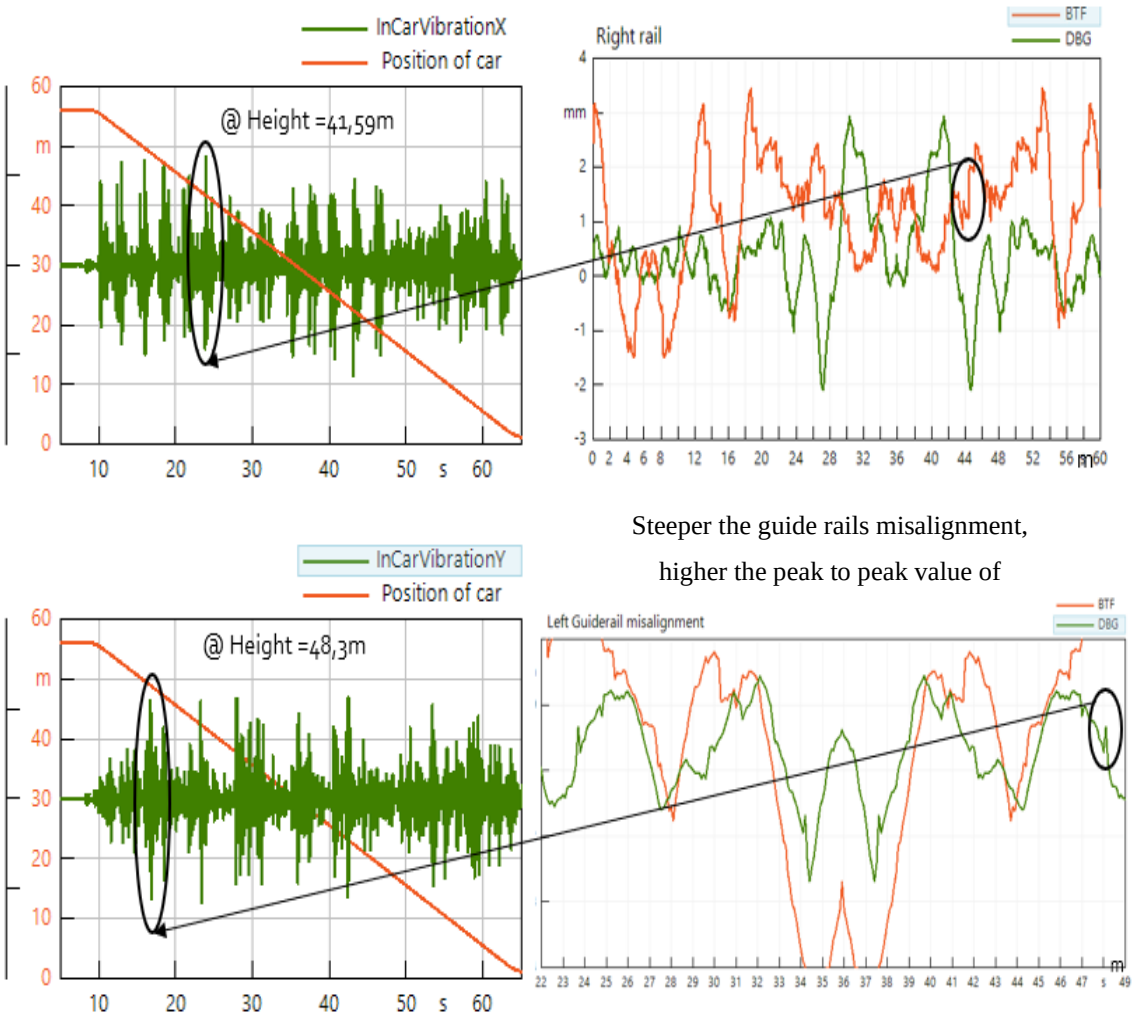


**Figure 40.** Impact of travel height of 55 m on guide rail misalignments on lateral vibrations.

The guide rail misalignment has an impact on the vertical vibration as well as can be seen from the graph in Figure 41. Sharper the spikes in the guide rail misalignment, the higher the peak-to-peak value can be found in vertical vibration. Sharper spikes in the guide rail misalignment act as the source of excitation in the model for vertical vibration. This effect of misalignment is seen in the vertical vibration because of the squeezing effect of the guide shoes on the flexible floor. The squeezing effect here means when the guide shoes are passing through higher misalignments (higher guide shoes forces), the flexible floor panels can bend (up or down) creating space for guide shoes to displace toward each other. This phenomenon is taking place because the guide shoes are rigidly connected to the floor panels and floor panels are modeled as flexible and are stiffened by translation and rotation stiffness values. Further development of the model is going on to avoid the displacement of guide

shoes. Higher vibration can be seen in Figure 41 when the car is closer to the motor due to higher transmission of vibration from motor to car when the rope length is at the shortest.

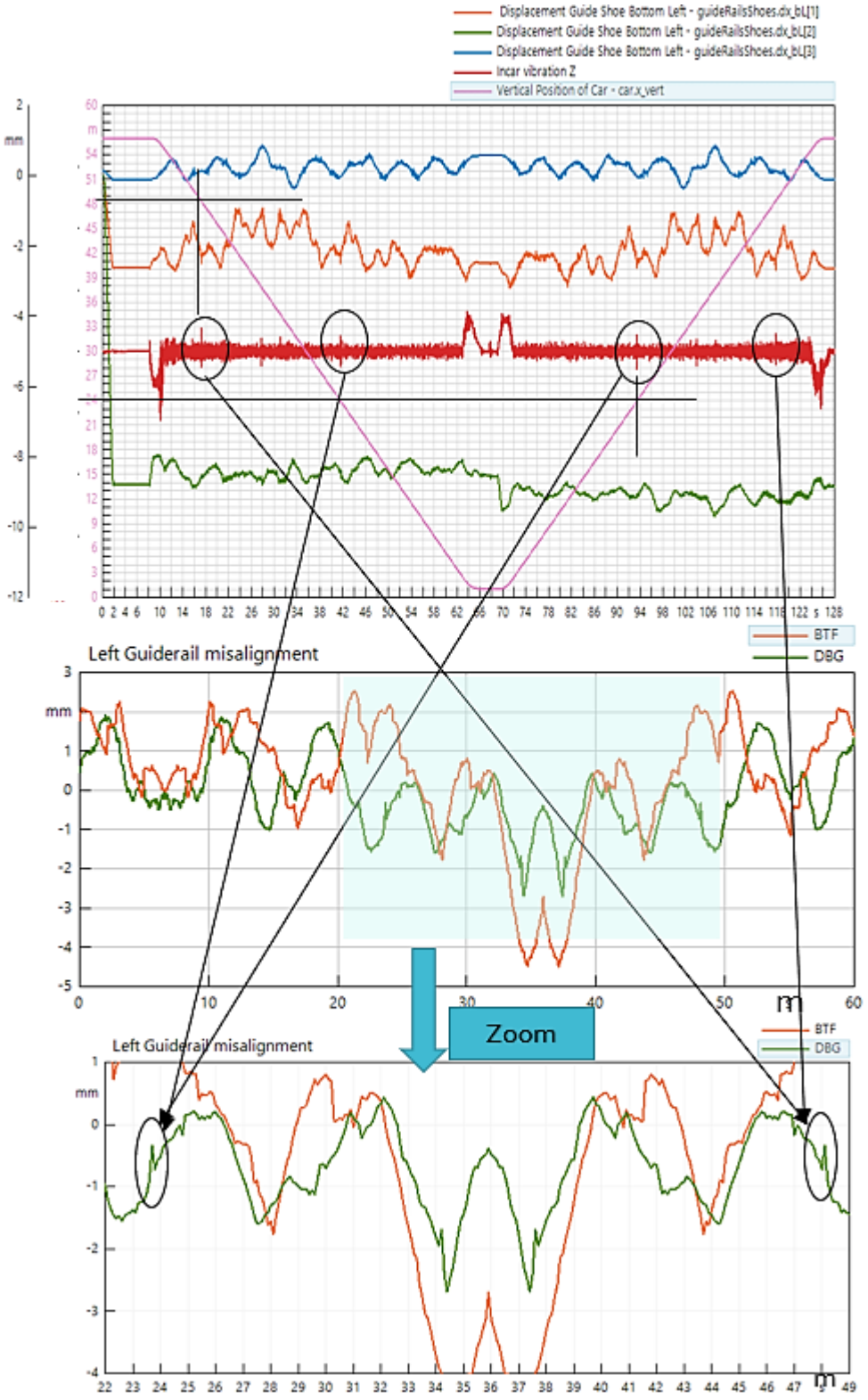


**Figure 41**. Travel height impact on Vertical vibration.

### 4.2.5 Acceleration case

The nominal acceleration and deceleration of the elevator is 0.5 m/s^2 and this acceleration and deceleration is reduced to 0.3 m/s^2. The purpose of this change is to study its influence in all model's in-car vibration. During the simulation, it is expected that vertical vibrations at the time of acceleration or deceleration phase must reduce with lower acceleration. From the rotational analog of Newton's second law, torque is directly proportional to the angular acceleration, which also can be seen from Figure 42 motor torque plot. At lower (0.3 m/s^2) acceleration, less torque is required which means less excitation produced at the motor and transferred to the elevator car via suspension rope. The reduction of the highest peak of vibration at acceleration phase of Elevator 1, Elevator 2, Elevator 3 and Elevator 4 models are 28.49 gals, 32,81, 41.7 and 38,78 gals respectively. Acceleration change created a slight shift in the nominal vibrations in the lateral direction.

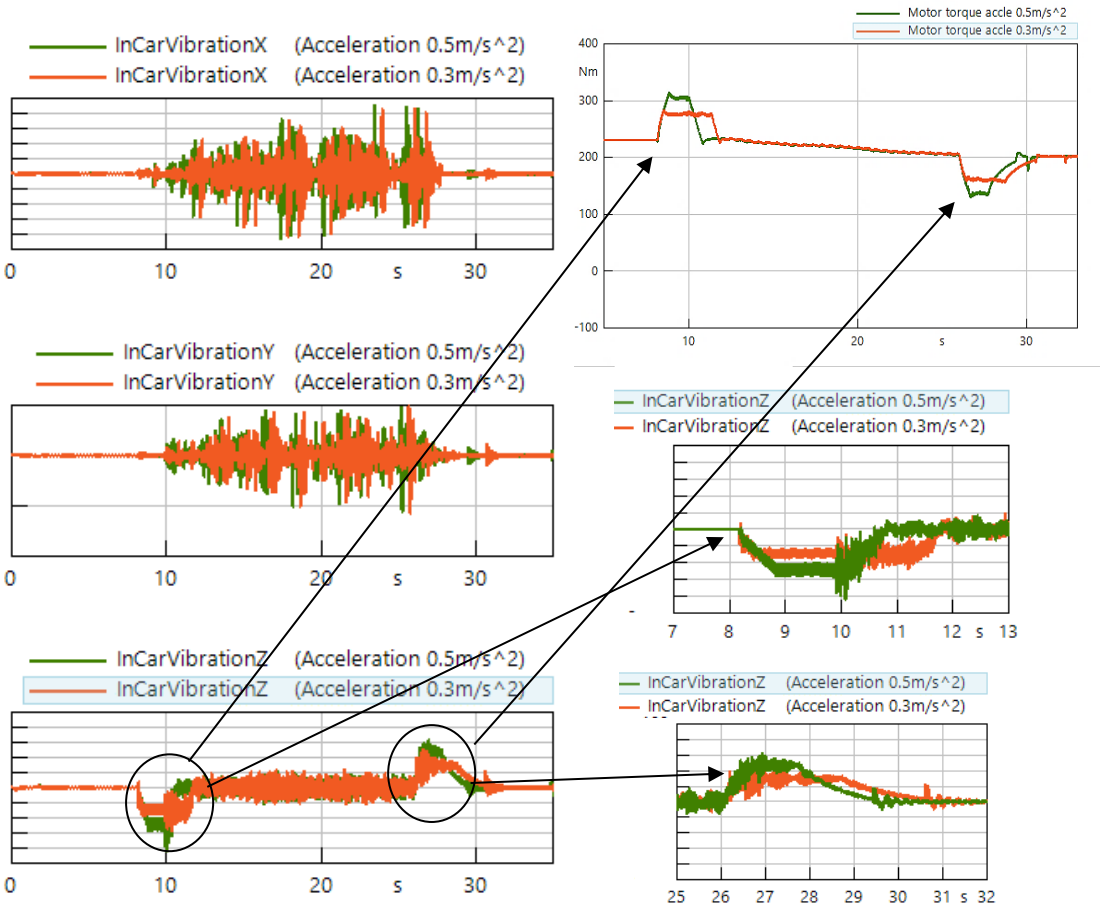


**Figure 42.** Impact of acceleration changed on vibration.

### 4.2.6 Balancing ratio case

The balancing ratio implies the total load on the car side of traction sheave to the total load on the counterweight side. The motor application is reduced when the balancing ratio is close to 50%. In this situation, the work done required for completing the down run or up run by elevator is minimum, hence the least motor torque is required. The variation of balancing ratio had been done by changing the weight of the counterweight in the SimulationX model. In this study, the balancing ratio of 40% and 50% have been used. 40% is considered to be the worst balancing ratio while 50% is considered as the best balancing ratio. The car mass or load has been kept constant in all the cases therefore no significant changes in the lateral vibration can be seen. However, in the vertical vibration one can see from Figure 43 that at 50% balancing ratio, the peak to peak value has been the least. This is because at 50% balancing ratio the motor torque production to carry out work is least which leads to less excitation being transferred to the car through suspension rope. This phenomenon also can be seen in the load case variate simulation for elevator model with sliding guide shoes, where at load 360 kg the vertical vibration is registered to be least.

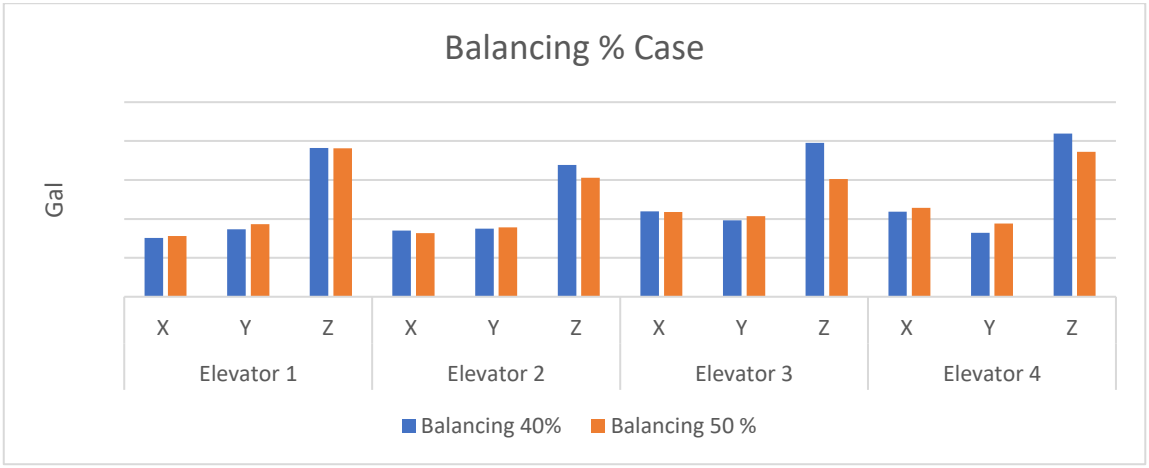


**Figure 43.** Balancing ratio impact in peak to peak value of in-car vibration.

### 4.2.7 Traveling cable case

The weight of the moving cable is attached to the bottom of the elevator car. When the elevator travels from the lowest level to the top floor, the weight of the traveling cable increases, and it reduces on the down run. Depending on where it is attached and the linear density of the cable, it might cause a dynamic imbalance in the car which has an influence on ride comfort. For all four simulation models, the linear density of the cable ranges from

0.435 kg/m to 1,842 kg/m. According to the results shown in Figure 44, traveling cable linear density has little influence on lateral vibration, and in vertical vibration, the vibration amplitude is lowest when the traveling cable linear density is 0.908 kg/m. This is suspected to be happening due to some resonance taking place in the remaining cases.

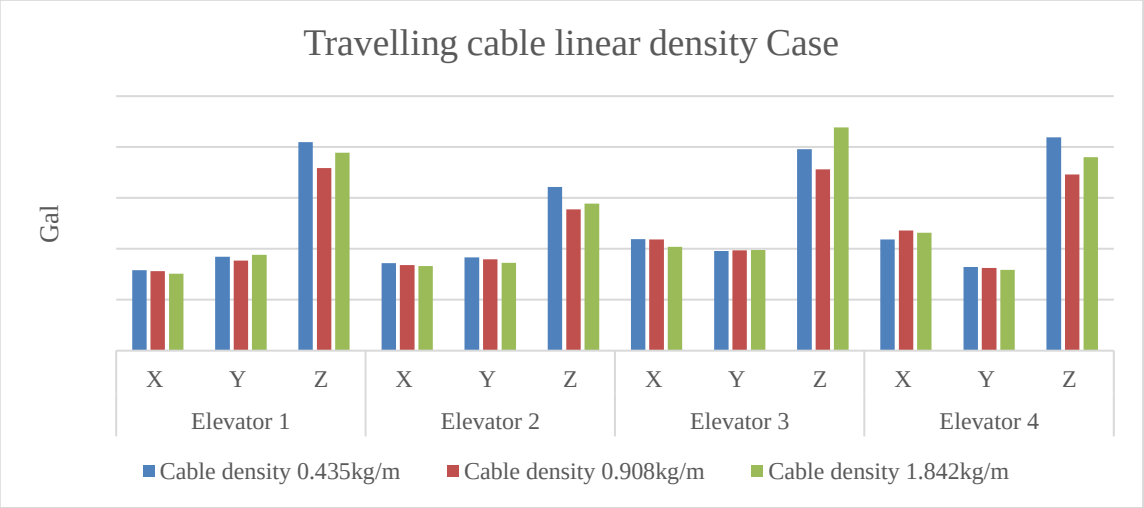


**Figure 44.** Travelling cable impact in peak to peak value of in-car vibration.

### 4.2.8 Compensation chain linear density case

The compensation chain, like the traveling cable, is linked to the bottom of the elevator car and also the counterweight. The overall weight of the car progressively grows during the uprun and reduces during the down run, whereas the total weight of the counterweight changes in the opposite direction. Compensation chains are typically used to provide ease on the hoisting mechanism when the elevator is operating without any passengers or with fewer passengers than of the capacity. Normally for the low-rise elevators, there is no compensation chain used since the travel height are these elevators are low. In this case, two alternative compensation chains are utilized and simulated with linear densities of 1.5 kg/m and 3 kg/m using all four models to determine if the model is sensitive compensation chain. As a result of the increased linear density of the compensating chain, one may expect increased vibration during up run and decreased vibration during down run. According to the results given in Figure 45. The linear density of the compensation chain has little impact on lateral vibration, and there is no apparent pattern in the vertical vibration peak to peak value. This is caused by the unpredictability that exists in the model.

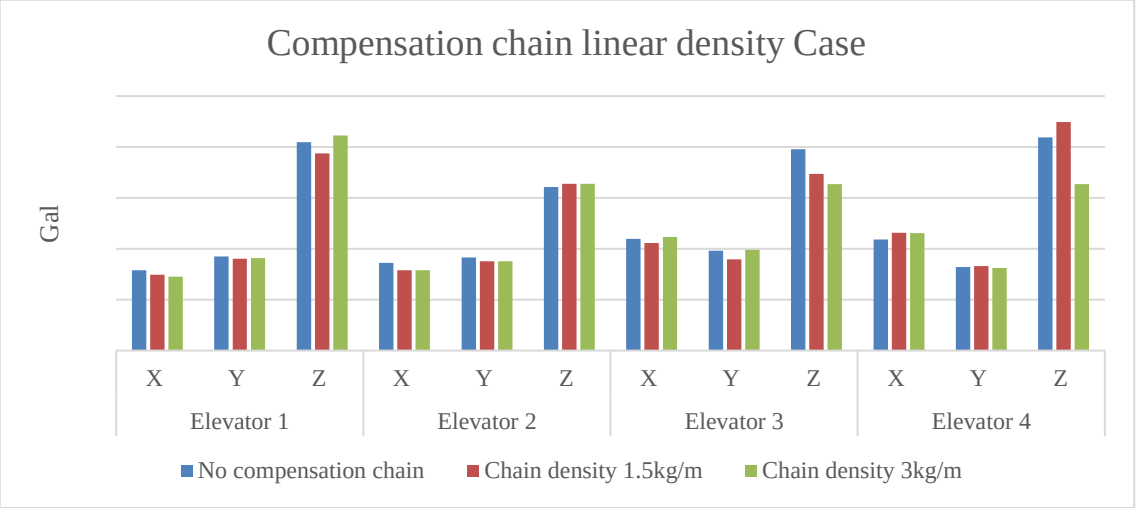


**Figure 45.** Compensation chain impact in peak to peak value of in-car vibration.

White noise was set as constant to avoid randomness in the model to investigate compensation chain impact. Elevator 1 was used for this study, and all three variations (0 kg/m, 1.5 kg/m, 3 kg/m) of liner density is used. The results of these simulations are shown in Figure 46. The peak to peak value of both lateral and vertical vibration has been seen to be decreasing when the compensation chain linear density has increased. However this change in the peak to peak value is taking place with 1 gal of vibration, this is because the change in the total weight after adding or subtracting to the car is only 56,7 kg (with companion chain linear density 3 kg/m) which is negligible to affect vibration. Nevertheless, as expected the vibration is reduced. In the graph, it is seen that when the elevation car has compensation chain weight (starting of simulation run in the green box) the vibration in all directions is less than when the elevator car has no compensation chain weight (end of simulation run in red box).

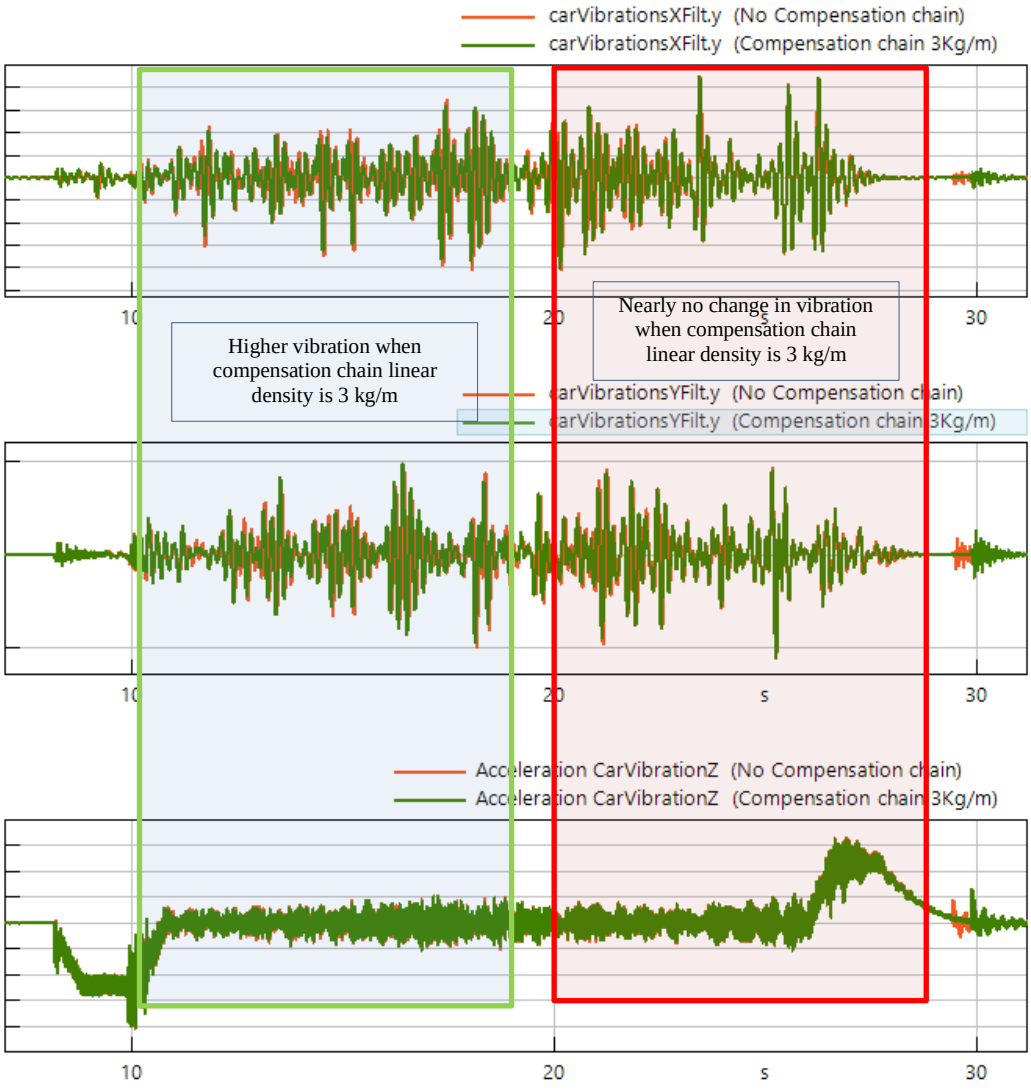


**Figure 46.** Compensation chain impact in-car vibration of Elevator 1.

### 4.2.9 Study of assumptions in the model

Sensitivity studies of different nominal run cases revealed that the model had a modest quantity of randomness. To study the root causes of this randomness in the model, Elevator 3 model is used. Three consecutive simulations were performed without making any changes in the model and the results indicated a 3 gals, 2 gals, and 4 gals fluctuation in Peak to peak values of X, Y and Z direction vibrations respectively. The model contains white noise to provide additional generic excitation to motor and car. The implementation of generic excitation in the model to account for possible excitation sources such as friction and other noise. To understand the impact of white noise on the vibration, three consecutive simulations were performed without white noise in the model. The results of these

simulations are plotted with and without white noise in the model as shown in Figure 47. The variation in peak to peak value in the model with white noise is because on each run the white noise produces a random signal and hence random excitation to the model can be randomly, however in the given boundary line. There is no change in the peak-to-peak value in both lateral and vertical direction simulations without white noise but lose in the vertical vibration. The loss of vertical vibration is due to a lack of initial excitation to waken the eigenfrequency present in the model. This study concluded with white noise in the model there is some level of randomness in the model and must be avoided.

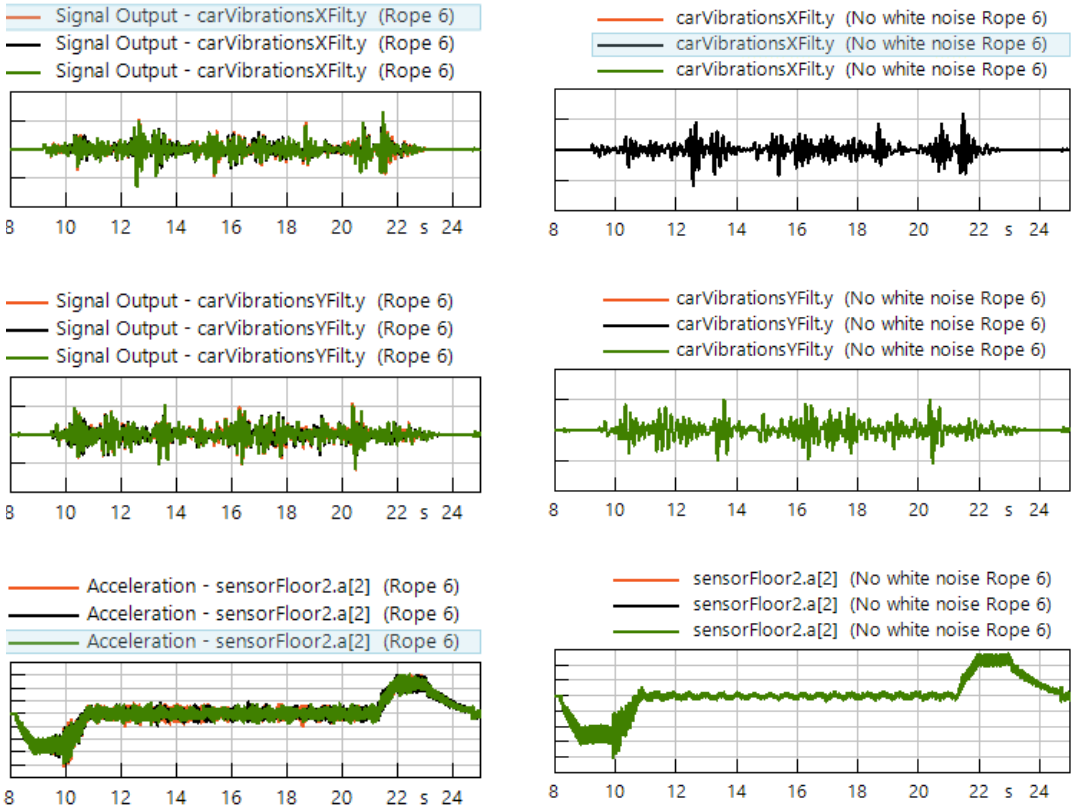


**Figure 47.** Vibration with white noise (Left) and without white noise(right) in the model.

The seed set during the startup phase totally determines the pseudo random signal in white noise. Automatic and manual initialization modes are available to the user. The seed is generated by the application based on the system time in automatic *initMode*. The seed can be entered manually in manual *initMode* as Figure 48 . The manual *initMode* assures that simulation results are repeatable which will avoid the randomness from the model as seen in the Figure 49.

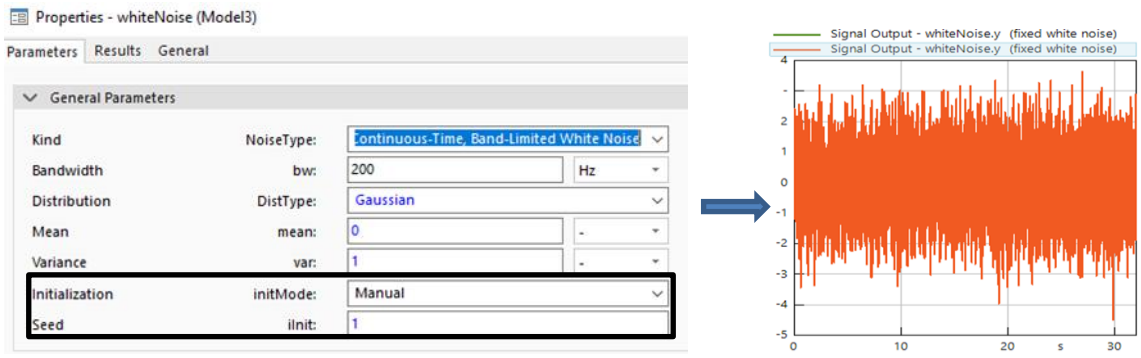


**Figure 48.** White noise setting from constant output.

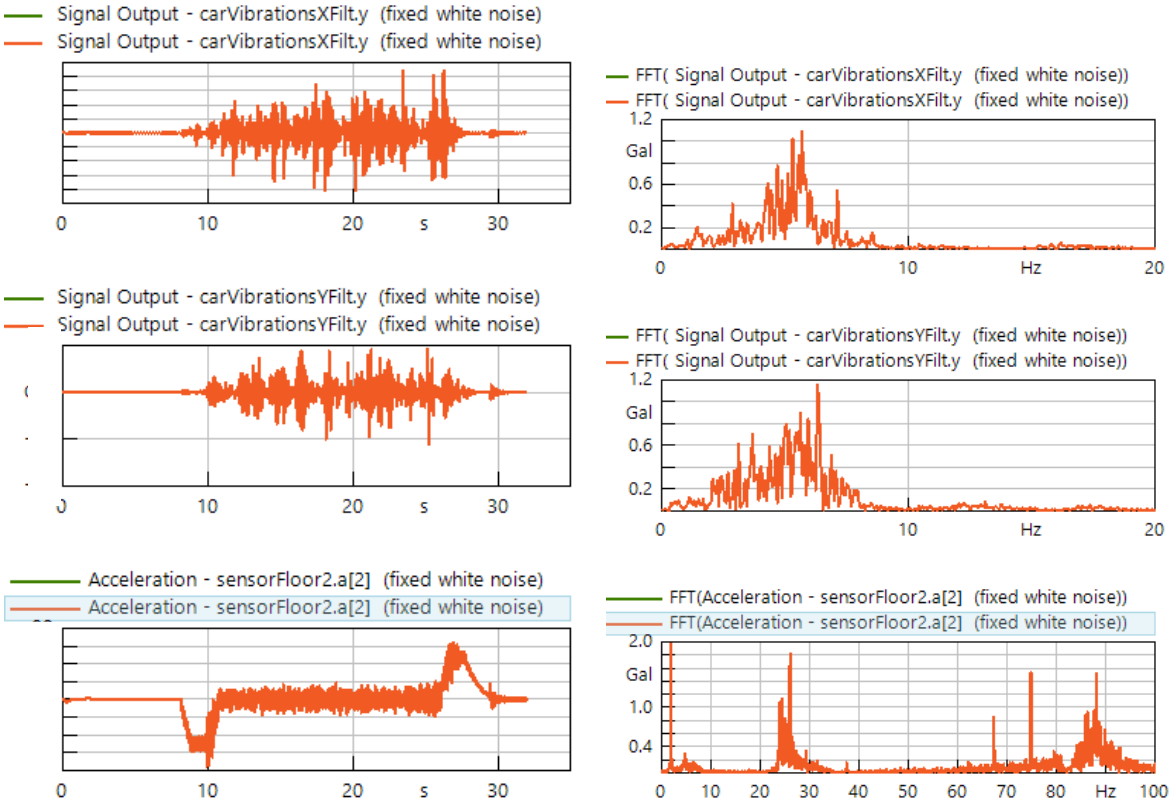


**Figure 49.** Vibration and frequency domain of constant white noise to motor and car.

The anomalies found in the result were investigated and root causes were found to be either because of white noise excitation or flexible floor modeling. The white noise excitation replicates the real model to produce results with small variations. This phenomenon is also found when multiple measurements are taken for the same real elevator. This is a useful feature to have in the model, but it is inapplicable for sensitivity analysis when even a small change in peak to peak value is important.

The sensitivity analysis of several configurations at nominal run confirmed that the model is sensitive and robust. In the majority of situations, the model behavior was found to be as projected. There were clear patterns in the dynamic response of the model as well as in the peak to peak value of vibration. However, the amount of change in peak to peak values found in the real model under these configurations needs to be validated with measured data

## 4.3 Load case results and analysis

In the chapter, the results of sag and bounce, car buffer crash and counterweight buffer crash situation are presented and analyzed.

### 4.3.1 Sag and bounce

The Elevator 1 model has been used for sag and bouncing phenomena. The sag model is validated with measured data. During the simulation and measurement of sag and bouncing, the load used is 89 kg. The car sag is measured by finding the position of the car in relation to the landing door positioning before and after loading. A 3-dimensional DC accelerometer is used to measure car bounce. The loading time is set to be at 5 seconds and the loading off time is at 15 seconds. The sag found in the measurement is less than 2.4 mm and, in the model, it is found to be 2.24 mm. The comparison of simulated and measured graphs of bouncing acceleration is represented in Figure 50. The simulated result of car bouncing is well-fitting with the measured curve and its peak to peak value is 99.25 gals and simulated is 97.34 gals. For this validation of bouncing vibration, the axial stiffness is multiplied by 0.6 to represent the non-linearity of rope at the lowest floor. The saturation time used is 0.2 seconds. The slight difference at the starting of the curve comes due to differences in the saturation time used in the model and in real-time. This parameter is challenging to capture as it happened in a fraction of time. The difference at the end of the curve comes from the difference in the damper parameter used in the model, which again it challenging to know the exact value.

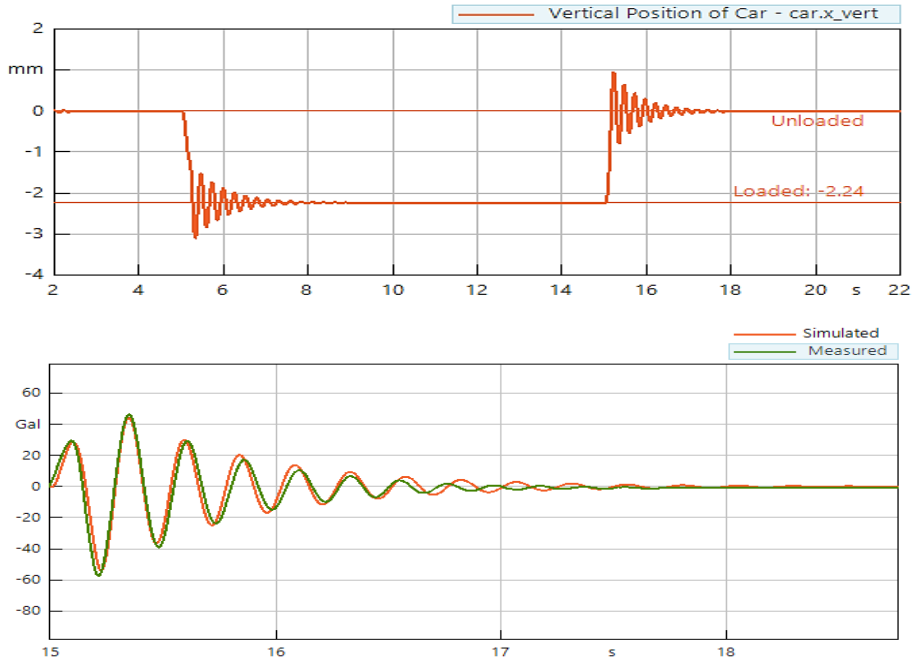


**Figure 50.** Sag and bouncing of the elevator (up) and vibration at bouncing (down).

### 4.3.2 Car buffer run

Elevator 1 has been utilized for car buffer run study and the simulation run has been started from the third floor to the buffer run. Figure 51 represents the result of the vertical velocity of the car, counterweight and angular velocity of traction sheave at buffer run. The collision between the car and buffer has taken place at 15.54 seconds. The velocity of the car after the collision has come to zero but at 15.90 seconds, it has started to rise and reached 0.7 m/s. At the same time, the velocity of the counterweight is -0.7 m/s and the angular velocity of the traction sheave is 7.2 rad/s. From this phenomenon, it can be concluded that when the car is striking against buffer, the impact of collision leads to bouncing of counterweight. And because the counterweight is 210 kg more than car weight, it pulls the car upward. Due to a lack of braking torque, the traction sheave is not stopped after brake activation, allowing this scenario to occur. Therefore, the brake torque value is reviewed and found out that the motor is equipped with two brake pads hence twice the brake torque value (2*350 Nm) must be used in the SimulationX model. The vertical velocity result with a new brake torque value represents the reality much more, however, there is still a small effect of counterweight as presented in Figure 51 on the right side.

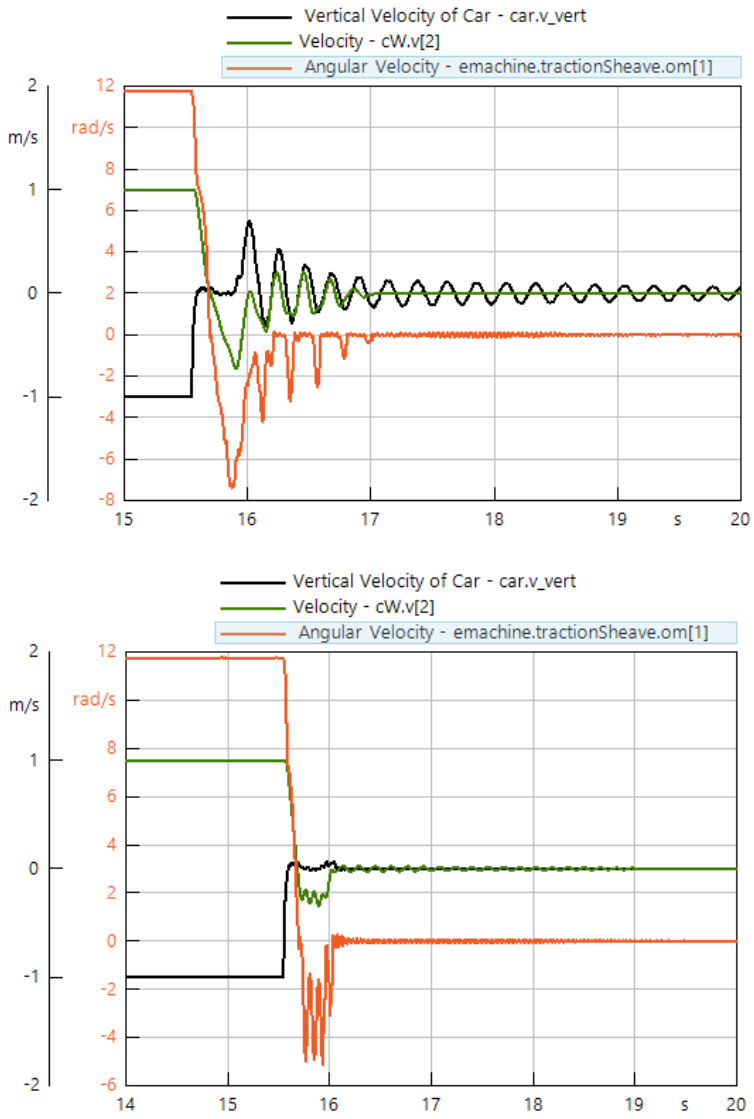


**Figure 51.** Buffer run impact at vertical velocity at brake torque value (up) and twice brake torque value(down).

Figure 52 illustrates the buffer forces dispersion after the impact when the car is empty (Load 0 kg) and when loaded with full capacity (Load 630 kg). The collision between the car and the buffer (in between 15.5 to 15.6 seconds in Figure 52) of the fully-loaded car is taking place slightly earlier than that of the car due to the change in initial position of the car as the elongation of the rope is different under different load conditions. After the dispersion of the impact at load 630 kg, the buffer force is higher than that of the empty car. The car pulling phenomenon can also be seen in the buffer force for both cases. For both cases, the maximum buffer force is closed to -4e+4 N. The comparison between two load cases shows that the model is sensitive to the load and results are obtained s expected. This study was not verified

since the measured data from the real buffer was unbillable; thus, validation is necessary for better understanding and a more reliable model.

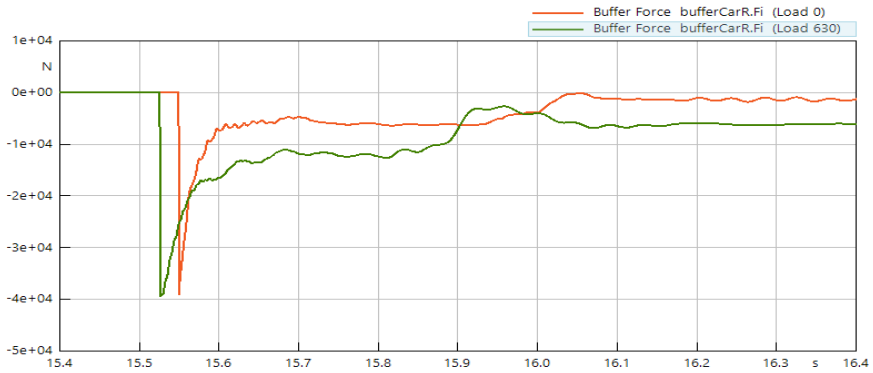


**Figure 52.** Buffer force at load 0 kg and 630 kg.

### 4.3.3 Counterweight buffer run

Elevator 1 has been utilized for the counterweight buffer run and the simulation run has been started from the sixth floor to the counterweight buffer run. Figure 53 represents the result of the vertical velocity, buffer force of counterweight at buffer run8 at 0 kg and 630 kg load case. No significant difference other than the change in the time of buffer impact can be seen in the curves and this is due to no change in the load of the counterweight. This study was not validated since the measured data from the real buffer was unbillable; thus, validation is necessary for better understanding and obtaining a more accurate model.

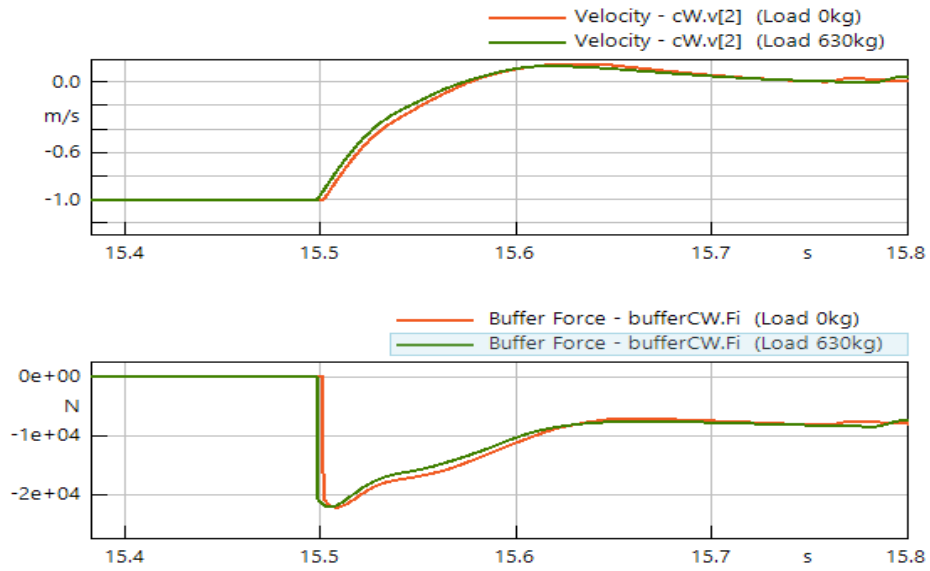


**Figure 53.** Velocity and buffer force of counterweight at 0 kg and 630 kg in-car load.

## 4.4 Analysis and discussion

In this thesis, the elevator system is modeled based on a preexisting elevator model and validated from the laboratory data for position, velocity and vibrations of the elevator car. During the validation, not only the measured and simulated curves are shown to have a high correlation, but the model's inability to turn the floor eigenfrequency lower than 81 HZ was discovered and resolved. In the same way, in the sensitivity analysis, not only the model's sensitivity and robustness were validated, but also a model with randomness and a significant effect of squeezing of guide shoes was discovered. Finally, load scenarios were successfully modeled and assessed. The objectives of this thesis were fulfilled effectively, and numerous obstacles were encountered and solved along the way, increasing the reliability of the model predicting the dynamic behavior of elevator systems.

The most critical components, with their parameters contributing to the researched phenomena, are required to be modeled for an accurate representation of the system. However, the level of detail required in the model is entirely dependent on the type and accuracy of the outcomes expected. The most significant components in an elevator system are the motor, motor mount, rope, guide rails, guide shoes, car mount, pulley beam, elevator car, and counterweight. The collective effect of each component and its parameters results in car vibration. The level of detail modeling required for each component for studying their response in-car vibration is presented in section 3.2. The initial excitations are also crucial to include in the model since they can cause subsequent resonances to occur. Similarly, a flexible car model is required for capturing the influence of local mode and its potential resonances. This provides the answer to the first research question of the thesis.

When the elevator family changes, the parameters of components change as well. The input parameters provided in Table 2 in Chapter 3 must be updated as per new elevator specifications that represent a specific elevator. The inputs can be categories into 4 main parameters i.e. geomaterial information, mass properties, stiffness and damping of components. These parameters have a high influence on vibration. Thus, these are the most important parameters to update while changing from one elevator family to another elevator family and maintaining the accuracy of the results. This is the solution to the thesis's second research question.

While discussing the third research question, to model any load case or malfunction in the model, the phenomena happening in the real situation must be identified and requirements to represent the phenomena must be known before replicating in the virtual model. As in sag and bounce modeling, it was understood that the in-car load is added in a fraction of a second and its result is measured in the displacement of car position after loading and unloading and vertical vibration while unloading.

As explained in chapter 2.1.2 for prescriptive maintenance a larger set of data (real or synthetic data) are required. Synthetic data can carry all kinds of information about the model along with malfunctions information which can be implemented in the simulation model. These data are used for creating algorithms from machine learning. With the high-quality synthetic data availability, artificial intelligence is used for failure signatures recognition and maintenance indications. During training a prescriptive maintenance algorithm, industry higher-level information can be provided to detected possible upcoming malfunction and suggesting possible ways to solve it. In short, the synthetic data provide the raw material for deep machine learning and artificial intelligence to create signature failure patterns which are then used in the prescriptive maintenance.

# 5 CONCLUSION AND FUTURE WORK

The main aim of this thesis was to model, validate and perform sensitivity analysis of the elevator at the system level in the SimulationX software. For this purpose, four elevators were modeled with their components and characteristics. The preexisting physics-based simulation model based on the KONE elevator system was utilized as a reference model.

The elevator model of Elevator 1 and Elevator 2 were successfully validated with respective measured data based on peak to peak values of the lateral and vertical vibrations. Validation comparisons show several discrepancies between test data and simulation data curves in terms of their form and amplitude. The major cause is the discrepancies in characteristics between the real and simulated elevators, such as stiffness and damper values of different components, as well as guide rail misalignments. During the comparison of the influence of rolling and sliding guide shoes on vibration, it was discovered that increasing the stiffness value of guide shoes resulted in an increase in peak to peak value and vice versa. The friction coefficient value between the guide rail and the guide shoes demonstrates the relationship between power loss at guide shoes and motor torque requirement.

The sensitivity analysis of the model provided important findings which could be further utilized to develop the elevator model. Higher spikes in the guide rail misalignment have a significant influence on the vertical vibration peak to peak value due to the squeezing effect of the guide shoes on the flexible floor however, in reality, there is a squeezing effect but much smaller and hardly its effect is seen in the vertical vibration. Thus, in the future, the model requires further modification to limit the effect of this phenomenon. In addition, sensitivity analysis also shows that the model also includes a modest level of randomness. The randomness in the model caused the inconsistency of multiple configurations study results. The utilization of white noise excitation in the car and motor was identified to be the fundamental cause of this randomness. For each simulation, the white noise was configured to generate random signals thus causing random excitation. However, randomness can be avoided by configuring the white noise to generate a constant signal. Overall, the simulation model demonstrated its sensitivity and robustness in projecting the dynamic behavior of elevator systems in nominal scenarios.

The three most common load case scenarios of an elevator - sag and bounce, car buffer run, and counterweight buffer run were simulated and analyzed. The sag and bounce were validated with the measured data and the comparison between simulation results to test results showed a good correlation. These load case modeling demonstrated the possibility to model and analyze several other types of load cases or malfunctions which further can be simulated with several configurations to understand the case behavior with changing configurations.

In the future, Elevator 3 and Elevator 4 can be validated with measured data from that specific real elevator. The specific measured guide rails misalignment of the model elevator rated load 630 kg and elevator rated load 480 kg can be utilized in the model and compare with their simulated and measured in-car vibration data to validate the model. The roller guide shoes model containing pretension and end stopper, while sliding guide shoes having a clearance in the y-axis direction can be used in the model to represent maximum functionalities of real guide shoes. The nonlinear stiffness value of sliding guide shoes can also be introduced in the model. The guide rail can be modeled to be flexible. This advancement in the model will enable it to capture almost all dynamic behavior while also increasing its sensitivity and robustness.

Several other parameter configurations can be simulation at nominal scenario. Many elevator malfunctions such as flat roller of guide shoes, incorrect installation of guide rails, lack of lubricant oil causing high friction between roller guide shoes and rails for sliding guide shoes, tilting of the car due to load imbalance and many more, can be modeled, their impact in-car vibration can be studied and synthetic data can be generated. The generated synthetic data from these nominal run configurations and malfunctions can be validated from real data when possible and then can be used for machine learning and artificial intelligence to find signature patterners in the time domain or the frequency domain. Prescriptive maintenance can be established using a combination of data captured by sensors and data generated from physics-based simulation to not only anticipate failure but also provide recommendations on how to effectively resolve the problem.

## REFERENCES

Amirouche, F. 2006. [Chapter 5:] Rigid-Body Kinematics. In: Fundamentals of Multibody Dynamics: Theory and Applications. Birkhäuser Boston, Pp. 41-55.

Aspentech. 2021. Prescriptive Maintenance. [Aspentech webpage]. (Updated date unknown). [Referred 19.8.2021]. Available: https://www.aspentech.com/en/apm-resources/prescriptive-maintenance

Baharudin, M. E. 2016. Real-time simulation of multibody systems with applications for working mobile vehicles. Lappeenranta University of Technology, Pp. 41-43.

Baobing, W. & Baras, J. S. 2013. HybridSim: A Modeling and Co-simulation Toolchain for Cyber-Physical Systems. IEEE/ACM 17th International Symposium on Distributed Simulation and Real Time Applications, Pp. 70-75.

Brezina, T., Hadas , Z. & Vetiska, J. 2011. Using of Co-simulation ADAMS-SIMULINK for Development of Mechatronic Systems. Proceedings of 14th International Conference on Mechatronics, MECHATRONIKA. Trencianske Teplice, Slovakia. 1-3.6.2011. IEEE. Pp. 59-64.

Centomo, S., Dall'Ora, N. & Fummi, F. 2020. The Design of a Digital-Twin for Predictive Maintenance. 25th IEEE International Conference on Emerging Technologies and Factory Automation (ETFA). Vienna, Austria. 8-11.9.2020. Pp. 1781-1788.

Çınar, Z. M., Abdussalam N. A., Zeeshan, Q., Korhan, O., Asmael, M. & Safaei, B. 2020. Machine Learning in Predictive Maintenance towards Sustainable Smart Manufacturing in Industry 4.0. Machine Learning and AI Technology for Sustainability, 12: 19. Pp. 8211.

Edrmedeso. 2020. Simulation Leadership Forum. [Edrmedeso webpage]. Updated December 22, 2020. [Referred 1.8.2021]. Available: https://digitallabs.edrmedeso.com/blog/gkn-vs-liu-vs-gbs-simulation-leadership-forum

Flores, P. 2015. Definition of Multibody System. In: Concepts and Formulations for Spatial Multibody Dynamics. SpringerBriefs in Applied Sciences and Technology, Pp. 1-63.

Ford, P. J., Amiri, E. & Mendrela, E. 2016. Electric elevator drive with position control. Electrical Engineering, 98. Pp. 307–319.

Hahsler, M., Bolaos, M. & Forrest, J. 2017. Introduction to stream: An Extensible Framework for Data Stream Clustering Research with R. Journal of Statistical Software, 76: 14. Pp. 1-45.

Herrera, I., Su, H. & Kaczmarczyk, S. 2014. Influence of the Load Occupancy Ratio on the Dynamic Response of an Elevator Car System. Applied Mechanics and Materials, 706. Pp. 128-136.

Huang, Q., Li , Z. & Xue, H. 2018. Multi-body dynamics co-simulation of hoisting wire rope. The Journal of Strain Analysis for Engineering Design, 53: 1. Pp. 36-45.

Ishii, T. 1994. Elevators for skyscrapers. IEEE Spectrum, 31: 9. Pp. 42-46.

Kelvin, M. K. 2007. A simulation study of predictive maintenance policies and how they impact manufacturing systems. University of Iowa, Pp. 1-2.

Kheir, A. 2015. Tall Buildings and Elevators: A Review of Recent Technological Advances. Buildings, 5:3. Pp. 1070-1104.

Klein , P. & Bergmann, R. 2018. Data Generation with a Physical Model to Support Machine Learning Research for Predictive Maintenance [web document]. Trier: 2018 [Referred

16.3.2021]. Business Information Systems II University of Trier. Pp. 12. Available in PDF-file: http://ceur-ws.org/Vol-2191/paper22.pdf

KONE. 2013. [ Slideshare webpage]. (Updated date unknown). [Referred 13.3.2021]. Available: https://www.slideshare.net/suleymanaliyev/general-presentation-ikma24736261

Kovacevic, J. 2017. What is Prescriptive Maintenance? [web document]. Updated 5.6.2017. [Referred 12.6.2021]. Available: https://hpreliability.com/what-is-prescriptive-maintenance/

Lemiao, Q., Zili, W. & Shuyou , Z. 2020. A Vibration-Related Design Parameter Optimization Method for High-Speed Elevator Horizontal Vibration Reduction. Shock and Vibration, Pp. 1-20.

Liu, Y., Yu, H., Li, G. & Li, Z. 2015. Modeling and Simulation of the drive system of elevator based on AMESIM. Proceedings of the 3rd International Conference on Material, Mechanical and Manufacturing Engineering. Guangzhou, China. 27-28.6.2015. Atlantis Press. Pp. 1120-1124.

Mathworks. 2021. Modeling Joint Connections. [Mathworks webpage]. (Updated date unknown). [Referred 26.5.2021]. Available: https://se.mathworks.com/help/physmod-/sm/ug/joints.html

Modelon. 2020. FMI. [Modelon webpage]. (Updated date unknown). [Referred 6.3.2021]. Available: https://www.modelon.com/functional-mock-up-interface-fmi/

Nikravesh, P. E. 2004. An Overview of Several Formulations for Multibody Dynamics. Springer, Pp. 189-196.

Parrott, A. & Warshaw, L. 2017. Industry 4.0 and the digital twin [web document]. Deloitte: September 2017 [Referred 26.6.2021]. A Deloitte series on Industry 4.0, digital manufacturing enterprises, and digital supply networks. Pp. 20. Available in PDF-file:

https://www2.deloitte.com/content/dam/Deloitte/kr/Documents/insights/deloittenewsletter-2017/26_201706/kr_insights_deloitte-newsletter-26_report_02_en.pdf.

SimulationX. 2016. Getting started. [SimulationX webpage]. Updated January 2021. [Referred 6.2.2021]. Available: http://doc.simulationx.com/4.0/1033/Default.htm#-Tutorials/GettingStarted.htm

Spiegelhauer , M. & Schlecht, B. 2020. Efficient modelling of flexible cable-pulley systems. Forsch Ingenieurwes, 85. Pp. 67-75.

Westin, C. 2018. Modelling and Simulation of Marine Cables with Dynamic Winch and Sheave Contact [web document]. Ottawa: June 2018 [Referred 29.2.2021]. Master's degree thesis. Carleton University Ottawa. Pp. 151. Available in PDF-file: https://carleton.ca/mdl/wp-content/uploads/Westin-Cassidy-MASc-ENG-August-2018.pdf

Yin, C. & Mckay, A. 2018. Introduction to Modeling and Simulation Techniques. The 8th International Symposium on Computational Intelligence and Industrial Applications. Tengzhou, Shandong, China. 2-6.9.2018. Pp. 2-4.